

INVESTIGATION OF TENSION-COMPRESSION FATIGUE
BEHAVIOR OF A NOTCHED CROSS-PLY
FIBER REINFORCED POLYMER MATRIX COMPOSITE AT ELEVATED TEMPERATURES
A
THESIS

19941228 036

DEPARTMENT OF THE AIR FORCE
AIR UNIVERSITY
AIR FORCE INSTITUTE OF TECHNOLOGY

Wright-Patterson Air Force Base, Ohio

DISCLAIMER NOTICE



THIS DOCUMENT IS BEST QUALITY AVAILABLE. THE COPY FURNISHED TO DTIC CONTAINED A SIGNIFICANT NUMBER OF PAGES WHICH DO NOT REPRODUCE LEGIBLY.

AFIT/GAE/ENY/94D-8

**INVESTIGATION OF TENSION-COMPRESSION FATIGUE
BEHAVIOR OF A NOTCHED CROSS-PLY
METAL MATRIX COMPOSITE AT ELEVATED TEMPERATURE**

THESIS

Matthew W. Yocum
Second Lieutenant, USAF

AFIT/GAE/ENY/94D-8

THIS QUANTITY IS LIMITED 2

AFIT/GAE/ENY/94D-8

INVESTIGATION OF TENSION-COMPRESSION FATIGUE BEHAVIOR
OF A NOTCHED CROSS-PLY METAL MATRIX COMPOSITE
AT ELEVATED TEMPERATURE

THESIS

Presented to the Faculty of the Graduate School of Engineering
of the Air Force Institute of Technology

Air University

In Partial Fulfillment of the
Requirements for the Degree of
Master of Science in Aeronautical Engineering

Matthew W. Yocum, B.S.E.S.

Second Lieutenant, USAF

December 1994

Accession For	
NTIS CRA&I	<input checked="" type="checkbox"/>
DTIC TAB	<input type="checkbox"/>
Unannounced	<input type="checkbox"/>
Justification	
By	
Date	
Availability Codes	
Dist	Avail and/or Special
A-1	

Approved for public release; distribution unlimited

Acknowledgments

As with any research effort of this magnitude, the single credited name shown on the title page of this work does not serve to do justice to the amalgamation of individuals whose advice, instruction, guidance, and hard work silently graces the following pages.

I would like to voice my thanks most deeply to Mr. Mark Derriso, whose experience, knowledge, and friendship made my stay at AFIT enjoyable and the work bearable. Also, thanks to the Model Shop for handling the many designs and redesigns of the buckling guide, and cutting out toys for me to play with. I would like to extend a thanks to Mr. Ken Burns of the ASD Machine Shop for his willingness to find better drilling techniques for the notch, as well as all the gang at the WL Materials Division for all their help with cutting, polishing, sectioning, and microscopy work.

Thanks to Dr. Walter Jones of AFOSR for making this research possible. And thanks especially to Dr. Mall who provided direction, answers to innumerable questions, and many hours of proofreading.

I am forever thankful to my family, whose continual prayers unquestionably remind God to keep an eye on and protect this one lone individual. Thank you to my parents for being such good friends.

And I am grateful for the friendly voices of good books and the even friendlier silences in the company of good friends. Thanks to Keats, Simmons and Bradbury and all those who have “heard the music.”

Matt Yocum

Table of Contents

Acknowledgments	i
Table of Contents.....	ii
List of Figures	v
List of Tables	ix
Abstract.....	x
I. Introduction	1
II. Previous Works	6
Introduction.....	6
Room Temperature (RT) Testing	6
High Temperature (HT) Testing	9
III. Experimental Set-up and Procedures	12
Material.....	12
Material Preparation	12
Specimen Preparation	13
Test Apparatus	16
Buckling Guide.....	19
Acetate Replication.....	21
Test Procedures.....	22
Post-Failure Analysis.....	26
IV. Results	29

Introduction.....	29
Monotonic Tensile Test	30
Macromechanic Considerations.....	32
Fatigue Life.....	37
Stress-Strain Curves.....	39
Stiffness and Strain Curves.....	46
Micromechanic Considerations	50
Crack Initiation and Growth	52
Fractographic Analysis	58
Metallographic Analysis	72
V. Analysis and Discussion	83
Introduction.....	83
Maximum Applied Stress Criterion.....	85
Stress Range Criterion	87
Effective Strain Range Criterion.....	89
Crack Initiation and Growth Comparison.....	91
Notched and Unnotched Specimen Fatigue Life Comparisons	98
LISOL Analysis	104
VI. Conclusions and Recommendations	115
Appendix A: Stress-Strain Curves.....	119
Appendix B: LISOL Files.....	125
Bibliography	128

Vita131

List of Figures

Figure 1. Tension-Compression Load-Time Relationship, $R = -1$	5
Figure 2. Specimen Dimensions	14
Figure 3. Test Apparatus.....	18
Figure 4. AFIT Buckling Guide Design.....	20
Figure 5. Effect of Buckling on Hysteresis.....	24
Figure 6. Sectioning Plan of a Specimen.....	28
Figure 7. Monotonic Tensile Test Stress-Strain Curve.....	31
Figure 8. Talreja's Model for Regimes of Cross-Ply Laminate S-N Curve.....	35
Figure 9. Model of Regimes for Notched Cross-Ply Laminate S-N Curve	35
Figure 10. Regimes of S-N Curve for Unnotched Cross-Ply Laminate.....	36
Figure 11. Regimes of S-N Curve for Notched Cross-Ply Laminate.....	36
Figure 12. Failure S-N Curve.....	40
Figure 13. Crack Initiation S-N Curve.....	41
Figure 14. Failure and Crack Initiation S-N Curves	41
Figure 15. Stress-Strain Curves Throughout Fatigue Life of ± 225 MPa Fatigue Test	43
Figure 16. Tensile Portion of Stress-Strain Curves	44
Figure 17. Compressive Portion of Stress-Strain Curves	45
Figure 18. Normalized Stiffness vs. Fatigue Cycles.....	47
Figure 19. Max and Min Strain vs. Fatigue Cycles	47
Figure 20. Normalized Stiffness vs. Normalized Fatigue Life	48

Figure 21. Max and Min Strain vs. Normalized Fatigue Life.....	48
Figure 22. Edge Replica of 90° Fiber Debonding (400x).....	53
Figure 23. Crack Initiation Sites (19.6x)	55
Figure 24. Crack Bifurcation of Major Crack (50x).....	56
Figure 25. Crack Length vs. Fatigue Cycles	57
Figure 26. Four Specimens Fracture Surfaces	60
Figure 27. Monotonically Loaded Specimen Fracture Surface.....	61
Figure 28. ± 300 MPa Fatigue Loaded Test Fracture Surface	62
Figure 29. Brittle Cleavage Region Near Hole on Fracture Surface (45x).....	65
Figure 30. Brittle/Ductile Transition Region (50x)	66
Figure 31. Matrix Necking and Ductile Void Coalescence in Ductile Region (400x)	67
Figure 32. Fatigue Crack Shape Prior to Failure	69
Figure 33. Fatigue Striations Emanating from 90° Fibers (500x)	70
Figure 34. 90° Fiber Break at Molybdenum Cross-Weave (370x).....	71
Figure 35. 90° Fiber Debonding (500x).....	73
Figure 36. Region of 0° Fiber Breaks (100x)	74
Figure 37. 90° Fiber Break (500x).....	75
Figure 38. Reaction Zone Crack on 90° Fiber (560x)	76
Figure 39. Fiber Bridging of Major Crack (120x)	78
Figure 40. Effect of Fiber Bridging	79
Figure 41. 0° Fiber Debonding Causing Fiber Bridging of Major Crack (700x)	80
Figure 42. Transgranular Cleavage of Major Crack (220x).....	82

Figure 43. Maximum Stress S-N Curve: TC HT vs. TT HT	86
Figure 44. Stress Range S-N Curve: TC HT vs. TT HT.....	88
Figure 45. Effective Strain Range S-N Curve: TC HT vs. TT HT	90
Figure 46. Crack Growth vs. Normalized Fatigue Life Comparison: TC HT vs. TT HT	95
Figure 47. Stiffness Response Comparison: 170 TC HT vs. 400 TT HT.....	97
Figure 48. Maximum Stress S-N Curve: TC Notched vs. TC Unnotched.....	99
Figure 49. Stress Range S-N Curve: TC Notched vs. Unnotched	100
Figure 50. Maximum Stress Comparison of Fatigue Lives, Notched and Unnotched	102
Figure 51. Stress Range Comparison of Fatigue Lives, Notched and Unnotched....	103
Figure 52. LISOL Unit Cell Model.....	105
Figure 53. Maximum Fiber Stress vs. Fatigue Life: TC HT vs. TT HT	109
Figure 54. Maximum Matrix Stress vs. Fatigue Life: TC HT vs. TT HT	109
Figure 55. Fiber Stress Range vs. Fatigue Life: TC HT vs. TT HT.....	111
Figure 56. Matrix Stress Range vs. Fatigue Life: TC HT vs. TT HT	111
Figure 57. Maximum Fiber Stress vs. Cycles : Notched TC vs. Unnotched TC	113
Figure 58. Maximum Matrix Stress vs. Cycles : Notched TC vs. Unnotched TC....	113
Figure 59. Fiber Stress Range vs. Cycles : Notched TC vs. Unnotched TC.....	114
Figure 60. Matrix Stress Range vs. Cycles : Notched TC vs. Unnotched TC	114
Figure 61. Stress-Strain Curves : ± 150 MPa Test	120
Figure 62. Stress-Strain Curves : ± 170 MPa Test	121
Figure 63. Stress-Strain Curves : ± 278 MPa Test	122
Figure 64. Stress-Strain Curves : ± 300 MPa Test	123

Figure 65. Stress-Strain Curves : ± 375 MPa Test124

List of Tables

Table 1. Test Matrix	25
Table 2. Test Results.....	39
Table 3. TC HT: Crack Initiation Cycle Value Validity	92
Table 4. TT HT: Crack Initiation Cycle Value Validity	93
Table 5. TC HT: Percentage of Life Until Crack Initiated	93
Table 6. TT HT: Percentage of Life Until Crack Initiated.....	94
Table 7. Matrix Microstress Range Comparison: TC HT vs. TT HT.....	108

Abstract

With the ability to now perform tension-compression fatigue loading without the effects of buckling, this study seeks to fill the gap in the characterization of the damage mechanisms for Metal Matrix Composites (MMCs). In particular, this study examines the effects of tension-compression fatigue loading on a cross-ply laminate lay-up, $[0/90]_{2s}$, of SCS-6/Ti-15-3 with a notch (center hole) at the elevated temperature of 427 °C (800 °F). Stress and strain data were taken to evaluate the macromechanical behavior of the material. Replication of the specimens throughout fatigue testing was used to determine crack initiation as well as the progression of the cracks during the loading. Fractography and metallography were performed to characterize the damage on the microscopic level.

The applied stress (S) and fatigue lives (N), S-N, curves for both crack initiation and fatigue life were established. Replica analysis in conjunction with fractographic and metallographic analysis of failed specimens established the picture of the crack propagation and the damage mechanisms. Four cracks were found to develop around the periphery of the hole. On further cycling, two of these became dominant and proceeded through to the edge of the specimen, inducing fracture. The crack proceeded through a brittle cleavage region in the matrix until a critical crack length was reached, at which time the crack grew catastrophically through the specimen causing a ductile region and matrix necking around the fibers.

The effects of the tension-compression fatigue condition on the notched MMCS were compared with the tension-tension fatigue condition. It was found that on a

maximum applied stress basis, the fatigue lives under the tension-compression cycling were shorter than its counterpart under the tension-tension cycling. The same findings among the two cases were also found based on the effective strain range basis. The reason for the shorter fatigue lives was due to the additional damage from the compressive portion of the fatigue loading, as well as earlier crack initiation and a faster crack growth rate for tension-compression loading.

A further comparison was made between tension-compression high temperature fatigue loading of notched and unnotched specimens. On both a maximum stress and stress range basis, the notched test fatigue lives were shorter than the fatigue lives of the unnotched condition. This was due to the presence of the center hole which added an additional stress concentration within the specimen.

Finally, another comparison was made among four conditions that included tension-compression and tension-tension fatigue loading for both notched and unnotched specimens. This showed that the addition of the center hole had no difference on the fatigue life of the material under tension-tension fatigue loading, but it had a considerable effect on fatigue life under tension-compression fatigue loading.

INVESTIGATION OF TENSION-COMPRESSION FATIGUE BEHAVIOR OF
A NOTCHED CROSS-PLY METAL MATRIX COMPOSITE
AT ELEVATED TEMPERATURE

I. Introduction

A crucial dichotomy exists in the engineering world. On one side, there are certain technologies and structures whose progress is on hold for the necessary materials to be developed. On the other side, the development of certain new materials leads to the formation of previously unknown technologies and structures. The key to this disparity is that the materials serve as the essential ingredients to progress in today's ever-expanding engineering achievements.

Composite materials have aided the aerospace industry in setting and reaching goals of greater speeds and higher altitudes that could not have been possible with purely monolithic materials. Metal matrix composites (MMCs) blend the best characteristics of handling high temperature conditions and maintaining excellent mechanical properties and have made it possible for these goals to be reached.

The various temperature and loading conditions that will be experienced by future aircraft make it necessary for a complete understanding of the material's behavior in a multitude of conditions. A manufacturer must have a complete assessment of the mechanical properties and failure modes at many different combinations of temperature and loading conditions.

Several studies have been done that investigate various fatigue conditions of MMCs. Johnson investigated the damage development in fatigue testing of continuous fiber reinforced MMCs (11). Gabb, Gayda, and MacKay studied isothermal and nonisothermal fatigue behavior of an MMC (7). Also, Mall and Portner (14) characterized the fatigue behavior of a cross-ply laminate of SCS-6/Ti-15-3 MMC at an elevated temperature.

Almost all of these studies were performed under tension-tension cycling conditions. However, components in real life structures will be subjected to some combination of tension and compression cycling. Therefore, a need exists for investigation of tension-compression fatigue behavior of MMCs.

Tension-compression fatigue behavior studies are extremely difficult to perform due to premature buckling of the thin specimens obtained from the available MMCs of eight or so plies. To perform the compressive fatigue testing on the material, it is necessary that a guide be developed to prevent the thin specimen from buckling yet would not impart any additional strength to the specimen. Boyum (6) designed the AFTT buckling guide which allowed such compressive stress fatigue studies to be performed. Boyum studied the fatigue behavior of an unnotched $[0/90]_{2S}$ MMC laminate under tension-compression loading at elevated and room temperatures. Her buckling guide design opened the door for further studies of tension-compression fatigue behavior under various conditions of temperature, lay-ups, and notched/unnotched specimens. Thus, this study is an extension of this area of fatigue conditions involving compression. Specifically, this study will investigate the fatigue behavior of a notched cross-ply MMC

at elevated temperature under tension-compression loading, which has not been performed to date. Further, this study is the extension of the previous study by Baker (4) who investigated the fatigue behavior of a notched (center hole) cross-ply MMC laminate under tension-tension cycling at elevated temperature.

The material investigated in this study is SCS-6/Ti-15-3, which contains silicon carbide fibers embedded in a titanium alloy matrix. The alloy making up the matrix is a combination of titanium (76% by weight), vanadium (15%), and aluminum, chromium, and tin (3% each). This material is a good model system to study the behavior of Titanium metal matrix composites, and has been used extensively in previous studies (4,6,17). The laminate used in this study had a cross-ply lay-up, $[0/90]_{2s}$.

Fatigue tests were performed at an elevated temperature of 427 °C (800 °F). This temperature is the common elevated temperature used by many previous investigators (4,6,17). Thus, it will be possible to make direct comparisons with these earlier studies by using this temperature.

This study used specimens with the most common form of stress concentration, a center hole. The center hole represents many conditions in aerospace applications such as rivet points, cutouts for cable routing, battle damage, and windows. This research will aid in establishing safe guidelines for operating limits for aircraft parts constructed with SCS-6/Ti-15-3. The specimens in this study with width of 19.05 mm (0.75 in) had a hole diameter of 3.175 mm (0.125 in) as was used by Baker's notched specimens in his similar study under tension-tension loading conditions (4:6).

Eight specimens were tested in this study. One specimen was subjected to a monotonic tensile test at 427 °C to characterize the baseline performance of this material. The remaining seven tests were fatigued under the load control method with a loading frequency of 10 Hertz (Hz) at different stress levels. The load ratio for all tests was $R = -1$ for the fully reversed tension-compression loading condition. The load-time relationship for the fatigue tests is shown in Figure 1.

Damage progression was monitored during the test by taking edge and face replicas. These provided a physical record of the damage for later examination. Also, information was obtained concerning damage progression by checking the changes in modulus and strain while the test was running.

Following testing, fractographic analysis of the fracture surfaces was performed to gain insight in the nature of failure. Examination of the face replicas provided information on crack development and growth. The applied stress (S) and fatigue life (N), S-N, curves for both crack initiation and fatigue lives were established under tension-compression cycling and compared with Baker's study involving tension-tension cycling, as well as crack growth curves as a function of fatigue cycles. An in-depth metallographic analysis was performed to understand the damage mechanisms of notched SCS-6/Ti-15-3. In summary, a comprehensive picture of the fatigue behavior of a notched cross-ply metal matrix composite when subjected to the fully reversed tension-compression cycling at elevated temperature was established.

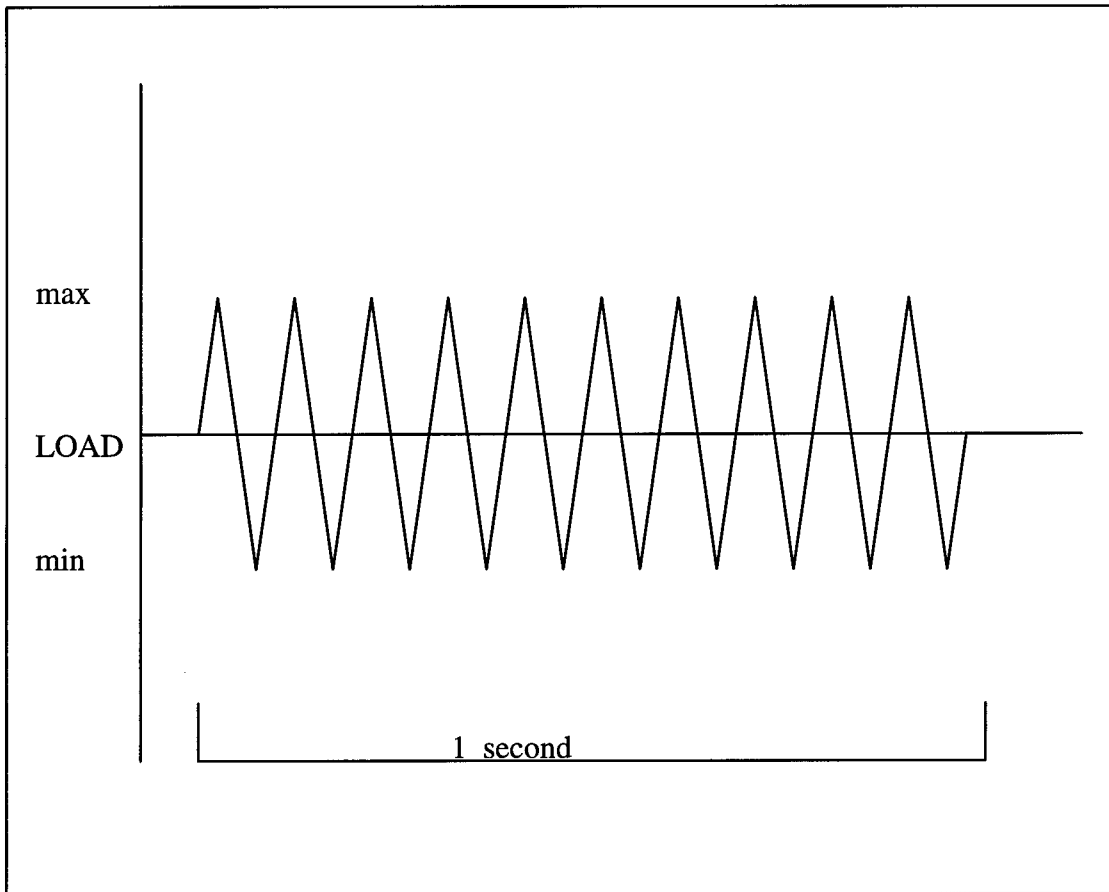


Figure 1. Tension-Compression Load-Time Relationship, $R = -1$

II. Previous Works

Introduction

The previous works which are pertinent to this study include studies of both notched and unnotched specimens in tension-tension and tension-compression fatigue, all at both room and elevated temperatures. All previous works discussed in this chapter were conducted using metal matrix composites (MMCs) with a variety of lay-ups. A brief background is presented in this chapter of these various studies which are related to the present work, and these studies are separated into room temperature testing and elevated temperature testing.

Room Temperature (RT) Testing

Hillberry and Johnson investigated the crack initiation of notched SCS-6/Ti-15-3 at room temperature (9:1-14). They used both center holes and double edge notch specimens, all with a laminate lay-up of $[0/90]_{2S}$ and a fiber volume fraction of 0.325. The fatigue tests were run under load control with a tension-tension (TT) loading condition and a 0.1 stress ratio at a frequency of 10 Hz. They also conducted strain controlled fatigue tests on the matrix material, and these tests were run with a strain ratio of 0.1 and a frequency of 10 Hz. Each specimen was observed using a telemicroscope, and edge and face replicas were taken to check damage throughout the fatigue tests. Crack initiation was defined to have occurred when at least one crack measured between 0.2 and 0.4 mm long.

In this particular study, Hillberry and Johnson adapted an effective strain parameter first developed by Smith, Watson, and Topper (20:767-768) to account for residual stresses during composite cool down (9:5-7) and local stress concentrations at the notch tip. The modulus of the fiber was much greater than the modulus of the matrix, therefore the assumption was made that the matrix was effectively under strain control. Thus, the strain is proportional to the stress, and as a result, the strain concentration factor is approximately the same as the stress concentration factor. The predictions closely agreed with the experimental results.

Newaz and Majumdar (16:1-22) investigated crack initiation in a unidirectional laminate of SCS-6/Ti-15-3 with a center hole. Their purpose was to characterize the crack initiation and crack growth from the center holes, as well as determine the crack initiation sites and whether the cracks were through-the-thickness cracks. The experiments were tension-tension fatigue tests under load control with a stress ratio of 0.1 and a frequency of 10 Hz. The fatigue tests were stopped prior to failure for sectioning and polishing so that metallographic examination could be performed.

They found that the fatigue loaded specimens developed four major cracks around the periphery of the hole. These cracks are through-the-thickness matrix cracks, and they bridge the fibers. Newaz and Majumdar used the Hencky-Von Mises distortion energy theory (8:373) to predict the point around the hole where yielding would begin. The major cracks formed between 65° and 72° from the loading axis, which was accurately predicted from the Hencky-Von Mises yield criterion. It is believed that the initiation is controlled by the local inelastic strain of the matrix (16:11).

They also performed several monotonic tensile tests using the same material and the same notch condition. These specimens developed cracks 90° from the loading axis. They determined that the monotonic specimens failed due to fiber failure while the fatigue tested specimens failed due to matrix failure.

Naik and Johnson (15:1-35) investigated the damage initiation in notched SCS-6/Ti-15-3 using the laminate lay-ups of $[0]_8$, $[0_2/\pm 45]_2$, $[0/\pm 45/90]_2$, and $[0/90]_{2s}$. Some specimens contained center holes while the others contained double edged notches. The fatigue tests were performed under load control tension-tension at a stress ratio of 0.1 and a frequency of 10 Hz. Two different types of loading were used on these tests. The first type was a constant amplitude load over the life of the entire specimen. The second type was an incremental approach. In this type of loading, the specimen is fatigued for 50,000 cycles at one load level and then 50,000 cycles at the next higher load level.

One of their conclusions was that debonding and matrix cracking served to reduce the effect of the stress concentration. They observed only matrix cracks and no fiber cracks. They also noticed that heat treated specimens and the as fabricated materials behaved in a similar manner.

Boyum (6) investigated the fatigue behavior of unnotched cross-ply SCS-6/Ti-15-3 under room temperature tension-compression (TC) and tension-tension (TT) loading. This was the first fully-reversed fatigue testing to be performed on an MMC. An important milestone was accomplished to achieve the tension-compression loading condition, and this was the development of the AFIT buckling guide (6:24-27). This was the first buckling guide of its type to be used in fatigue testing.

Boyum compared the results of the TC RT fatigue testing for the cross-ply lay-up with the TT RT results. It was found on a maximum applied stress basis as well as an effective strain range basis that the tension-compression specimens had shorter fatigue lives than the tension-tension specimens, and this was caused by the additional damage and plasticity sites which existed only in the tension-compression load case.

High Temperature (HT) Testing

Mall and Portner (14) investigated the fatigue behavior of unnotched cross-ply laminate SCS-6/Ti-15-3 at 427 °C. This study was performed to examine the damage initiation and progression in this material at the elevated temperature. The fatigue tests were all performed in load control under the tension-tension loading condition with a load ratio of 0.1 and a frequency of both 0.02 and 2 Hz. Damage was monitored throughout the test by acetate edge replication and quantified in terms of the initial modulus and the value of the modulus during the test. They found that the two different frequencies had different strains at failure which indicated two different modes of failure. For the high frequency test, brittle cleavage fracture of the matrix was the dominant influence on specimen failure. Cleavage fracture occurs when a crack follows a preferred crystallographic plane along the grains. At high frequency the material tended to strain harden. For low frequency tests, which were exposed to the high temperature for longer periods of time, the fibers failed prior to matrix failure. The matrix age hardened significantly.

Verilli and Gabb (23) studied the high temperature fatigue behavior of an unnotched tungsten/copper composite. The fatigue tests were under TC loading with a load ratio of $R = -1$. Performing the tests under strain control, the fatigue tests were run at 260 °C and 560 °C in a vacuum. Dogbone specimens with a shoulder radius of curvature of 368.3 mm and 63.5 mm were used for the fully-reversed and zero-tension tests, respectively. The larger radius of curvature for the fully-reversed tests was used to prevent the possibility of buckling and failure of the specimen at the shoulder. They found that tensile mean stresses are detrimental to the fatigue life of the material, while compressive mean stresses are beneficial to the fatigue life.

Along with the room temperature fatigue testing of TT and TC loaded specimens, Boyum (6) also studied the high temperature fatigue behavior of unnotched cross-ply SCS-6/Ti-15-3 under TC loading. These fully-reversed fatigue tests ($R = -1$) were run at a frequency of 10 Hz. Boyum found that on a stress range basis, the TC HT and TC RT had much longer lives than the TT RT specimens. This was due to the detrimental mean stress effects present in the TT RT case. The effective strain range was found to be a good parameter for comparing fatigue lives under different loading conditions.

Baker (4) studied the fatigue behavior of a notched (center hole) cross-ply laminate using the material SCS-6/Ti-15-3 at 427 °C under TT loading. The tests were run with a stress ratio of 0.1 and a frequency of 10 Hz. These fatigue tests by Baker used the same conditions and material as the focus of this study, however Baker's study was under TT loading and this study employs TC loading. Therefore, direct comparisons will be able to be made between the results of Baker's TT loaded, notched specimen fatigue

tests and this study's TC loaded, notched specimen fatigue tests (see chapter 5 for these comparisons).

Baker monitored crack initiation and progression around the periphery of the center hole through the use of front and back face replication (acetate replication is explained in detail in chapter 3). It was found that fatigue cracks initiated in the matrix at four locations on the front and back faces of each specimen. Two of the cracks became dominant through-the-thickness cracks and proceeded on to the edge of the specimen to induce fracture. The fracture surface was brittle cleavage in nature until the dominant or major cracks reached a fatigue critical crack length, at which time the fracture transitioned from brittle failure to ductile failure. The applied stress (S) and fatigue lives (N) S-N curves for both crack initiation and fatigue life were established.

It is clear that there is limited research in the area of fatigue testing on MMCs under tension-compression loading conditions. With the development of the AFIT buckling guide (6:24-27), it is now possible to begin tension-compression fatigue testing of various lay-ups under the differing conditions of temperature and notched/unnotched specimens. Thus, the current research in this study is a part of this new attempt to characterize the fatigue behavior of an MMC under tension-compression loading, in particular, that of a notched cross-ply laminate using SCS-6/Ti-15-3 at the elevated temperature of 427 °C.

III. Experimental Set-up and Procedures

This study investigated the fatigue behavior of a notched (center hole) cross-ply MMC laminate under a tension-compression loading condition at elevated temperature. Before explaining the results and presenting an analysis of this study, it is necessary to describe the material that was used and its preparation, as well as the test setup and procedure. This chapter will discuss in detail all aspects of the material, specimens, and test conditions and procedures.

Material

The material examined in this research is SCS-6/Ti-15-3 with a cross-ply laminate. This continuous fiber reinforced metal matrix composite (MMC) has an orientation of $[0/90]_{2s}$ and is capable of sustaining combined loading conditions.

Ti-15-3 is the reduced designation for Ti-15V-3Cr-3Al-3Sn which corresponds to the matrix alloy being composed of titanium (76% by weight) and vanadium (15%) as well as 3% each of aluminum, chromium, and tin. An EDAX (Electro-Dispersive Analytical X-Ray) was performed by Baker (4:17-18) that successfully confirmed this composition breakdown.

Material Preparation

The material used in this investigation was fabricated by Textron Specialty Materials Inc. They employed the Hot Isostatic Press (HIP) process when making

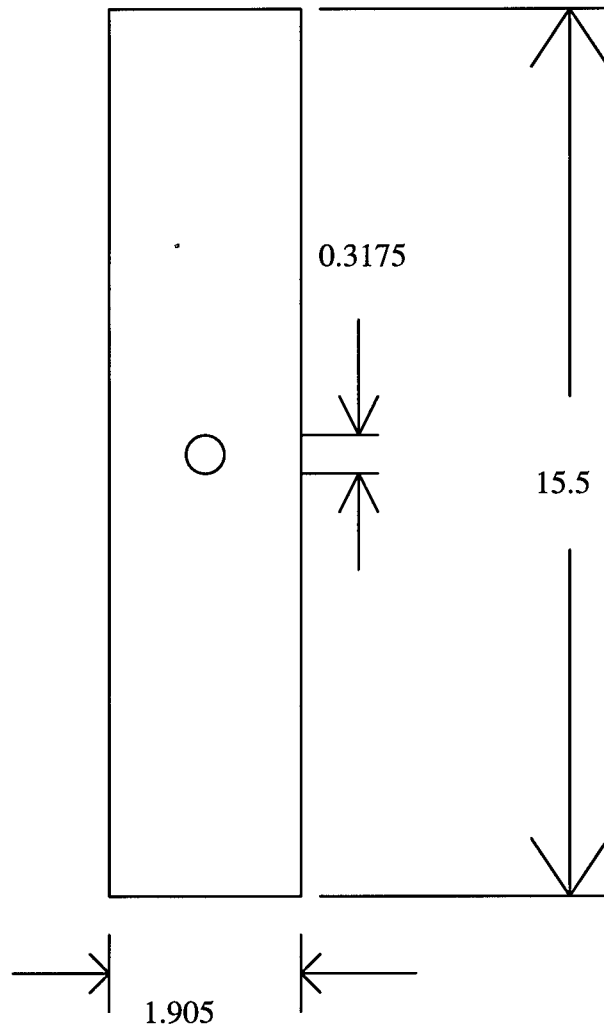
the .3048 m x .3048 m (12 in x 12 in) composite panel. HIPing is performed by alternating layers of the fiber and matrix and subsequently placing them in a high temperature pressure vessel. This vessel reaches temperatures in excess of 1000 °C and pressures of 35 MPa. The resulting lay-up forms a better consolidation of fibers and matrix than cold isostatic pressing, vacuum hot processing, pultrusion, or compression molding.

Specimen Preparation

The AFIT Model Fabrication Shop cut eight specimens from the panel with diamond encrusted blades which was required to cut through the extremely hard silicon carbide fibers. Each specimen was 15.5 cm long (6.1 in), 19.05 mm wide (0.75 in), and 1.77 mm thick (0.044 in).

Following the cutting process, the specimens were taken to the Aeronautical Systems Division (ASD) machine shop so as to drill a 3.175 mm (0.125 in) diameter hole in the direct center of each specimen. The holes were cut out by wire drilling, and to facilitate a smoother surface several finish passes were made with the wire. Figure 2 shows the dimension of the specimens used in this study.

After the drilling, the specimens were taken to the Wright Laboratory/Materials Division (WL/MD) Metals Laboratory to be heat treated. Technicians wrapped the specimens in Tantalum foil to protect from oxidation and to serve as a gettering surface for impurities ejected from the specimens during the heat treatment.



ALL DIMENSIONS IN CM

Thickness = 0.177 cm

Figure 2. Specimen Dimensions

The specimens were then placed in a vacuum oven with conditions of 700 °C and 1×10^{-6} Torr for 24 hours. Heat treating is performed to stabilize the beta phase of the material.

The next step was to polish the specimen edges at the WL/MD Metals Laboratory. Polishing is necessary to remove any existing flaws on the edges of the material that could possibly serve as stress concentrations. Also, one of the edges was finely polished to aid in edge replication.

Three specimens at a time were placed in a polishing fixture that allowed for polishing on the Buehler Maximet automatic polisher. The first stage of polishing was grinding, which was necessary to remove any major surface defects and flatten the edges. A number eight Metlap platen and 45 μm diamond slurry were used for grinding, followed by a 15 μm slurry to further reduce the size of the scratches. After each slurry was used, the fixture would be removed from the automatic polisher, and the edges would be examined using an optical microscope to determine how well the polishing was proceeding. This first grinding process was all that was required for the non-replica edge of the specimen. Any further polishing of this edge made it extremely likely for the extensometer to slip on that edge, as will be discussed later.

The second stage of polishing was to use 15 and 6 μm slurries on respective Perfmats, and this was only performed on one edge of the each of the specimens. Examination revealed that there were still scratches that existed along these edges. The third stage was to use Nylon mats with 3 and 1 μm slurries. It is important to be careful at this stage as the sharp edges of the specimen had a tendency to rip the mat. The final

stage of polishing resulted in the mirror finish and smoothed out the fine scratches in the matrix. A neoprene Chem-met mat was used with a chemical solution of Mastermet and distilled water. It was important to immediately rinse and steam clean the specimen after this step. If the Mastermet was allowed to dry, it would stain the specimen, and this can only be corrected by repolishing with Mastermet.

After polishing of the edges was completed, aluminum tabs were cut out. Epoxy was used to hold the tabs in place and the specimens were then cured for one hour at 67.2 °C (153 °F) in the Aero Lab oven.

The final process in preparing the material was to use a 400 grit Silicon Carbide sandpaper piece to smooth out any surface scratches near the hole. A small square was cut out a sheet of the proper grit sized sandpaper which was then wetted with water and rubbed along the face over the region around the hole. This had the effect of smoothing out any visible surface scratches near the hole and aided in obtaining better face replicas.

Test Apparatus

All tests were performed on a servo-hydraulic test stand (Material Test System 808) equipped with a 9979 kg (22 kip) load cell. Two parabolic lamps were attached to the test stand to provide the heating needed to reach the desired elevated temperatures. Cooled water was circulated through the upper and lower grips to protect the load transducer from the high temperature.

Strain measurements were obtained from an MTS model 632.50-b-04 1.27 cm (0.5 in) gage length extensometer which was cooled by chilled air. The extensometer

rods were replaced after every one or two tests due to breakage of the rod or dulling of the tip. Each time that a new set of rods were inserted, they were carefully calibrated to span over positive and negative strain values to ensure accuracy of the strain measurements during the tension-compression loading conditions.

The temperature was maintained at $427\text{ }^{\circ}\text{C} \pm 3\text{ }^{\circ}\text{C}$ over a 3.81 cm (1.5 in) gage length by a Micricon 825 microprocessor. This microprocessor provided feedback signal processing and output control of the heat lamps. Two type k chromel-alumel thermocouples were tack welded to the buckling guide to provide temperature information to the Micricon 825. To provide an even temperature distribution, the thermocouples were placed 19.05 cm (0.75 in) apart. A third thermocouple was placed .254 cm (0.1 in) away from the hole along the center line of the specimen. This thermocouple was employed to monitor temperature distribution. Figure 3 shows the test apparatus.

The fatigue test profile was acquired from a Zenith 248 computer through a program called LOADTEST, developed by Sanders (19). The profile for the test included the maximum stress to be reached during the test, the stress ratio, R , the maximum range of the load and strain, specimen area, load frequency, and maximum desired temperature. These specifications were sent to the microprofiler which drives the load transducer.

LOADTEST contains a data acquisition system for collecting key data throughout the test. The user would provide when the Data Acquisition Cycles (DACs) were to occur. The data would then be saved in a user specified directory under the name of the

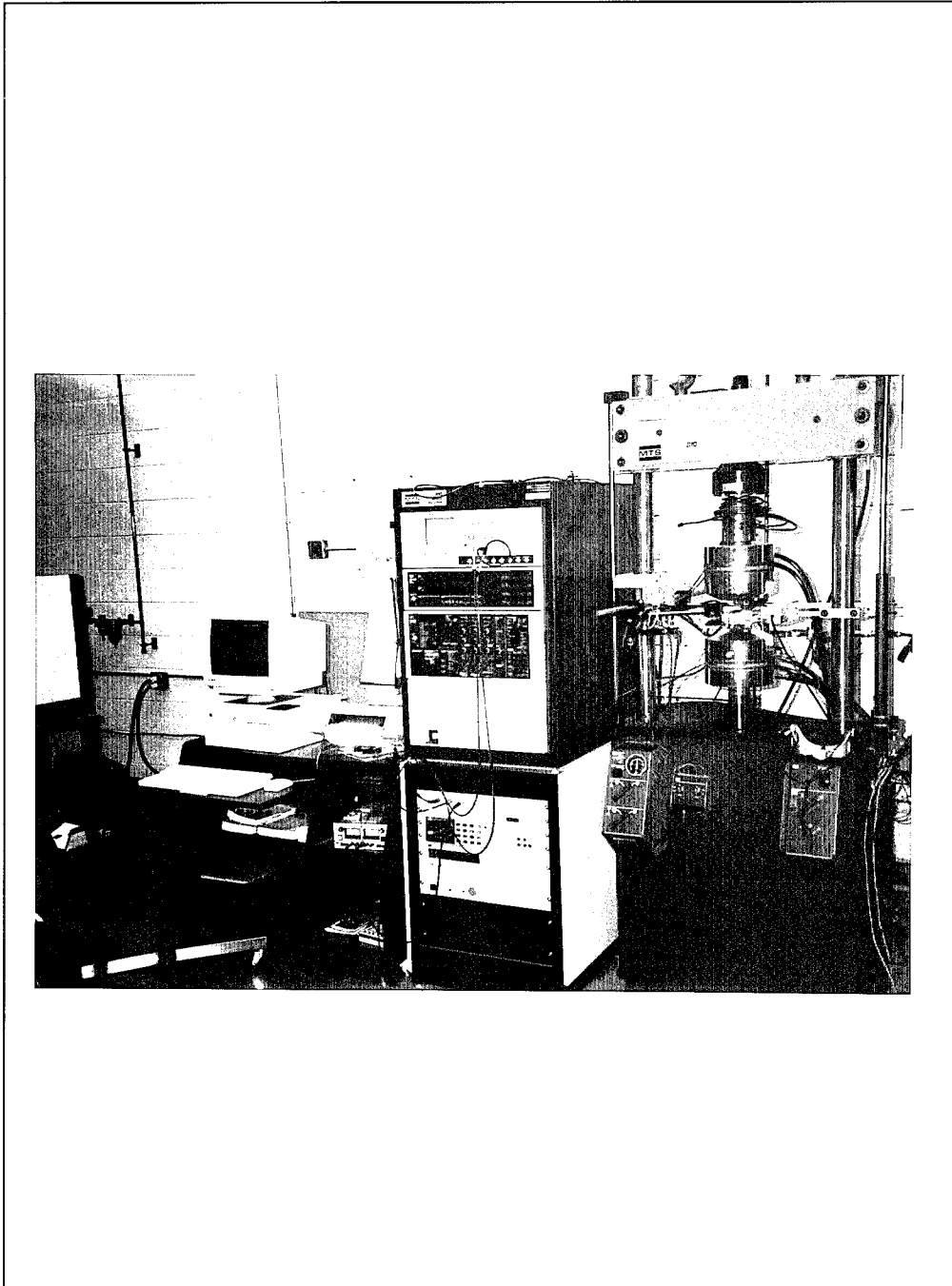


Figure 3. Test Apparatus

cycle number followed by “.dat”. As an illustration, 1.dat would contain the cycle number, the temperature during cycle 1, the secant modulus value for this cycle, and 512 pairs of stress and strain data taken during this cycle. Also, a file entitled “minmax.dat” was produced, which contained the cycle number, maximum and minimum stress values, maximum and minimum strain values, temperature and the material stiffness during the cycle.

Buckling Guide

This research effort continued with the use of the AFIT buckling guide, the only buckling guide designed to date specifically for use in tension-compression fatigue loading conditions (6). The Lockheed (1:24) and Battelle (13) buckling guides were designed strictly for static compression tests only, and these were shown in previous research efforts to be ineffective in fatigue loading.

The AFIT buckling guide, designed by Capt Beth Boyum (6: 24- 27), provided the general framework for the buckling guide that was used in this study. The overall dimensions of the buckling guide used in this research effort were altered to accommodate the larger size specimen and the flat edges rather than a dogbone specimen used with the original AFIT buckling guide design. See figure 4 for these dimensions.

This buckling guide allows for sliding between two portions of the guide. The sliding mechanism, allowing the guide to expand and contract with the specimen, decreases problems with friction experienced by static buckling guides. The two top pieces of the guide have a fork in the lower portion where they join with the sliding

mechanism. A countersunk, flathead bolt protrudes from the sliding mechanism and when capped with a steel locknut and washer, permits only axial sliding of the guide forks. This sliding mechanism locknut and washer restrict any out of plane movement

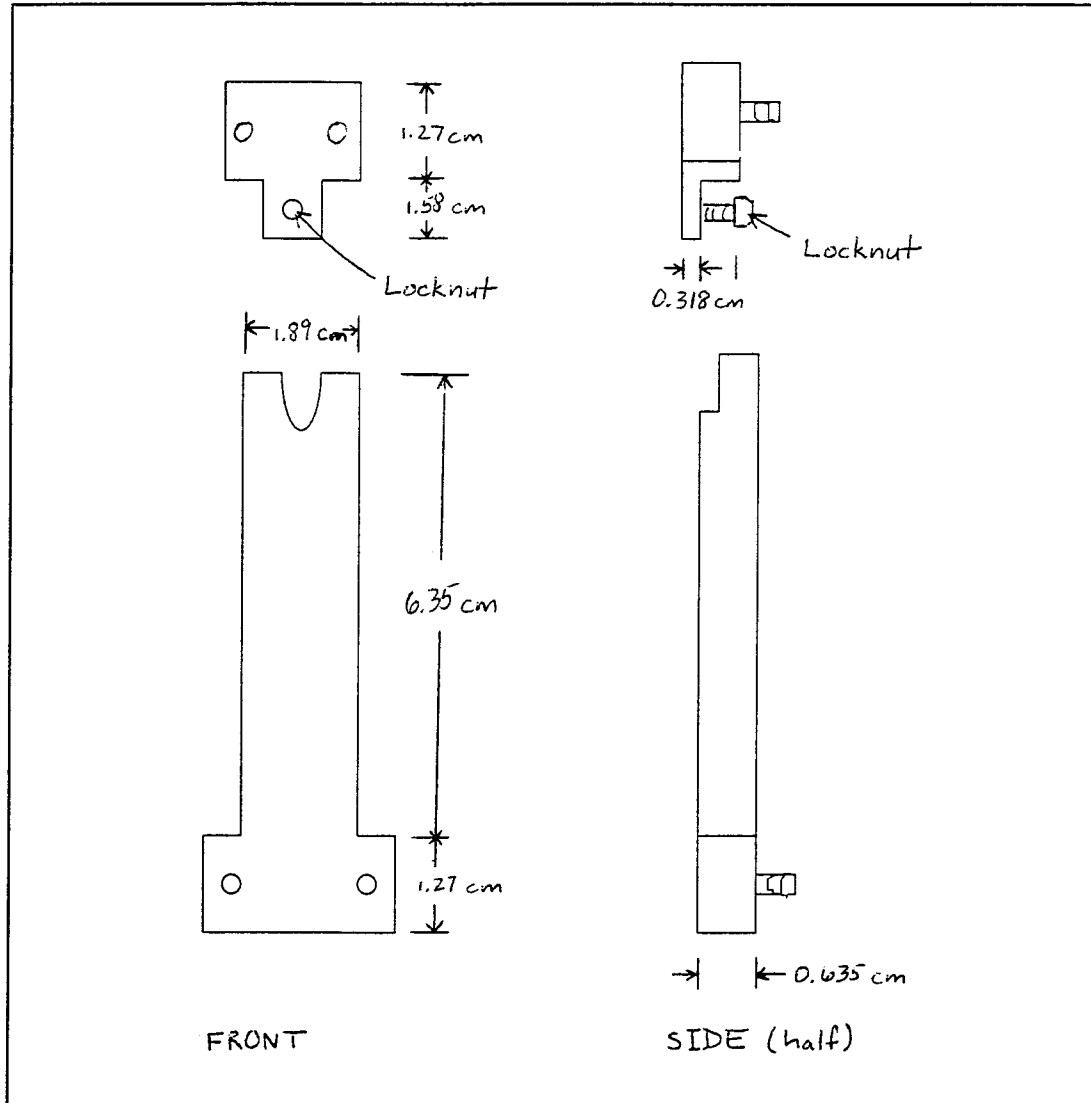


Figure 4. AFIT Buckling Guide Design

and therefore restrict any excessive buckling. After the specimen fails, the guide forks easily separate from the sliding mechanism, preventing the guide from becoming damaged.

The inside portion of the buckling guide that comes into contact with the specimen was skimmed off by an amount of 0.01 mm. This effectively allowed the specimen to buckle in an out of plane direction by this amount as the specimen was loaded in the compressive portion of the loading. Once the specimen traveled this small amount, it then came into contact with the guide, and forced the guide to resist any further out of plane motion and therefore stop any buckling.

The sliding mechanism bolts onto the lower portion of the specimen such that a minimum length of the specimen is left between the mechanism and the lower grips. This part of the buckling guide does not rest on the grips because this would provide an undesired heat sink.

Thermocouple wires were tack welded on the exterior of the AFIT buckling guide. The location of these wires was mentioned previously in the Test Apparatus section of this chapter.

Acetate Replication

One way of monitoring the damage that is accumulating throughout the specimen while being tested is through the use of replication. This method has been used in the past and is a reliable process that allows the tester to observe the initiation and progression of cracks on the edges and faces of the specimen.

The process of replication begins by placing the test on hold and allowing the temperature to reach ambient room temperature levels. The load is then increased to 50% of the maximum tensile load condition for that test. This is done in order to open up the cracks which will have closed on themselves when the load was returned to zero after placing the test on hold.

Next, a piece of acetylcellulose is cut out and taped to the portion of the specimen that is to be replicated. Acetone is sprayed from a jar onto the surface of the specimen, and the acetate is pressed to this surface for 30 seconds. For obtaining front and back face replicas, the buckling guide had to be removed from the specimen before this step. The acetate melts into the cracks and crevices of the specimen, imprinting an image of the surface which can be taken to an optical microscope for examination. To smooth out the replicas, they were sandwiched between two pieces of glass, which were subsequently clamped together and placed in the Aero Lab oven for approximately five minutes.

The Scanning Electron Microscope (SEM) offered the means to examine the face replicas. The particle measurement system of the SEM allowed these replicas to be studied for measurement and recording of the length of the cracks.

Test Procedures

An initial replication of the edge and both faces was performed on the specimen prior to the test to serve as a visual record of the undamaged material. Once this was completed, both pieces of the buckling guide were placed over the specimen and screwed

buckling guide was properly attached and was not allowing any buckling to occur.

Boyum (6:35) discovered that buckling showed a cusp in the compression portion of the load on the stress-strain graph. Figure 5 shows the cusp resulting from buckling. Notice that once buckling cusp was observed, this test was halted and the setup checked.

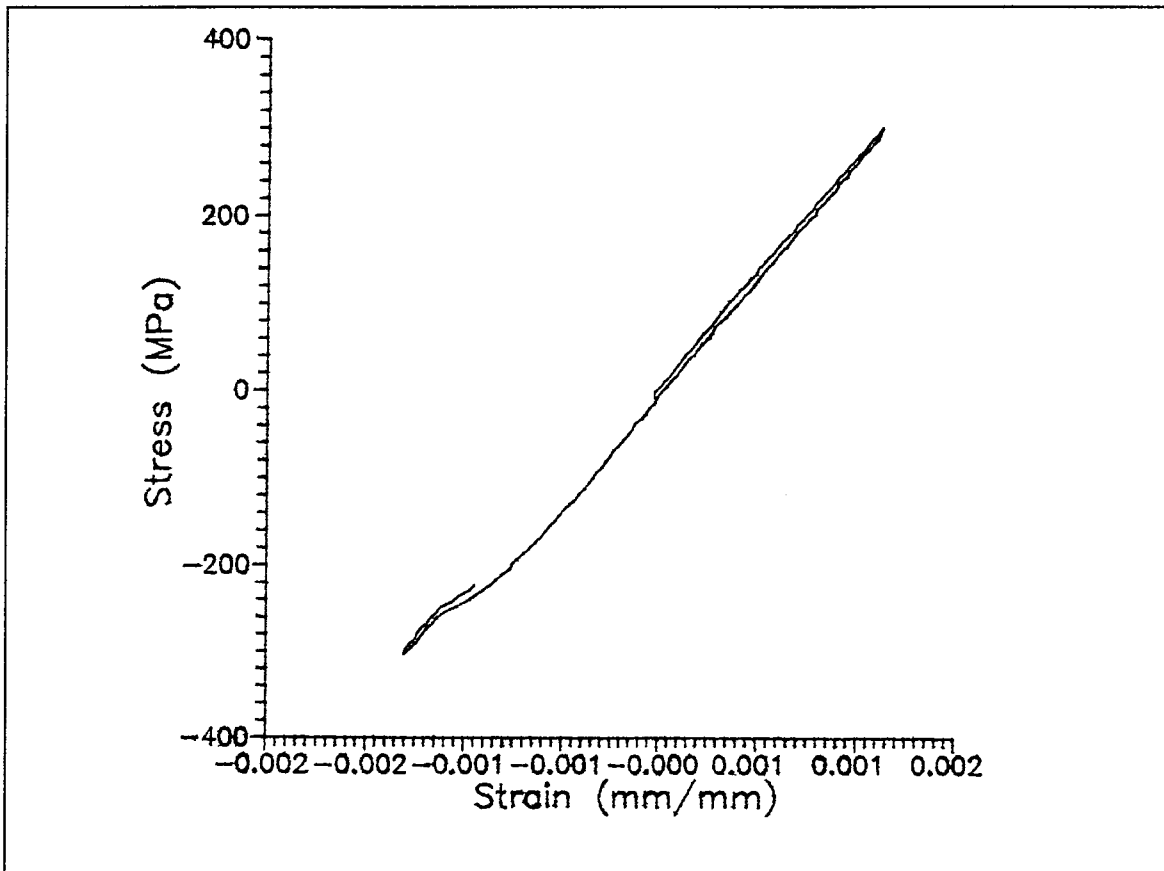


Figure 5. Effect of Buckling on Hysteresis

After this was completed, the load controlled fatigue was begun at a frequency of 10 Hz with a load ratio of $R = -1$. Once every logarithmic decade (i.e. 1, 10, 100, 1000, etc. cycles), the test was stopped and replicas were taken. If it was clear that cracks along the front or back face were soon to develop, then replication was performed more

often. However, the time turnaround for replication and the restart of the test was approximately three to four hours. The temperature had to be returned to ambient levels for the replicas to be taken. The edge replica was taken first with the buckling guide in place around the specimen. Following this, the buckling guide was removed gently, and front and back face replicas were taken. All replicas were checked on the optical microscope to ensure good images were obtained.

After replication, the buckling guide was carefully placed back over the specimen. It was not uncommon for the thermocouple wires to come off while doing this step. When this occurred, they were simply reattached once the buckling guide was securely in place and aligned properly. The temperature was returned to 427 °C and the strain was allowed to reach the hot strain value recorded prior to cooling down.

Eight tests were run, with one of these being an elevated temperature static test and one fatigue test not being allowed to reach failure. All of these had one extensometer rod on each side of the hole, which is commonly known as “enclosing the hole”. Table 1 shows the tests that were run and the associated stress levels.

Table 1 : Test Matrix

Test	Type	Maximum Stress (MPa)	Stress Range (MPa)
1	Monotonic	----	----
2	T-C Fatigue	300	600
3	T-C Fatigue	225	450
4	T-C Fatigue	278	556
5	T-C Fatigue	170	340
6	T-C Fatigue	375	750
7	T-C Fatigue	150	300
8	T-C Fatigue	270	540

Note: T-C = Tension-Compression

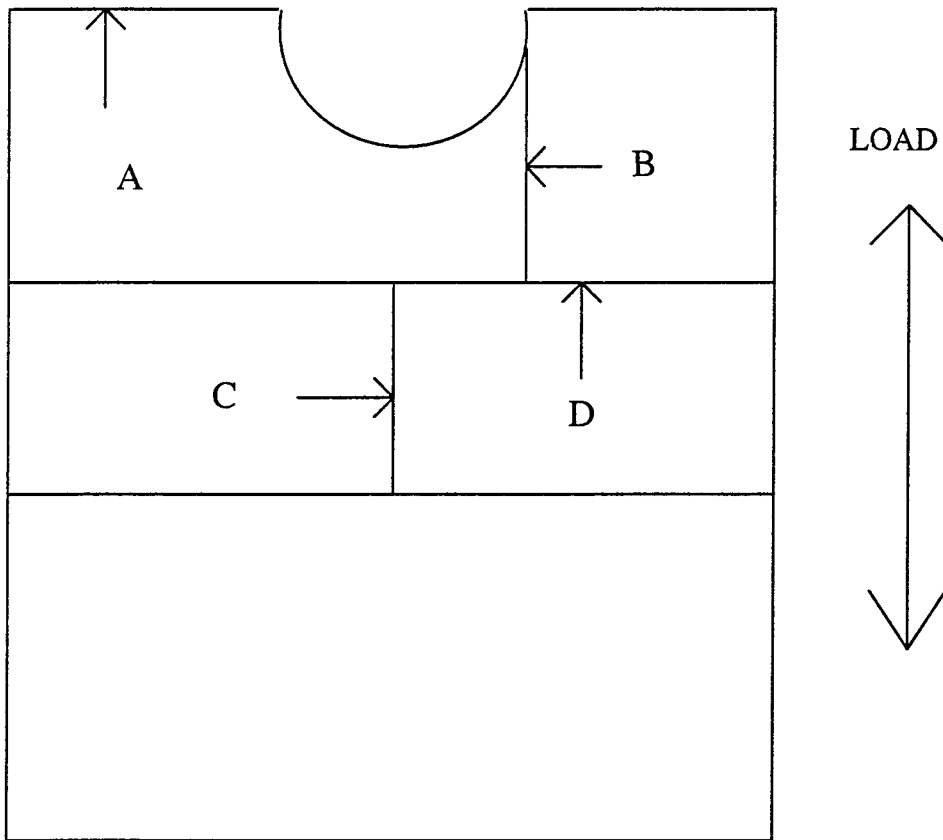
Post-Failure Analysis

After a specimen failed, the fracture surfaces were examined visually for color, fiber pullout, and the general appearance of the surface, which was all recorded. This initial inspection was followed by a sectioning of the specimen as seen in Figure 6. The fracture surfaces were then sputter coated with gold and then examined in the SEM to characterize the failure. Details of importance were the type of failure, such as brittle or ductile, transition zones, and cracking within the hole.

The remaining non-fracture surface sections were mounted in Buehler Konductimet, a conductive mounting compound, using a Simplimet mounting press. The specimen was first cleaned in an ultrasonic cleaner, mounted, and then polishing of the mount began. The sectioning is shown in Figure 6.

The first step in the polishing was to use the Maximet automatic polisher with a number eight platen using a 45 μm diamond slurry, followed by 15, 9, and finally 3 μm diamond. The mounted section was then placed on a Buehler Vibromet vibrating polisher with a 1 μm diamond slurry for 24 hours. This eliminated all scratches larger than one micron. The mount is then transferred to a Vibromet with 0.5 μm diamond slurry for 12 hours. Finally, the mount is transferred to Mastermet, the aggressive chemical polish which removes all scratches larger than 0.06 micron, for 45 minutes. After this polishing, the mounted section is then ready for examination under an optical microscope. This examination is intended to observe cracks within the matrix and/or fibers, debonding around the fibers, and matrix plasticity.

The last specimen was sectioned and mounted such that the hole and all of the cracks could be observed. The mounting procedure was the same as before. The specimen was hand ground on abrasive disks, and once the fibers became exposed the specimen was placed on a stainless steel mesh Vibromet with one micron diamond slurry for 24 hours. The specimen was then transferred to the half micron Vibromet for 48 hours followed by 45 minutes on the 0.06 micron Mastermet.



A = Fractured Surface

B = Transverse Face Near Hole (inside the specimen)

C = Transverse Face Away from Hole (inside the specimen)

D = Longitudinal Surface (inside the specimen)

Figure 6. Sectioning Plan of a Specimen

IV. Results

Introduction

As mentioned previously, the objective of this investigation was to study the fatigue behavior of a notched cross-ply SCS-6/Ti-15-3 at elevated temperature under tension-compression loading. For this purpose, fatigue tests were performed at 427 °C (800 °F) with a load ratio of $R = -1$ and a frequency of 10 Hz.

The fatigue damage mechanisms (both crack initiation and progression) were also investigated. To this end, damage was monitored in two fashions. First, while the fatigue tests were running, strain and stiffness changes were recorded and correlated to observed damage. Second, acetate edge and replicas of the face of the specimens were taken at various cycles during the life of the specimen. The face replicas were examined for crack initiation which was defined to be the point at which a crack exceeded 0.124 mm (0.0049 in) in length. This value was used in Baker's tension-tension study (4:35) and will also be used in this study so a direct comparison may be made between these cases as discussed in the next chapter. Crack lengths were measured at each replication interval by the Scanning Electron Microscope (SEM).

Failure was characterized by fractographic and metallographic examination. Fractured surfaces of the tested specimens were observed under the SEM for brittle/ductile transition, fiber pull-out, and surface coloration. Several specimens were also sectioned to look for signs of debonding and cracking, which may be present inside the specimens.

All stresses discussed in this section are based on the reduced area of the specimen. This means that the width of the specimen was considered to be the overall width (0.75 in) minus the diameter of the hole (0.125 in). This reduced width times the thickness of the specimen gave the reduced area.

Fatigue test specimen cracks formed at four points around the periphery of the hole. As they initially form, they are referred to as minor cracks. Two of these four cracks became dominant and continued to grow towards the edge of the specimen. These two cracks will be referred to as major or dominant cracks. The two cracks which do not grow as rapidly will be referred to as minor or secondary cracks.

In summary, this chapter will present all the results found in this study of the fatigue behavior of a notched (center hole) cross-ply laminate of SCS-6/Ti-15-3 under tension-compression loading at the elevated temperature of 427 °C (800 °F) at a frequency of 10 Hz and a load ratio of $R = -1$. All comparisons with Baker's tension-tension fatigue study (4) of the same material will be presented in the next chapter.

Monotonic Tensile Test

A monotonic tensile test at elevated temperature (427 °C) was performed on this batch of $[0/90]_{2S}$ material to establish the baseline performance. This was done with the extensometer enclosing the hole and using the stress based on the reduced area, which was the same condition that would be used on all subsequent fatigue tests. Figure 7 shows the stress-strain curve for the monotonic tensile test. It contained two linear portions, with the first "knee" in the stress-strain graph at approximately 140 MPa and the

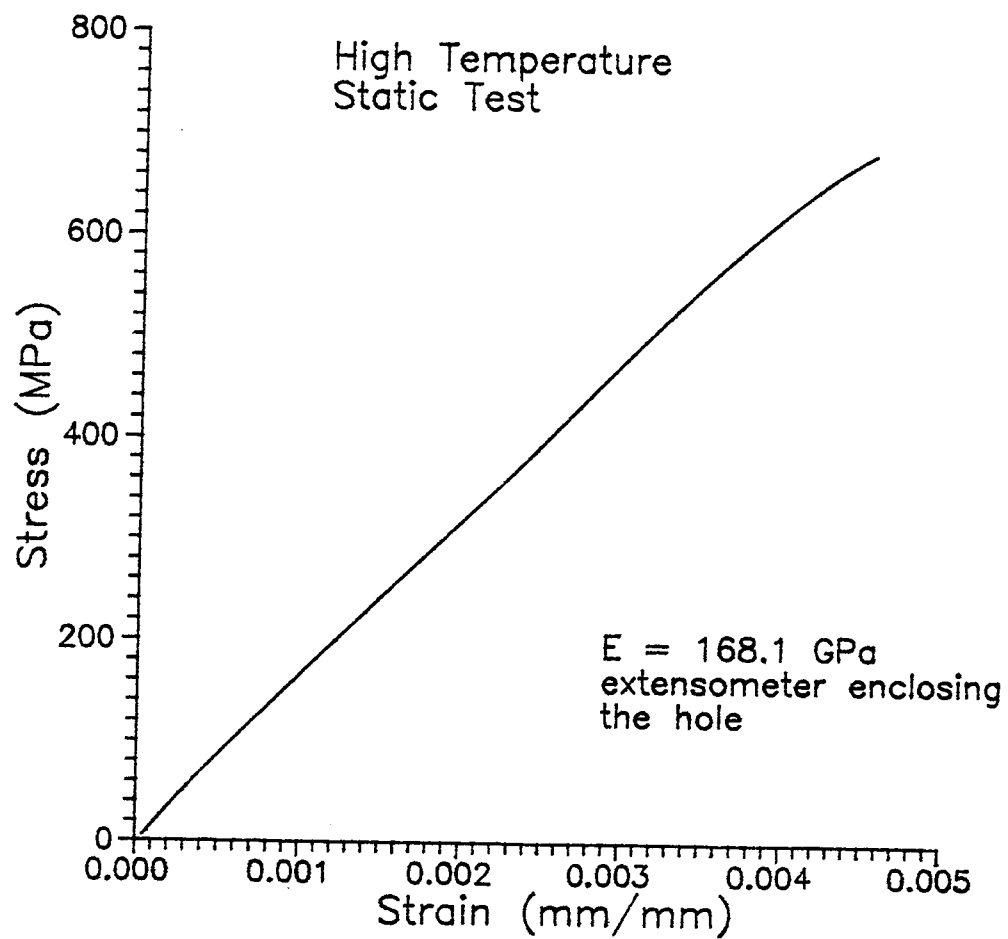


Figure 7. Monotonic Tensile Test Stress-Strain Curve

second at 440 MPa. This knee is a result of the debonding of the 90° fibers from the matrix. After this debonding, the stiffness decreases as a result of the reduction in the contribution of the cross-ply layers within the composite. The second knee in the graph is a result of the onset of nonlinearity of the matrix (6:41).

Baker performed a tensile test with the extensometer measuring the “far field” strain, which means the extensometer was placed over three hole diameters away from the center hole, and this had the effect of characterizing the material in an unnotched condition (4:44). That study found the first bilinear response occurred at 180 MPa. Boyum also recorded this value for the first knee on an unnotched cross-ply laminate lay-up of the same material (4:51), as well as revealing the second knee to occur at a stress level of 542 MPa. It is expected that the stress levels to reach the two knees in the stress-strain curve in a notched specimen would occur at lower values of stress than an unnotched specimen. The effect of the center hole places a sufficient stress concentration on the material to lower the values of stress to reach the bilinear responses in the stress-strain curve.

The ultimate strength of the monotonic tensile test specimen in this study was 670 MPa. The modulus of the material at elevated temperature was 168.1 GPa.

Macromechanic Considerations

The macromechanic behavior of a notched composite includes the fatigue life, stress-strain response during cycling, stiffness degradation, and the strain response during cycling. The fatigue life can be illustrated using the fatigue life diagram, i.e. the S-N

curve, with S being the stress level of the fatigue test and N the number of cycles to failure. For notched specimens an S-N diagram for crack initiation can also be produced using N as the value for the number of cycles to initiation of a crack within the tested material. The exact shape of the S-N failure curve varies depending on the matrix material, ply orientation, volume fraction of fibers, interface properties, type of loading, mean stress, frequency, and environment.

Several researchers have attempted to divide the S-N Curve into different sections that denote the type of failure mechanism acting as the dominant role. Majumdar and Lerch, following Talreja's approach (21), suggested that the S-N curve of a unidirectional MMC be broken up into three regimes: Regime 1, 2, and 3 (12:7). Regime 1 failure occurs strictly by overload of the fibers, Regime 2 describes failure primarily through matrix cracking, and Regime 3 consists of fatigue lives higher than 1 million cycles in which matrix cracks do not initiate or, if they do form, are quickly arrested. The transition between Regimes 1 and 2, as well between Regimes 2 and 3, consisted of mixed failure modes.

Boyum (6:39-42) further refined the regimes for a cross-ply laminate. Due to the presence of 90° fibers within the material, matrix cracks initiate much earlier in the cross-ply laminate as compared with the unidirectional laminate lay-up. For this reason, a major portion of the cross-ply S-N curve is occupied by the mixed mode transition between Regimes 1 and 2. This mixed mode region was called Regime 2a and characterizes the failure of cross-ply MMCs where the primary means of failure is a combination of both matrix cracking and fiber failure.

In the current work, an additional change will be made that takes into account the adding of a notch (center hole) for the cross-ply laminate lay-up of an MMC. The addition of a notch concentrates stresses and strains in its vicinity. The degree of this concentration is of a sufficient level that no specimen fails solely by overload of the fibers, i.e. there is always matrix cracking, regardless of the stress level of the fatigue test for the notched cross-ply laminate. Therefore, for this particular condition no Regime 1 failure occurs, and this region is removed from the S-N diagram. Talreja's concept of the regimes of the S-N diagram, as adapted by Majumdar and Lerch and amended by Boyum, as well as the concept used in this study for the notched cross-ply laminate MMC, are shown in Figures 8 and 9.

This type of fatigue diagram is generally used when a significant amount of experimental research has been accomplished so the exact locations of the transitions from one regime to the other are known. This amount of research was not possible in this study, therefore a method of demarcation is used which merely separates the tests which were performed into their respective regimes. It is important to note that these lines are not quantitative, but rather qualitative in nature, and they do not denote any specific value of the fatigue life. Figures 10 and 11 show this method for both the unnotched cross-ply laminate lay-up of an MMC as well as this study's notched cross-ply laminate.

In addition to the fatigue life approach, the macroscopic evaluation of a fatigued specimen can also be based on an examination of the stress-strain hysteresis curves throughout the fatigue life of the specimens. By using the tension-compression loading condition for the fatigue tests, it is useful to divide the stress-strain curves into the tensile

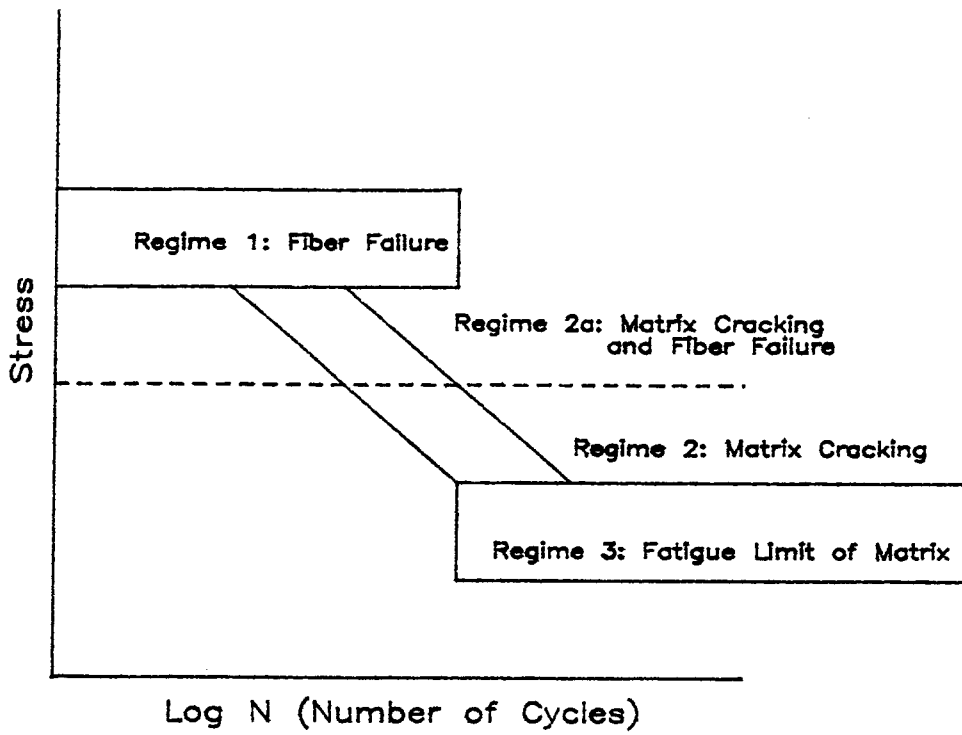


Figure 8. Talreja's Model for Regimes of Cross-Ply Laminate S-N Curve

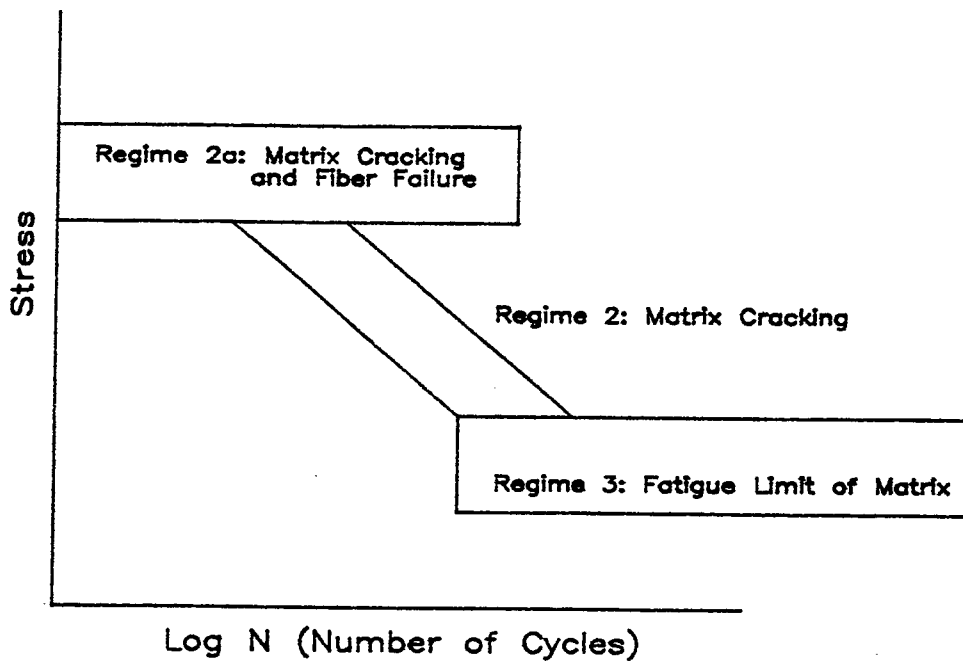


Figure 9. Model of Regimes for Notched Cross-Ply Laminate S-N Curve

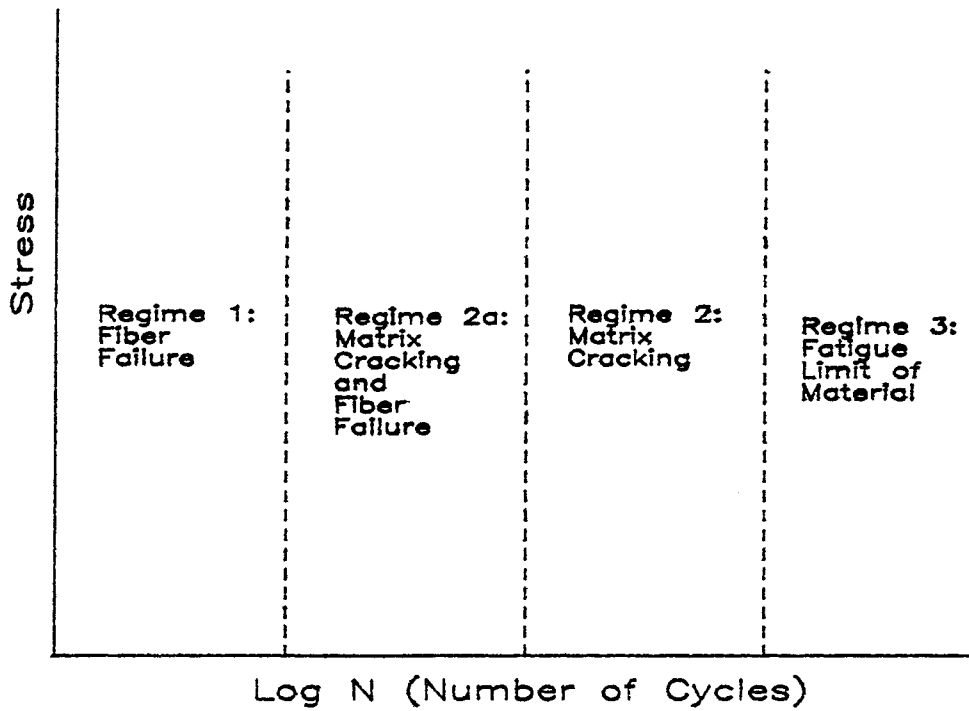


Figure 10. Regimes of S-N Curve for Unnotched Cross-Ply Laminate

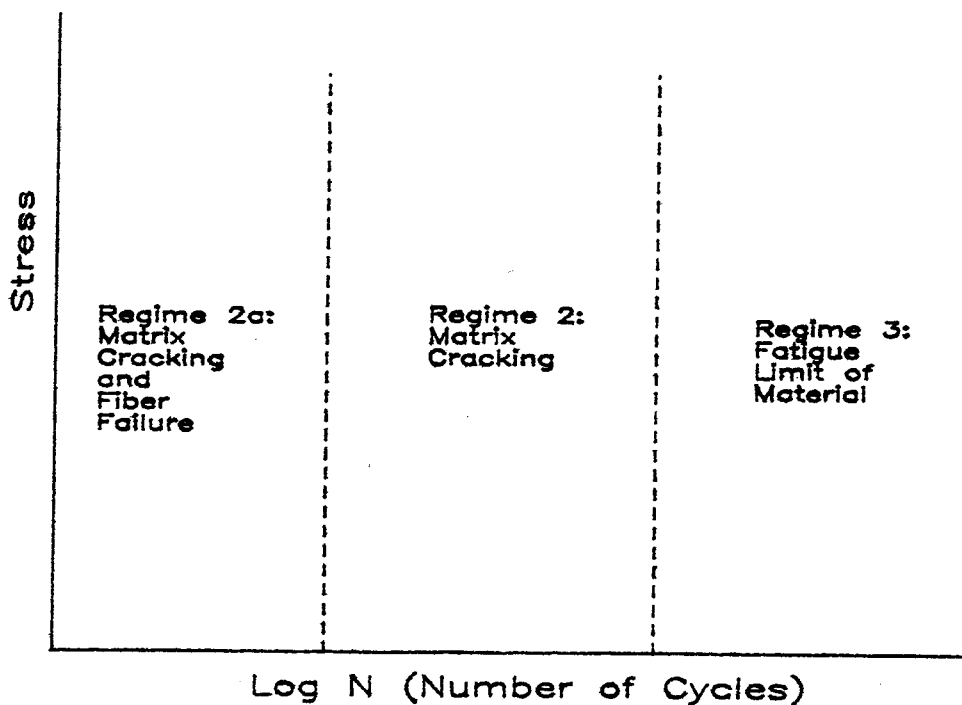


Figure 11. Regimes of S-N Curve for Notched Cross-Ply Laminate

portion of the loading, during which any cracks have opened, and during the compressive portion, in which the cracks have closed upon themselves. As the cracks open, damage should initiate or progress, and therefore the slope of the stress strain curve will fall. However, the compressive portion allows the cracks to close, and this would be indicated by a generally steady slope throughout the fatigue life of the material.

The stiffness, or modulus, degradation is another key method to observing the macromechanic behavior of a fatigue tested material. The stiffness of a material is the ratio of the applied stress to the resulting elastic strain:

$$E = \frac{\sigma}{\epsilon_{elastic}} \quad (1)$$

For the load-controlled fatigue tests used in this study, the stress remains a constant value, and the stiffness will change only with a change in strain. As stress is applied to the material during the fatigue cycling, there is deformation within the material which causes changes in strain. A drop in the stiffness indicates that damage has initiated or is progressing within the material.

Fatigue Life

The number of cycles to initiation and to failure at each stress level are presented in Table 2. These are the values used to establish the fatigue life diagrams in terms of the S-N curves shown in figures 12 through 14. These curves show the typical fatigue life of the tested material at 427 °C.

Table 2 has the data for the tests in the order of ascending stress level. The specimen ID shows when the test actually occurred in relation to the others. The first test was the monotonic tensile test performed on the material and is not listed in this table.

To observe when a crack initiated along the periphery of the hole was a difficult and time-consuming task. The test had to be placed on hold and allowed to cool down to an ambient room temperature level. The buckling guide was removed from the specimen, and front and back face replicas were obtained. These replicas were then gold-coated and placed in the SEM to see if any cracks had initiated. For more detail of how this was accomplished, see the acetate replication and test procedures sections of the previous chapter.

If a crack was not found, then the test was resumed and replication would be taken soon after the test was restarted, until the point at which a crack was discovered. Once a crack was found, the cycle at which it was discovered was annotated and is called the observed cycle to crack initiation. This does not really mean that this is the exact cycle at which the crack initiated. Rather, the crack initiated sometime between the cycle at which a crack was discovered and the previous cycle of replication, in which a crack was not found. Somewhere within this range is when the actual crack initiated. Table 2 shows the last replication cycle at which no crack was found (under the heading “Cycles Prior to Observed Crack Initiation”), and it also presents the cycle at which the first visible crack was observed. Tests 2 and 3 (300 MPa, 225 MPa) had no face replicas taken.

Table 2. Test Results

Specimen ID	Stress Level (MPa)	Stress Range (MPa)	Cycles Prior to Observed Crack Initiation	Observed Cycles to Crack Initiation	Cycles to Failure
7	150	300	10,000	100,000	2,451,504
5	170	340	0	11,000	958,615
3	225	450	---	---	225,785
4	278	556	0	1,000	72,033
2	300	600	---	---	18,925
6	375	750	0	1,000	6,716

Figure 12 shows the stress range plotted against the number of cycles to failure for each associated stress level. This shows the number of cycles which may be expected to cause failure at a given stress level for this material with a center hole at the elevated temperature of 427 °C when subjected to tension-compression fatigue.

Figure 13 gives the number of cycles to crack initiation for each stress range. The actual initiation for each test occurred somewhere between the initiation cycle shown and the previous cycle of replication in which no crack was detected, seen in Table 2. The point of initiation is the cycle of replication in which either the front or back face of the specimen revealed a crack. Figure 14 shows the crack initiation cycle curves and failure curves on the same diagram.

Stress-Strain Curves

The stress-strain hysteresis loops for the tension-compression fatigue tests in this study showed a unique response over the life of the tested specimen. During the initial cycles of a typical test, the hysteresis was minimal and the curve was approximately

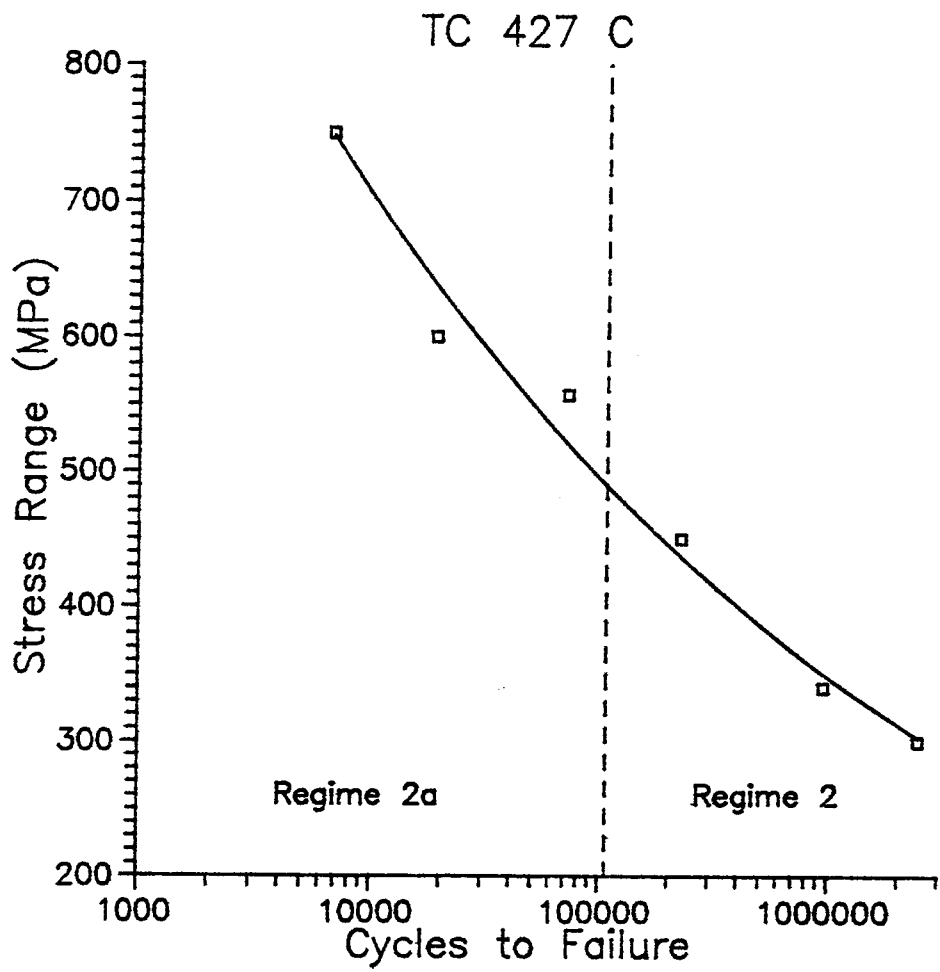


Figure 12. Failure S-N Curve

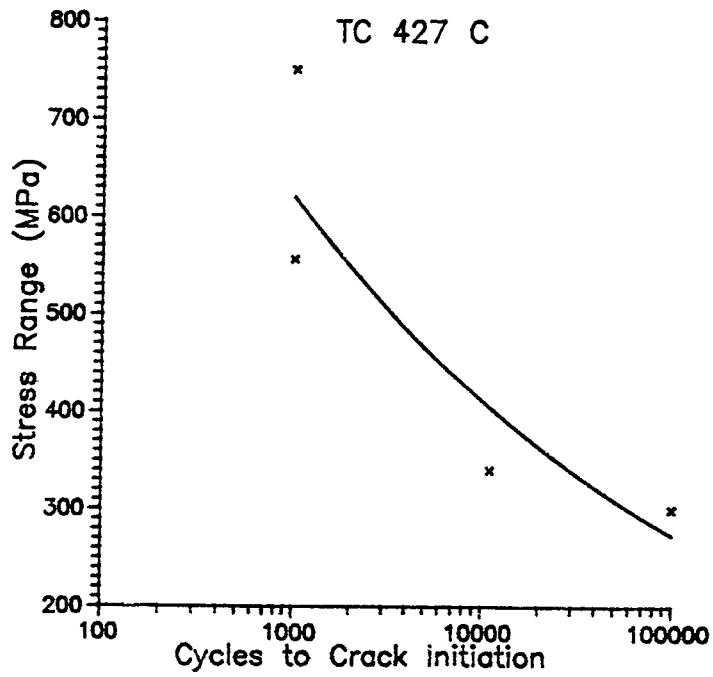


Figure 13. Crack Initiation S-N Curve

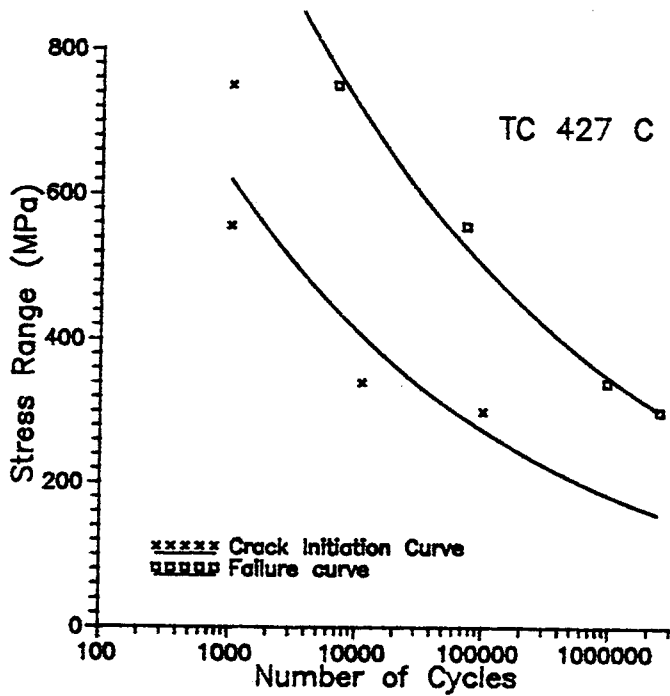


Figure 14. Failure and Crack Initiation S-N Curve

linear. As the test continued and damage began to accumulate within the specimen, a marked difference was seen between the tensile and compressive portions of the curve. Figure 15 shows specimen cycled from +225 MPa to -225 MPa at four different cycles during its fatigue life, starting from the initial cycle to the failure cycle (see Appendix A for the stress-strain curves of the other stress level fatigue tests).

This figure shows a significant decrease of the tensile stiffness as the test progressed compared with a mild degradation in compressive stiffness. This is due to the formation and progression of the four cracks and other accumulating damages. As a test begins, there are no cracks along the periphery of the hole, and hence the curve is nearly linear. As the cracks develop while the test continues, they will open under tensile loading and decrease the stiffness. However, the cracks will close back on themselves in compression, and therefore the stiffness will remain near its original value, with only a slight degradation as the test progresses. Figures 16 and 17 show the stress-strain curves again for the ± 225 MPa test at the same designated cycles as figure 15, yet the tensile and compressive portions of the curves are isolated with the corresponding values of stiffness for each cycle. A linear regression was performed for the modulus values from both the tensile and compressive portions of the stress-strain relationship during the first cycle. Stiffness values from this linear regression were within 2.5% of each other, making it reasonable to assume linearity for each portion of the stress-strain curves.

Notice that the compressive portion shows a slight increase in the stiffness at the beginning stages of the cycling, before eventually falling slightly below its original value. This was common among the tests conducted at low stresses (± 225 MPa and below). It

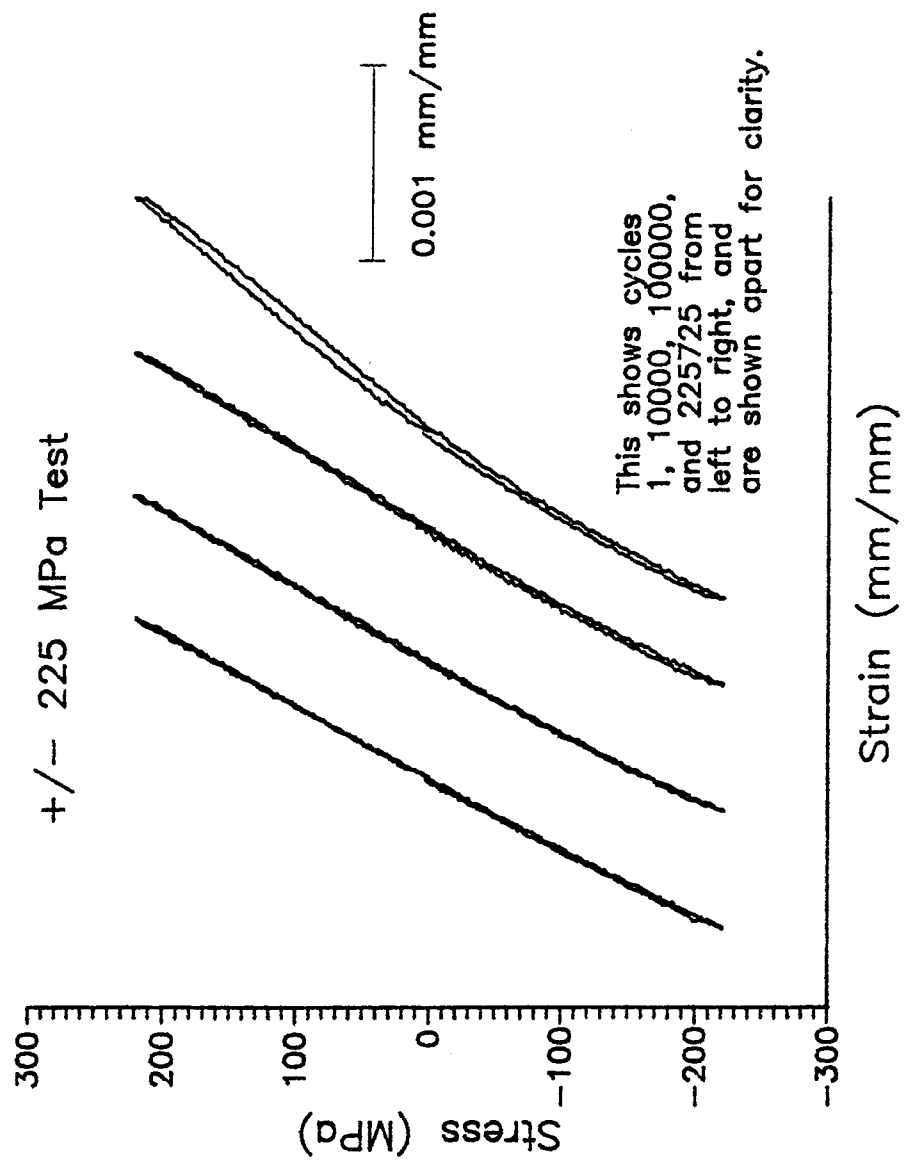


Figure 15. Stress-Strain Curves During Cycling of ± 225 MPa Fatigue Test

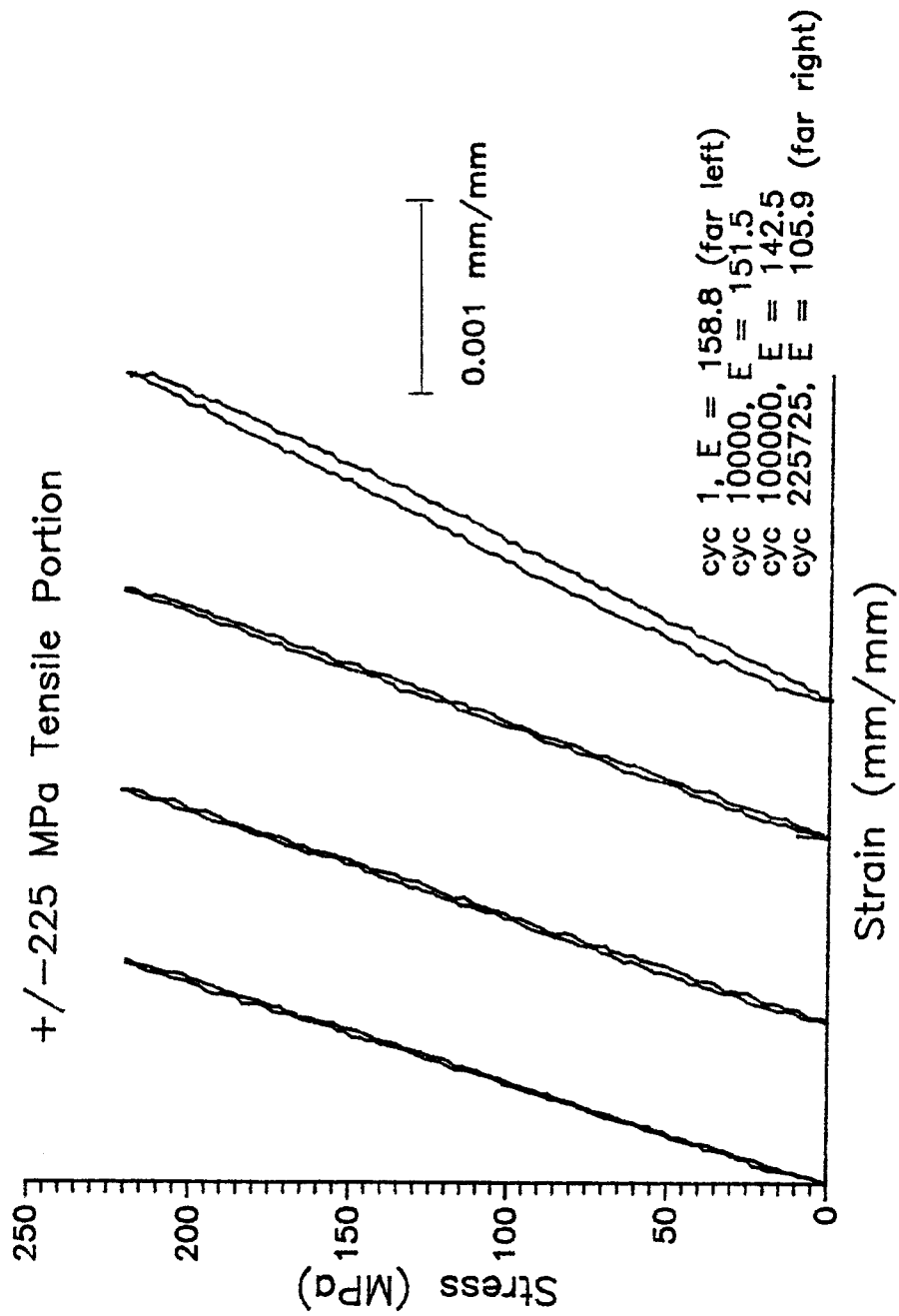


Figure 16. Tensile Portion of Stress-Strain Curves

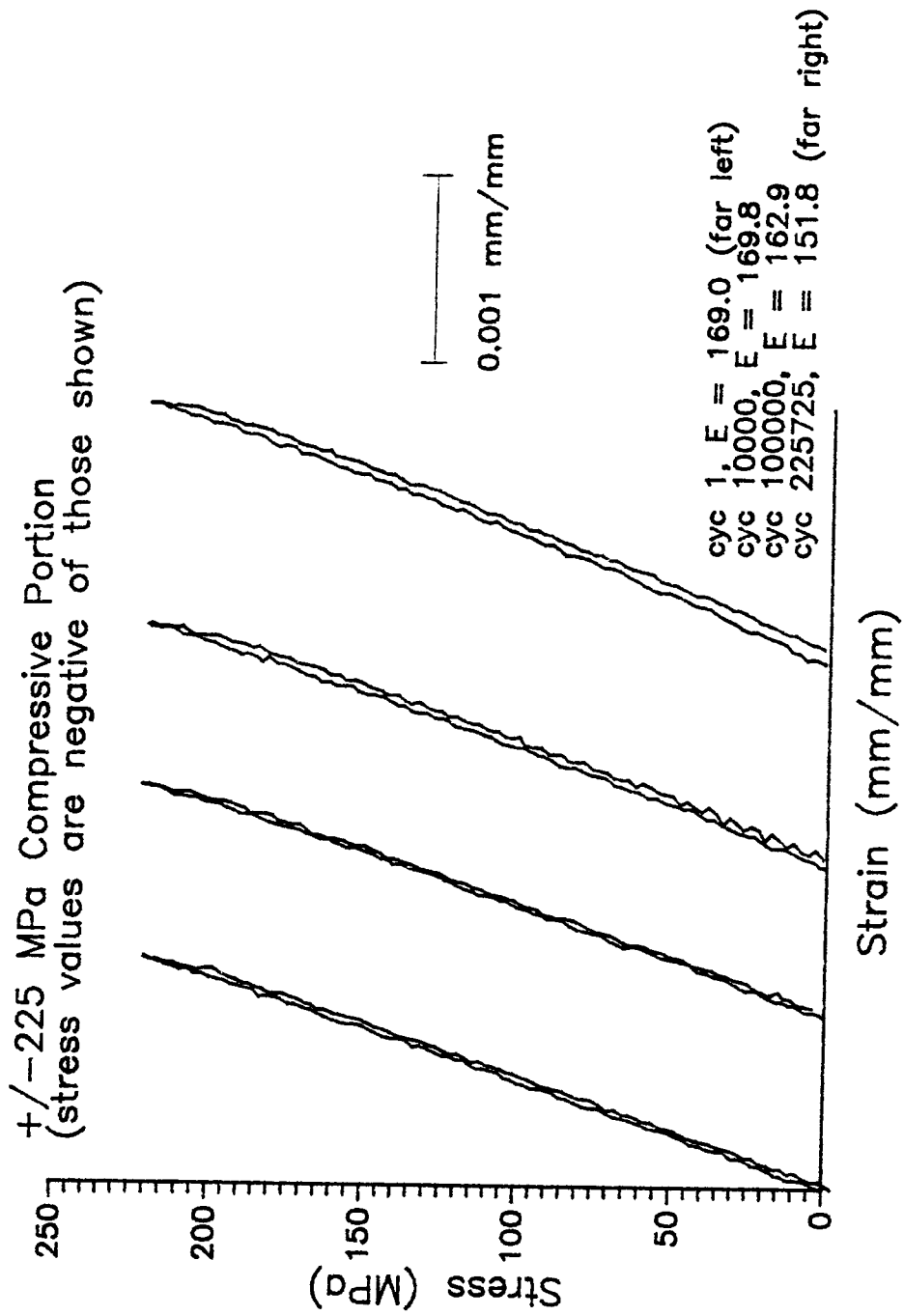


Figure 17. Compressive Portion of Stress-Strain Curves

has also been observed by both Boyum and Sanders that there is an increase in the stiffness of a material for low level stress fatigue tests at elevated temperature during a portion of the life of the specimen before significant damage has occurred (6:95,19:45). Sanders explained that this apparent strengthening of the material is caused by the transformation of β -phase to α -phase within the titanium matrix. This explains the slight increase in the stiffness on the compressive portion of the stress-strain graph for the ± 225 MPa test (a low stress test). This increase in stiffness would only be seen on the compressive portion of the graph of a tension-compression fatigue test because this would be when any existing cracks would have closed in on themselves.

Stiffness and Strain Curves

The increase in strain and stiffness reduction for four of the tests throughout their fatigue lives and normalized fatigue lives are shown in figures 18 through 21. To better compare tests at differing stress levels which have correspondingly different fatigue lives, it becomes useful to use the normalized fatigue life. To obtain this normalized fatigue life, the number of each cycle of a test is divided by the number of cycles to failure for that particular test (cycle/cycles to failure). This makes it easier to compare the trends of the strain increase and stiffness reduction at the different stress levels for different tests. Several observations can be noted from these figures.

As seen by Baker, Boyum, and Sanders (4,6,19) in their work with cross-ply MMCs, it was also seen here that the low stress test showed a slight increase in the stiffness before the development of damage in the specimen which led to a stiffness

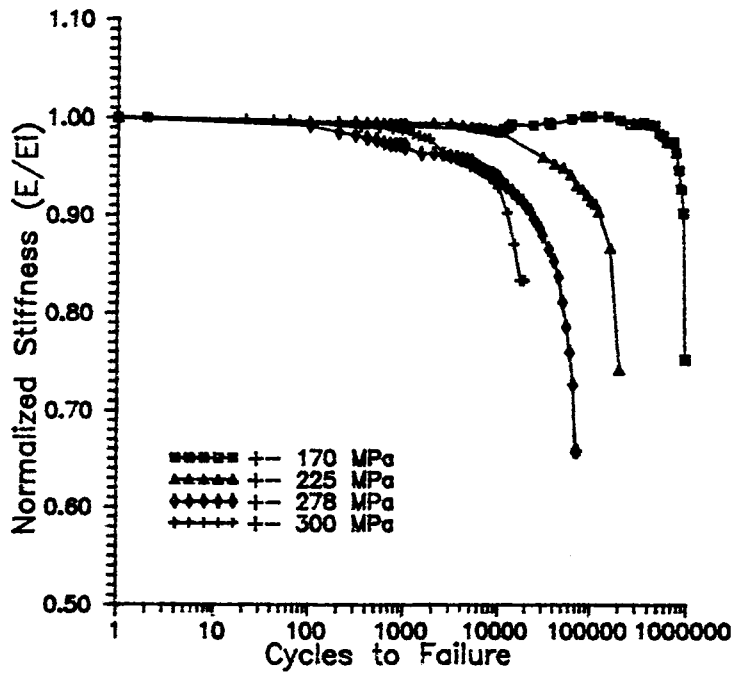


Figure 18. Normalized Stiffness vs. Fatigue Cycles

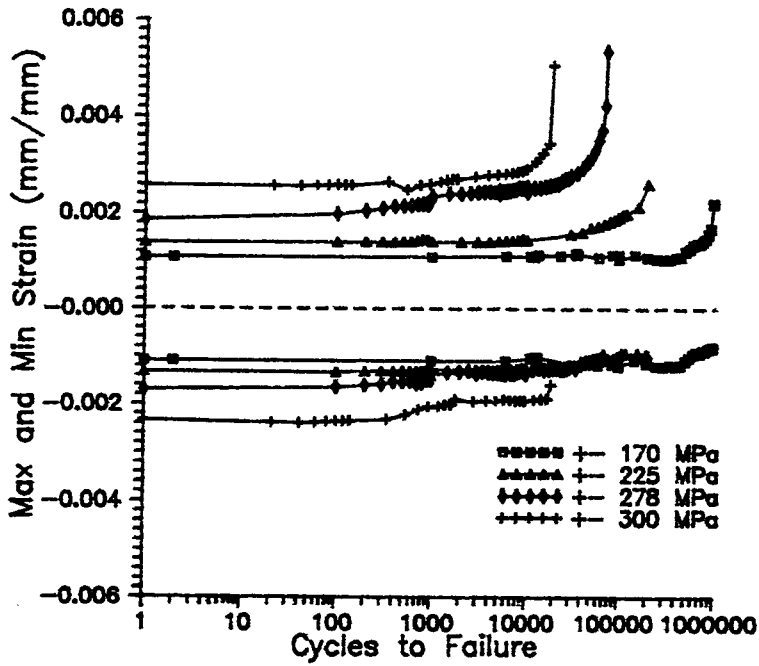


Figure 19. Max and Min Strain vs. Fatigue Cycles

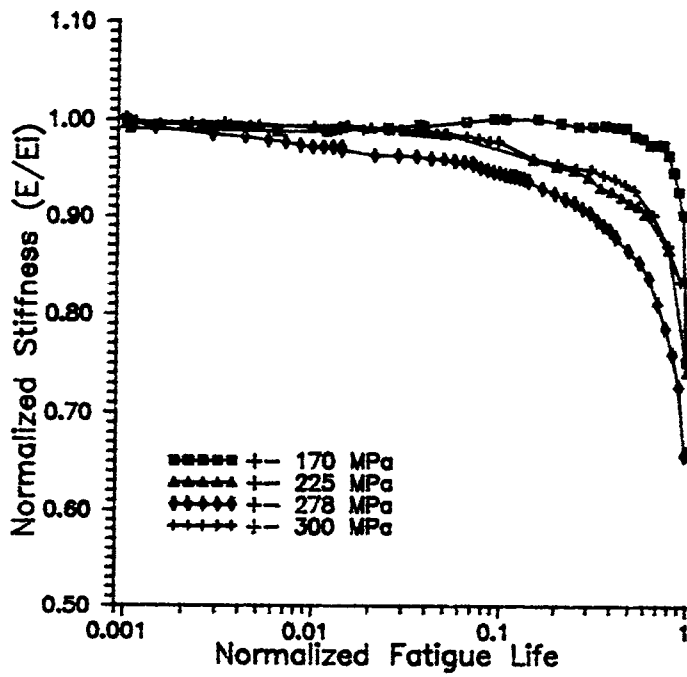


Figure 20. Normalized Stiffness vs. Normalized Fatigue Life

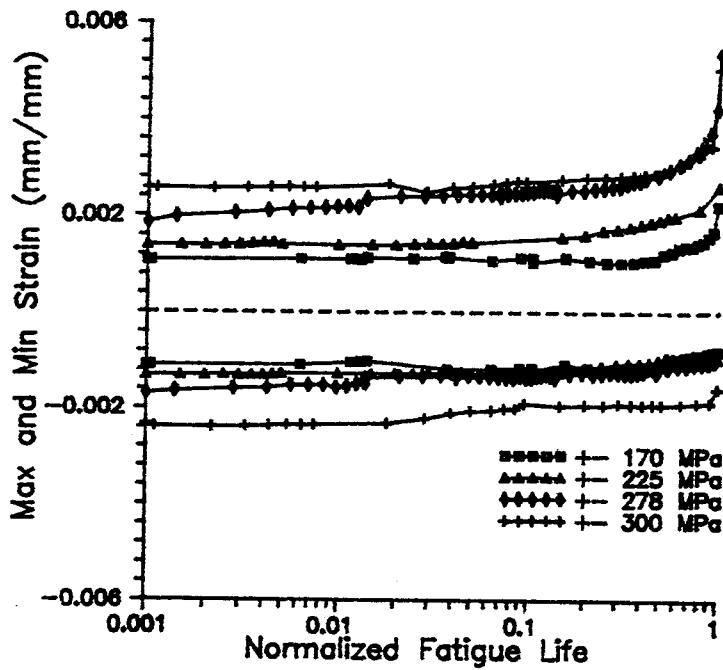


Figure 21. Max and Min Strain vs. Normalized Fatigue Life

decrease. Once the damage overrides the strengthening effects due to phase transformation (discussed in the previous section), the stiffness begins quickly to drop. This stiffness increase was also noted in the previous section in figure 17.

The trends for the ± 300 , ± 225 , and ± 170 MPa tests behaved as expected. As the stress level was reduced, the amount of stiffness degradation increased. A higher stress test has a higher prevalence of fiber failure while a lower stress test has a higher prevalence of matrix failure. Increased matrix cracking of the lower stress tests would account for more stiffness reduction before failure. The ± 278 MPa test had the highest stiffness reduction and, therefore, must have experienced the highest degree of combination of fiber and matrix failure. This combination of matrix cracking and fiber failure as the dominant failure mechanism is referred to by Boyum as a Regime 2a test (6:39). The fracture surface revealed that this particular test did indeed have the highest combination of matrix cracking and fiber failure, and is discussed later in this chapter under the fractographic analysis section.

From the maximum and minimum strain results, it is seen that the two lower stress level tests showed only a slight increase in strain values before failure. The ± 278 MPa and ± 300 MPa tests showed significant increases in strain prior to failure. Similar to Boyum (6:95), this may be caused by these mid-level stress tests experiencing both fiber and matrix damage.

The results of all these figures when combined together seems to indicate that the low stress tests (± 150 , ± 170 , and ± 225 MPa) experience Regime 2 failure, or matrix failure domination, before reaching a critical length when the crack develops up to the

end of the specimen and catastrophic failure occurs. The higher level stress tests (± 278 , ± 300 , and ± 375 MPa) appear to be Regime 2a failure, or a combination of fiber and matrix damage that lead to failure. No test exhibits the characteristics of Regime 1 failure, which is fiber failure domination. This is due to the stress concentration of the center hole which produces stresses that overwhelm the matrix near the borders of the hole. The fractography and metallography results given later will help to clarify this observation.

Micromechanic Considerations

Despite the indications of damage made from macromechanic observations, it is necessary to perform a micromechanic investigation. This will determine the manner in which damage has initiated and progressed during the fatigue test within the material.

The three methods used in this study for the micromechanic investigation included crack initiation and propagation monitoring, fractography, and metallography. By using each of these, the precise manner of fatigue damage initiation and progression can be determined.

Crack propagation during the fatigue life of a specimen is an important method of determining the microscopic behavior of the material. As mentioned previously in this chapter, cracks were monitored throughout each test by taking edge replicas as well as front and back face replicas. The length of the face cracks were determined by placing the replicas in the SEM and using a measuring system. This made it possible to chart the

length of the major and minor cracks within the material throughout the life of the specimen.

Fractography is the examination of the fracture surface using high magnification microscopes. Through the use of fractography, it is possible to determine the cause of the specimen failure and/or the fatigue crack growth process. Two basic types of fracture surfaces are characterized by either brittle cleavage failure or ductile void coalescence.

Brittle cleavage is caused by direct separation along the material's crystallographic planes due to the simple breaking of atomic bonds (5:40). This is generally associated with crack propagation through the material. The formed flat cleavage facets provide a high reflectivity, giving the fracture surface a bright, shiny appearance. On the contrary, the fracture surface formed by ductile void coalescence is generally dull. This type of surface is typically formed by an overload in tension within the matrix, causing extreme plastic flow and resulting in the classic cup and cone type fracture (5:40). Observing this type of fracture surface under the SEM reveals the surface covered with dimples, which show the coalesced voids.

Metallography is the examination of sectioned specimens under optical microscope used to reveal deformation mechanisms and damage. Damage is defined as the "formation of new and free surfaces within the specimen and consists of fiber and matrix cracking, fiber-matrix reaction zone cracking, and debonding of the fiber-matrix interface" (6:43).

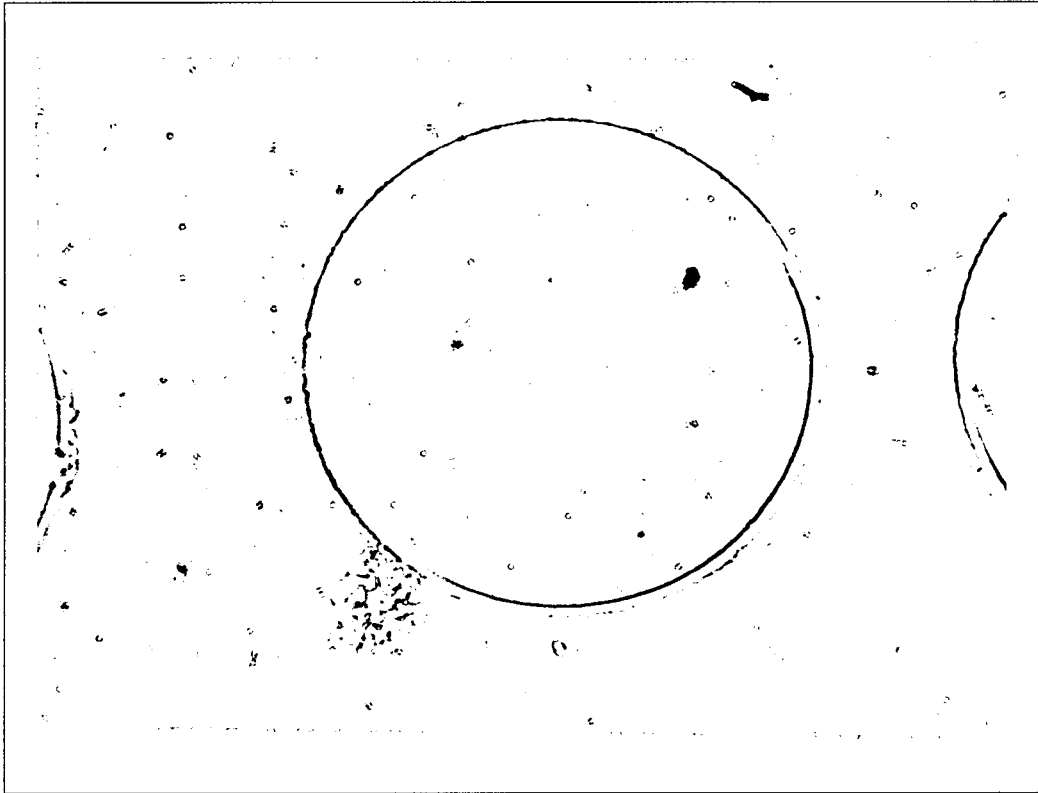
Fibers breaks occur in both the 0° and 90° fibers, and some may have resulted from machining or fabrication of the material. More commonly within fatigue tests, the

fiber breaks are a result of tensile overload. The damaged matrix transfers stress to the 0° fiber causing this overload. Reaction zone cracks refer to cracks in the fiber-matrix reaction zone, which is the area between the fiber and matrix in which the two have chemically reacted during fabrication. Matrix cracking, the most common form of damage initiation in this study, is a direct result of the specimen notch. These cracks in the notched specimen generally grow under cyclic loading until a fatigue critical crack length is reached. Debonding is another type of damage, in which there is a separation of the fiber from the matrix. Occurring in both the 0° and 90° fibers, this is generally between the carbon rich outer layer of the fiber and the reaction zone between fiber and matrix.

Crack Initiation and Growth

Replication was the method used to determine crack lengths at various cycles for each test. Edge replicas were examined under an optical microscope to determine if cracks were present or any other damage could be observed, and front and back face replicas were gold coated and placed in the Scanning Electron Microscope. The SEM was then used to find the length of each crack seen on the front and back face replicas.

Little damage transpired on the edges of the specimens during fatigue testing. Examination of the edge replicas revealed no transverse cracking within the matrix. The only observation made from the edge replicas was that the 90° fibers in the region near the hole, or within 2 hole diameters, debonded first (see Figure 22). The stress in the



←→ LOAD

Figure 22. Edge Replica of 90° Fiber Debonding (400x)

reduced area section would reach a level at which debonding of the 90° fibers occurred, which was usually within the first cycle of fatigue loading.

Four cracks developed along the edge of the hole on both the front and back face of each fatigue tested specimen. Similar to Baker's findings (4:55), these cracks developed between 60° and 80° from the loading axis. Figure 23 shows the presence of the four cracks from a face replica. Two of the four cracks continued to grow and become dominant. These major cracks proceeded on to the edge of the specimen, and after failure the length along the major cracks became the fracture surface for the specimen.

Many of the fatigue tested specimens exhibited a split in the major and minor cracks in which a tiny, discontinuous fatigue crack broke off from the main length of the crack and ran parallel to it for a short distance (see Figure 24). This splitting, referred as crack bifurcation, occurred in nearly all specimens, regardless of the stress level. These appear to be caused by the high stress region created by the presence of the hole. This crack bifurcation was also noted by Baker (4:57,58), however it was only noted in low stress tests. It would seem that the added compressive portion of the loading during tension-compression fatigue made crack bifurcation more prevalent at all stress levels and along both major and minor cracks.

Figure 25 shows the typical progression of the crack for the front face of the ± 170 MPa test. This is shown as a representative example of crack growth for all the fatigue tests in this study. As can be seen in this figure, the growth of crack continues throughout the life of the specimen. In the initial stages of the fatigue life of the specimen, the crack

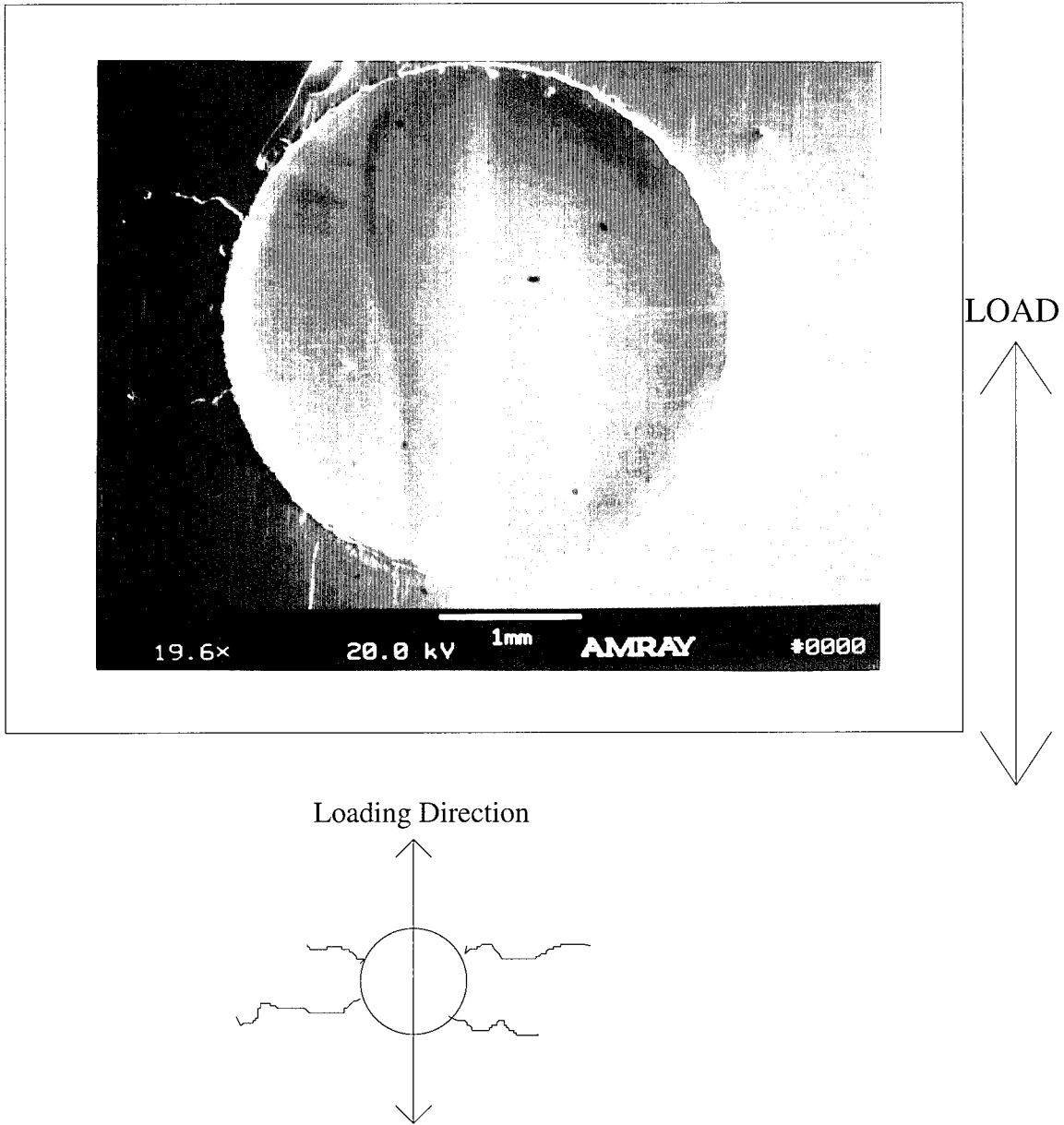


Figure 23. Crack Initiation Sites (19.6x)



Figure 24. Crack Bifurcation of Major Crack (50x)

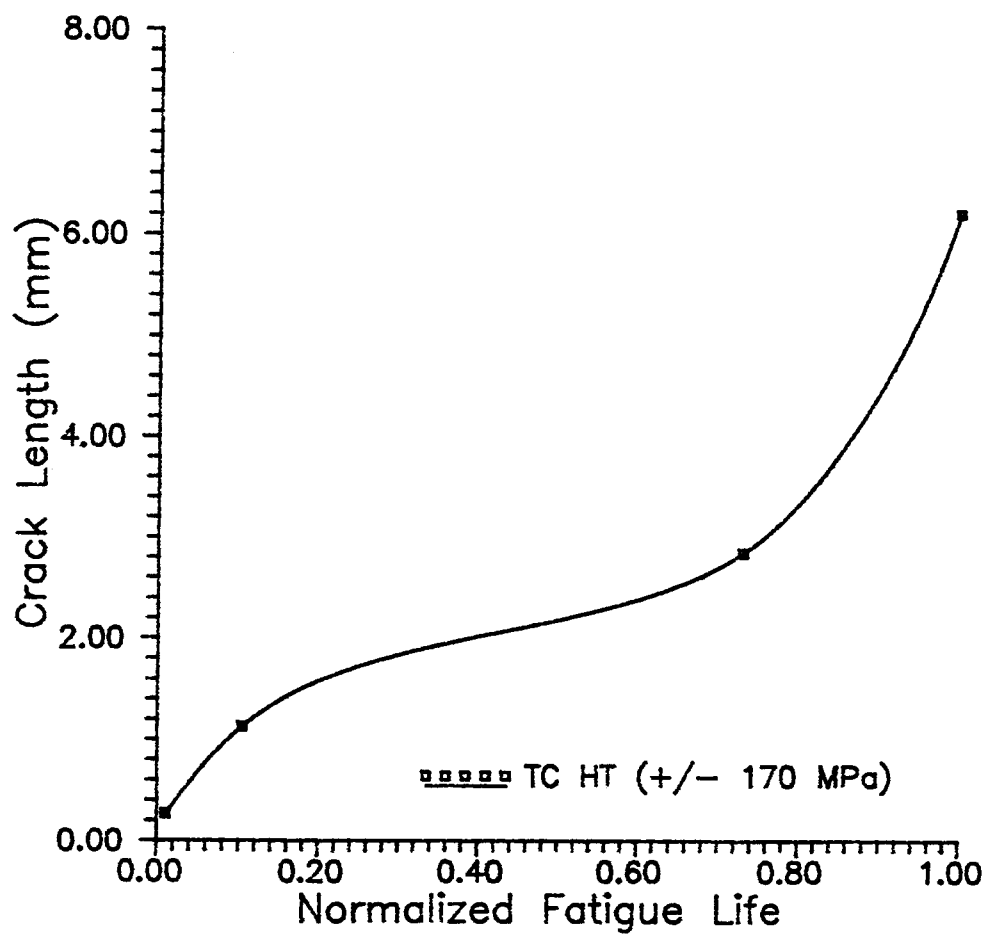


Figure 25. Crack Length vs. Fatigue Cycles

propagation is rapid, however it begins to slow slightly as the cycling continues. This is due to the fiber bridging of the fatigue crack, which will be discussed later in the metallographic analysis section of this chapter. Once the crack reaches a fatigue critical crack length, there is a rapid rise in crack growth, and it becomes unstable. The crack then grows catastrophically through to the edge of the specimen and fracture occurs.

Fractographic Analysis

The first step in performing a fractographic analysis for a notched specimen is to note the color, amount of fiber pull-out, and general fracture surface appearance. Examination of the color of the fracture surface gives a qualitative observation of the amount of time the surface was exposed to air and high temperature. At high temperature the air and titanium react to form an oxide layer which changes color as the exposure time increases (4:59). A shiny appearance indicates that there was a very short exposure time to air and elevated temperature. Increasing amounts of exposure time respectively lead to brownish-yellow, then a straw color, progressing to various shades of blue, and finally to purple. A crack history may be determined by noting the different regions of color on the fracture surface.

Another aspect to observe during the initial inspection is the degree of fiber pull-out along the fracture surface. Fiber pull-out occurs when “the fibers fracture at their weak cross sections that do not necessarily lie in the plane of composite fracture” (2:328). High fiber pull-out is an indication that some amount of fiber failure has occurred within that portion of the specimen. However, as stated earlier in this chapter under the

macroscopic considerations section, the effect of the center hole adds a stress concentration of a sufficient degree that matrix cracking is always present, regardless of the stress level. Thus, high fiber pull-out indicates that the dominant failure mechanism was Regime 2a failure, which is the combination of fiber failure and matrix cracking. Low fiber pull-out was an indication that matrix cracking alone served as the dominant failure mechanism, making it a Regime 2 failure.

All the fatigue test specimens had a different fracture surface appearance than the monotonically loaded tensile test specimen (see Figure 26). As seen in the picture, the specimen that was monotonically loaded to failure exhibited a fracture surface located at 90° from the loading axis. The fatigue tested specimens fractured along the dominant cracks, which were located between 60° and 80° from the loading axis. Figure 27 shows a close-up of the monotonically loaded specimen's fracture surface, and Figure 28 gives a closer view of a typical fatigue specimen's fracture surface (in particular, the ± 300 MPa test). These figures clearly show that cracks do not initiate in the same location for monotonic and fatigue loading.

The surface of the monotonic tensile test specimen showed a relatively high degree of fiber pull-out (see Figure 27) and a bright, shiny appearance uniformly over the cross-section. Fiber failure leading to a tensile overload of the matrix caused this specimen's failure. Newaz and Majumdar observed this type of failure for a monotonically loaded, notched unidirectional laminate specimen of the same material (16:1-22).

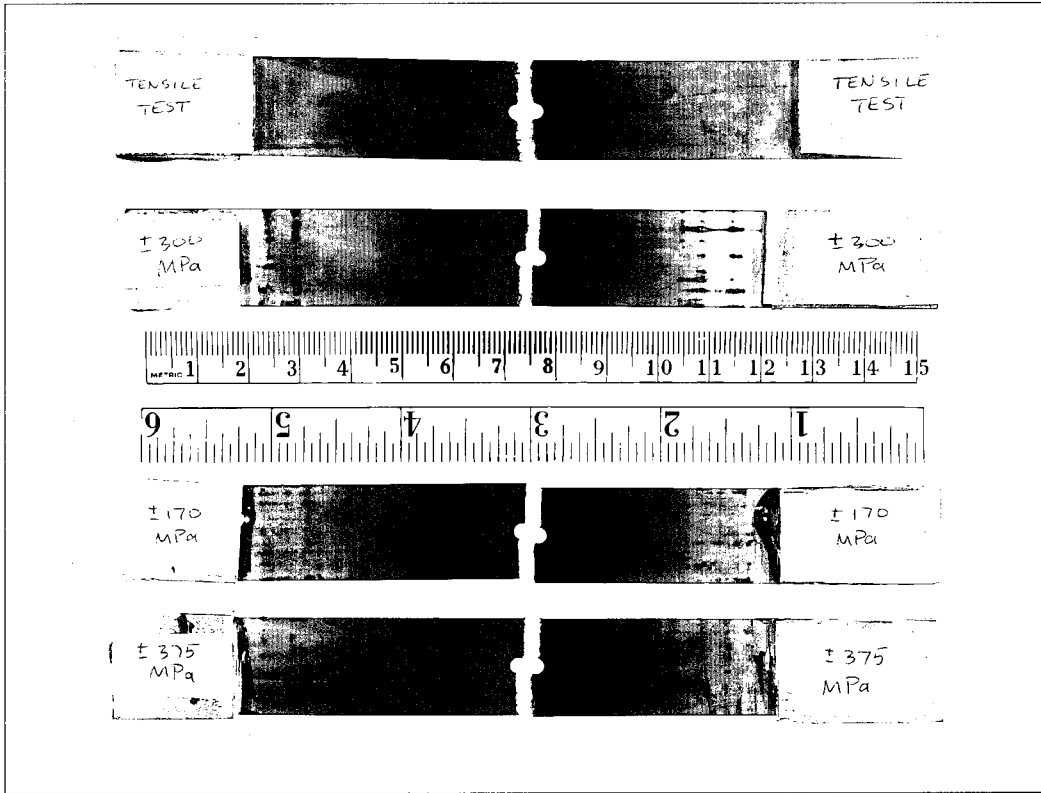


Figure 26. Four Specimens Fracture Surfaces

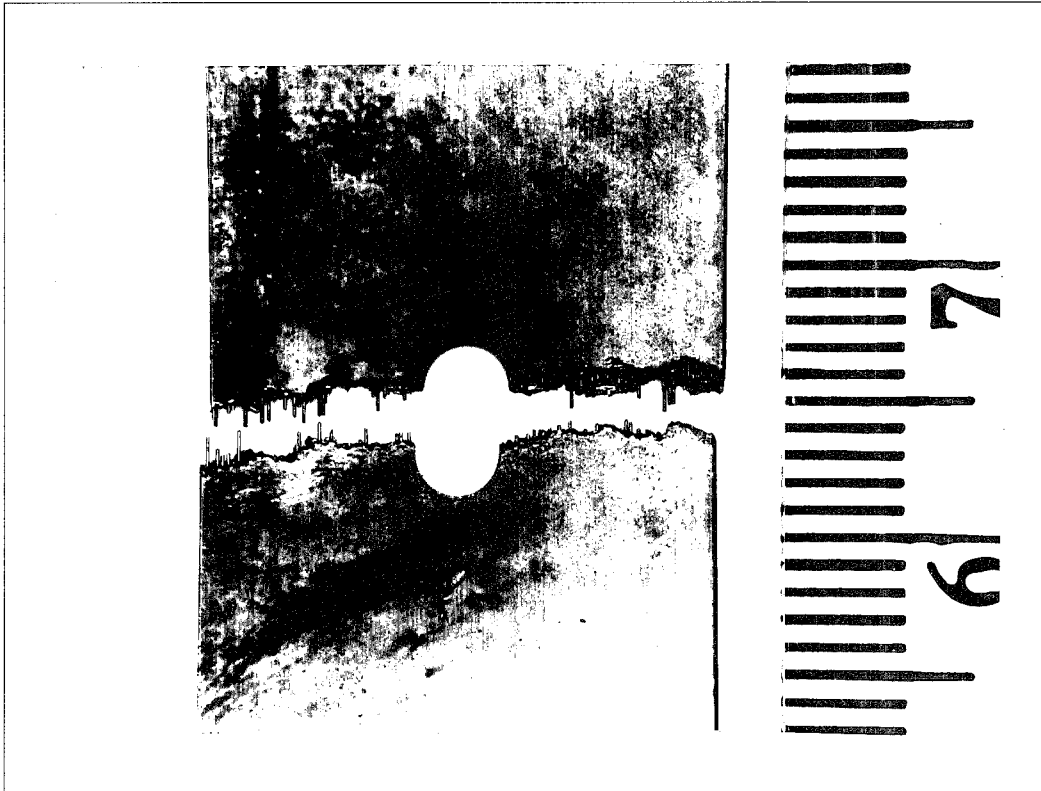


Figure 27. Monotonically Loaded Specimen Fracture Surface



Figure 28. ± 300 MPa Fatigue Loaded Test Fracture Surface

In this study, the low level stress fatigue tests (± 225 MPa and below) exhibited a relatively low degree of fiber pull-out. These tests were subjected to sufficiently low values of stress so that the fibers were generally not affected. Therefore, once the four cracks developed around the periphery of the hole, matrix cracking served as the dominant failure mechanism. This would indicate that the ± 150 MPa, ± 170 MPa, and ± 225 MPa tests all experienced Regime 2 failure. No test was run below a stress level of ± 150 MPa, and hence no test occurred within Regime 3, the fatigue limit of the matrix.

High stress fatigue tests (± 278 MPa and above) generally showed a high degree of fiber pull-out. The stress values were high enough to cause overload of many of the fibers, while the notch added the effect of matrix cracking. This indicates that the ± 278 MPa, ± 300 MPa, and ± 375 MPa tests were Regime 2a failure. It can clearly be seen in Figure 26 that the higher stress level fatigue tests shown (± 300 and ± 375 MPa) exhibited more fiber pull-out than the lower stress level fatigue test (± 170 MPa).

Also, the ± 278 MPa test experienced the highest degree of fiber pull-out, indicating that the test experienced the highest combination of fiber failure and matrix cracking. This corroborates the findings in Figures 18 through 21, in which the ± 278 MPa test showed the highest reduction in stiffness and highest increase in strain over the life of the specimen.

After the initial observation of the general fracture surface appearances of each specimen, it is then necessary to examine each specimen's fracture surface microscopically in the SEM. For all fatigue tested specimens, this examination revealed

that cracking at the hole is primarily brittle cleavage in nature (see Figure 29), with the fracture surface in this region relatively flat and dull in appearance. This brittle region showed little matrix plasticity and was caused by the major crack along the hole progressing due to the fatigue loading.

The fracture surface at the edge of the specimen is characterized by ductile dimpling. The transition from the brittle cleavage fracture to ductile fracture depends on the stress level of the fatigue test. A notched fatigue critical crack length can be defined as the length from the periphery of the hole to the brittle/ductile transition, seen in Figure 30. As the stress level of the fatigue test is increased, the notched fatigue critical crack length of the specimen decreases. As mentioned previously in the crack growth and initiation section of this chapter, the growth of the crack reduces the available area of the specimen to carry the load until a point is reached where the stress in the cross-section approaches the material's ultimate stress. Once the ultimate stress is reached, the crack reaches its notched fatigue critical crack length. The crack then shoots through to the edge of the specimen, breaking all the fibers along the way. After these fibers break, the matrix takes on the load and is immediately overloaded in tension. This results in the ductile region of the matrix, in which the matrix plastically deforms and necks around the fibers. Figure 31 shows this matrix necking and ductile void coalescence in the ductile failure region near the edge of the specimen.

No analytical model has been developed for this parameter of a notched fatigue critical crack length of an MMC. Indeed, Tsai explained that "since composite laminates exhibit very complex failure processes, the analytical model accounting for all the failure

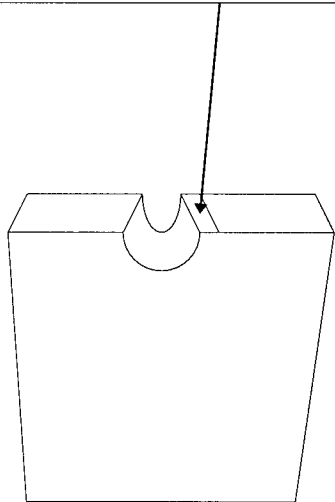
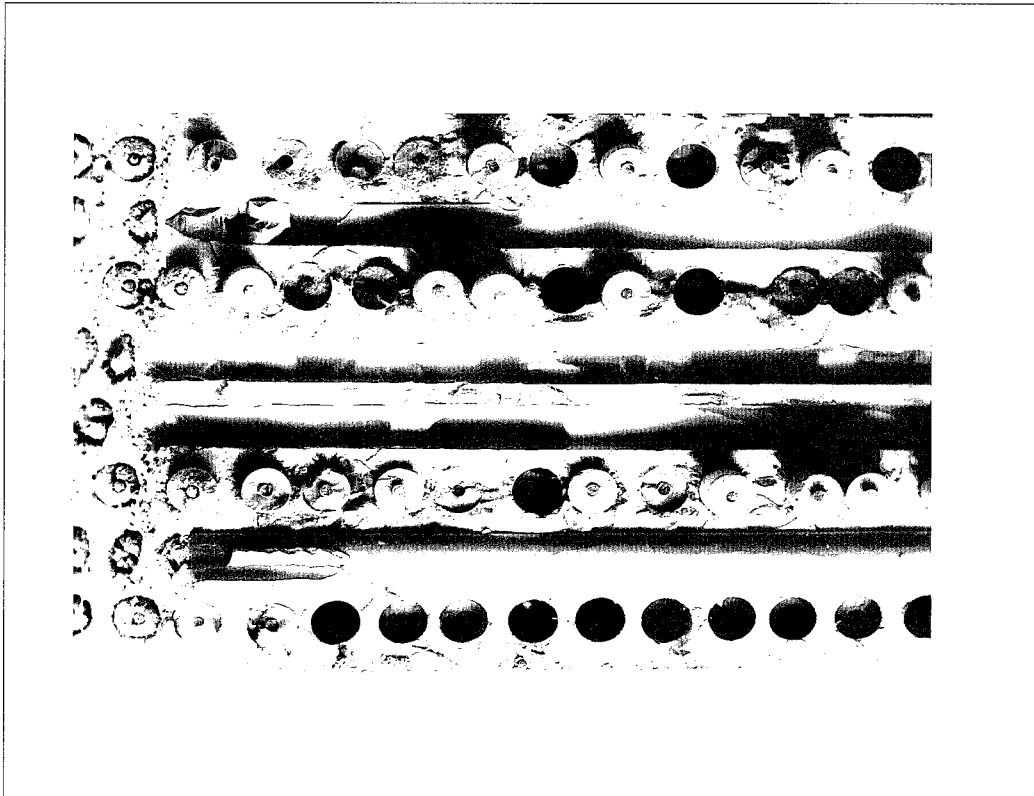


Figure 29. Brittle Cleavage Region Near Hole on Fracture Surface (45x)

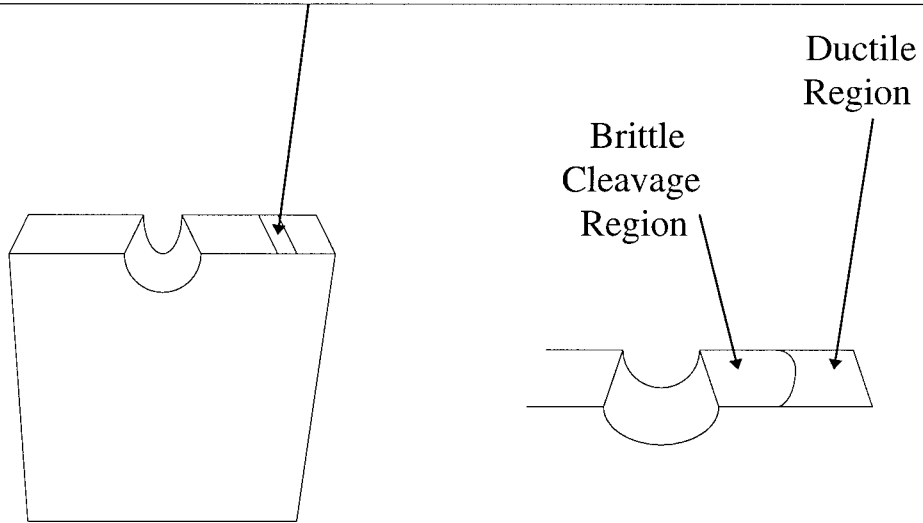
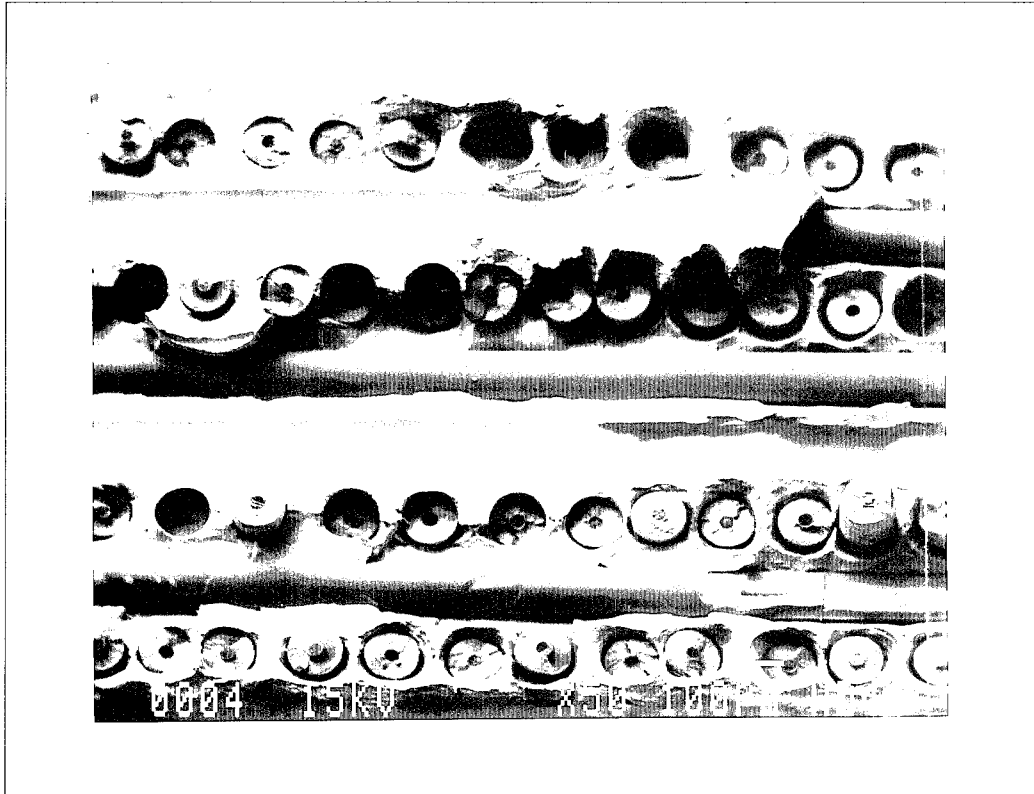


Figure 30. Brittle/Ductile Transition Region (50x)

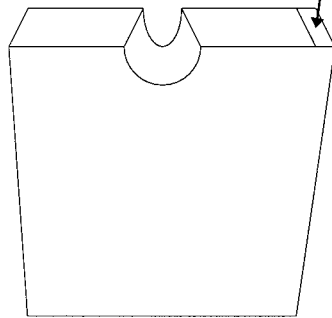


Figure 31. Matrix Necking and Ductile Void Coalescence in Ductile Region (400x)

processes has not been established” (22:19-30). This determination of the notched fatigue critical crack length in this study is a qualitative observation based on the fractographic results of this research effort and Baker’s tension-tension study (4:63).

Another observation can be made from the brittle/ductile transition region shown in Figure 30. The brittle surface is in the center of the specimen thickness while the ductile surface is on the face of the specimen. This shows that, at the point prior to failure, the fatigue crack had a parabolic shape (seen in Figure 32). This indicates that the brittle fatigue crack front was propagating internal to the specimen ahead of the face crack prior to failure.

In the brittle cleavage region, fatigue striations were found emanating from the 90° fibers within the matrix (see Figure 33). This is expected to find fatigue striations in the brittle cleavage region of the fracture surface, which is the region where the crack is progressing due to fatigue cycling. Fatigue cycling is known to cause striations in monolithic metals, and are seen in the titanium matrix of this MMC. The high temperature of the fatigue tests also helped in forming these striations by increasing the ductility of the matrix, which would aid in the formation of the fatigue striations.

In many specimens, the outer carbon coating of the 90° fibers had fractured or separated. Also, the 90° fibers at the juncture of the molybdenum cross-weaves fractured, due to the added stress concentration of the weave on the fiber (see Figure 34).

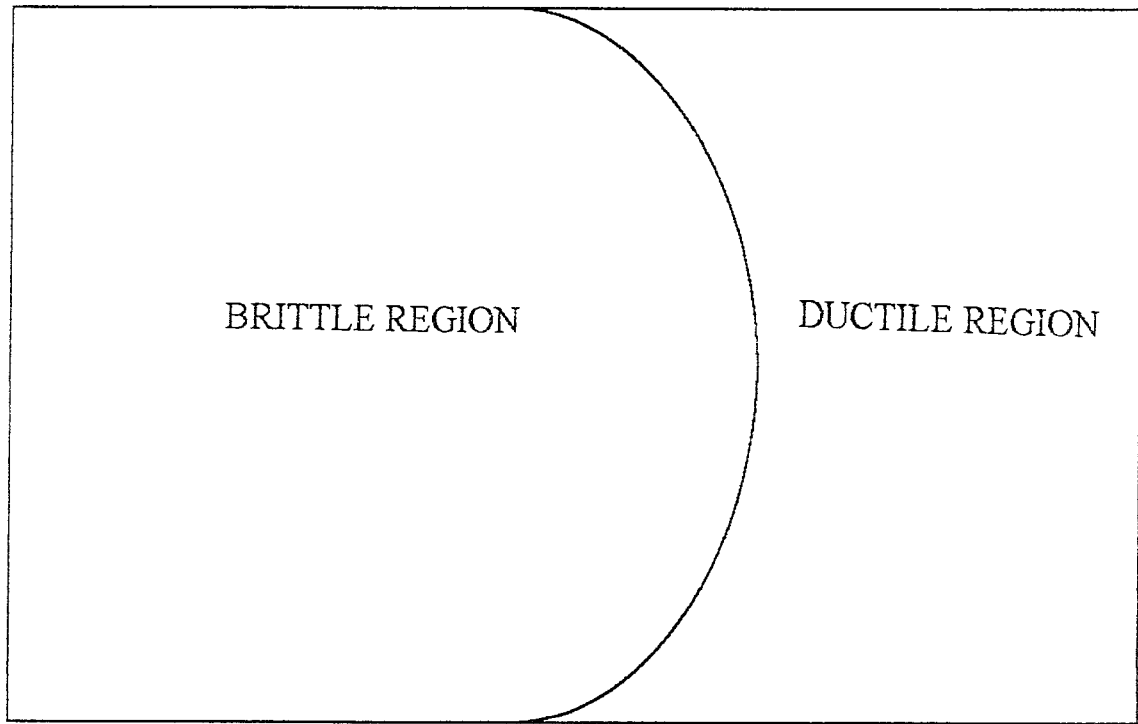


Figure 32. Fatigue Crack Shape Prior to Failure

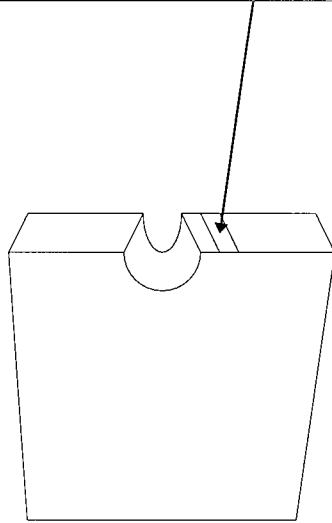
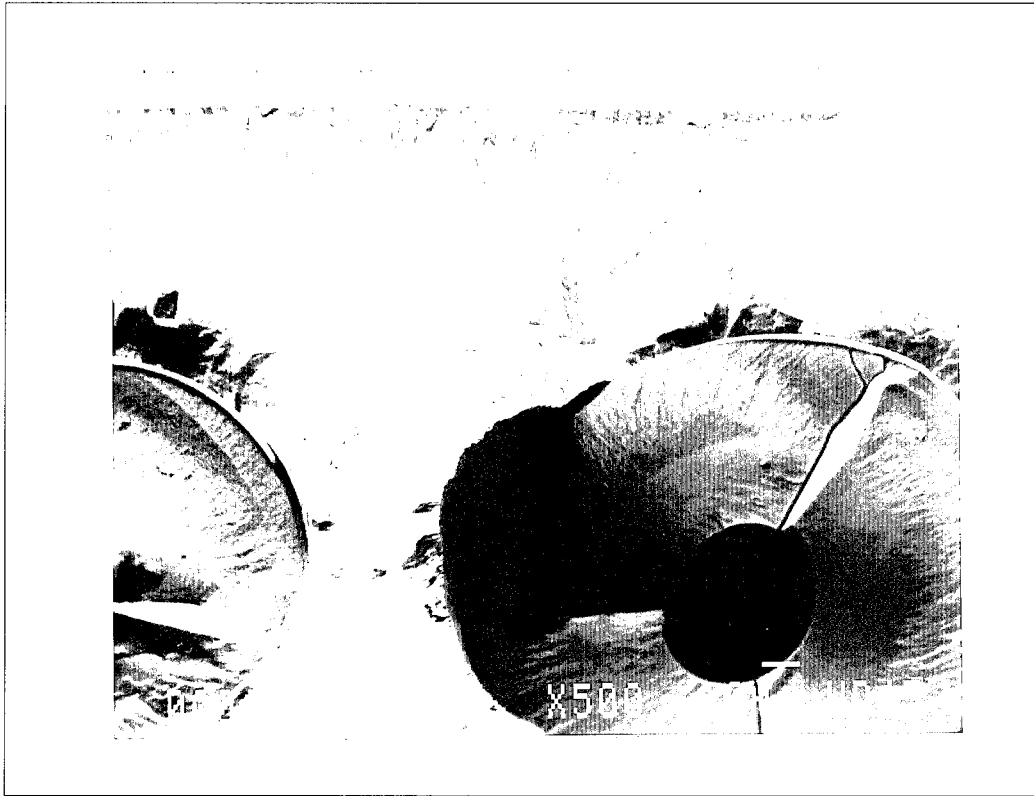


Figure 33. Fatigue Striations Emanating from 90° Fibers (500x)

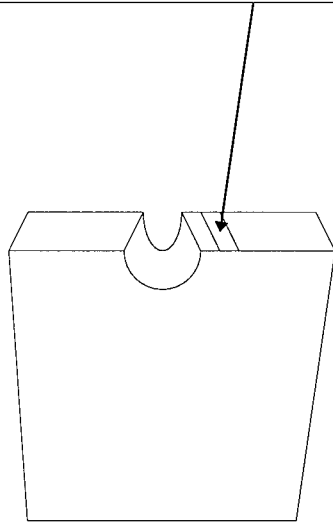
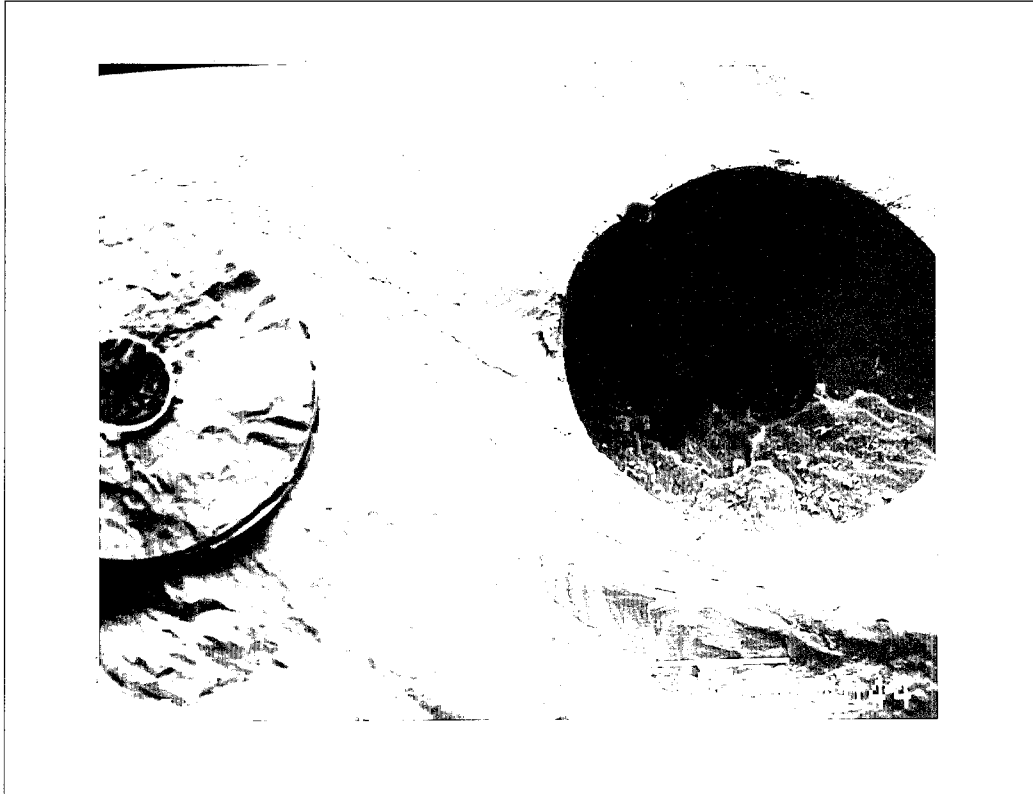


Figure 34. 90° Fiber Break at Molybdenum Cross-Weave (370x)

Metallographic Analysis

Metallography seeks to answer questions about what is happening in the material a short distance from the fracture surface. Each specimen was sectioned according to Figure 6 in Chapter 3.

Figure 35 shows the debonding of the 90° fibers. As mentioned earlier in this chapter, the debonding of these fibers usually occurred within the first cycle of fatigue loading. No matrix cracking was found in either the longitudinal or transverse sectioned specimens.

The high stress fatigue tests in this study have been determined to experience Regime 2a failure, which is the combination of matrix cracking and fiber failure as the dominant failure mechanisms. The sectioned specimens revealed that fiber breaks did exist for the Regime 2a tests. Figure 36 reveals a region where several 0° fibers broke away from the hole for the ± 270 MPa fatigue test. Many of the transverse sections also revealed fiber cracks in the 90° fibers, as seen in Figure 37 for the ± 300 MPa test. Tests that were run at stress levels of ± 225 MPa and below did not exhibit these fiber breaks. This is another indication that tests at this stress level and below experienced Regime 2 failure, with the dominant failure mechanism as matrix cracking.

All the fatigue tests revealed reaction zone cracks on the 90° fibers (see Figure 38). The reaction zone is made up of titanium carbides and titanium silicates and is very brittle, making this area prone to damage in the form of cracking. The combination of

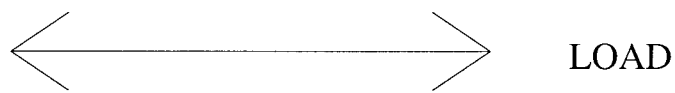
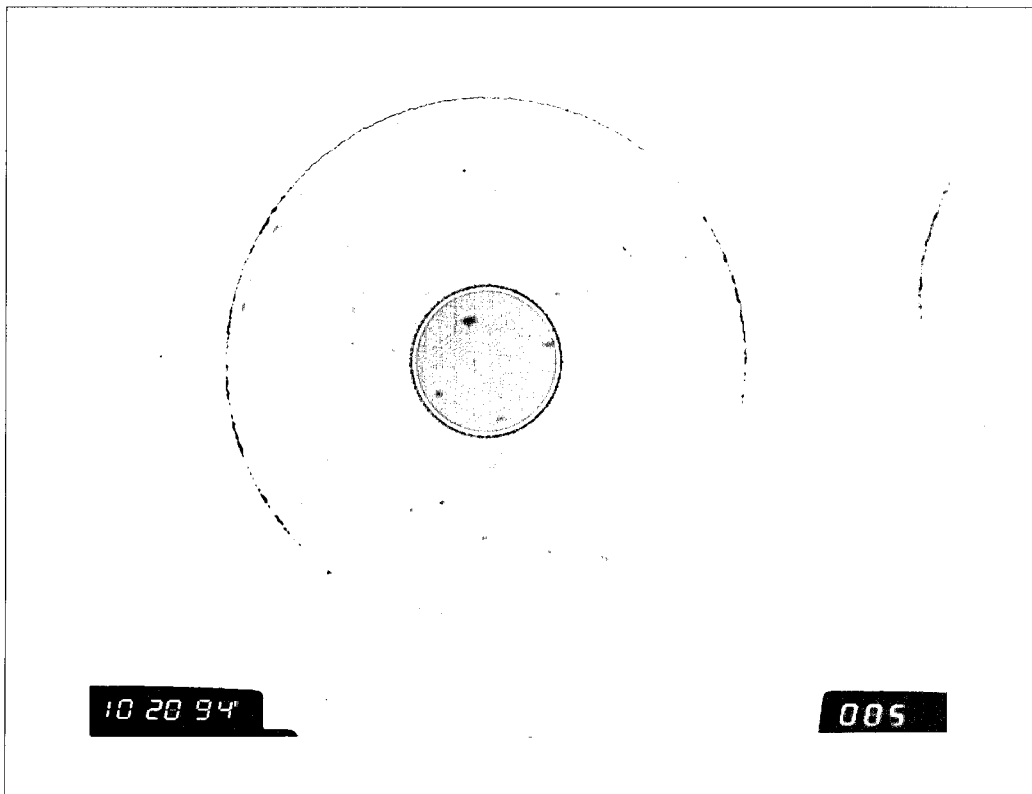


Figure 35. 90° Fiber Debonding (500x)

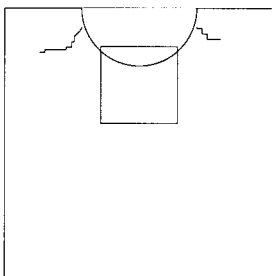
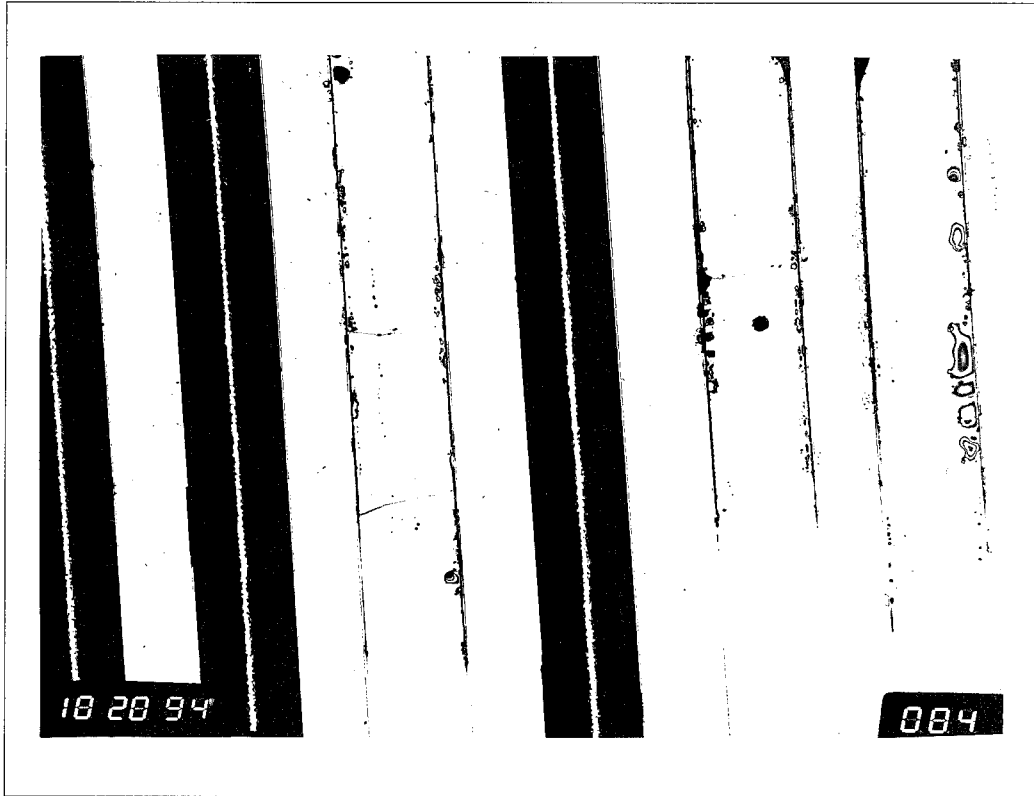


Figure 36. Region of 0° Fiber Breaks (100x)

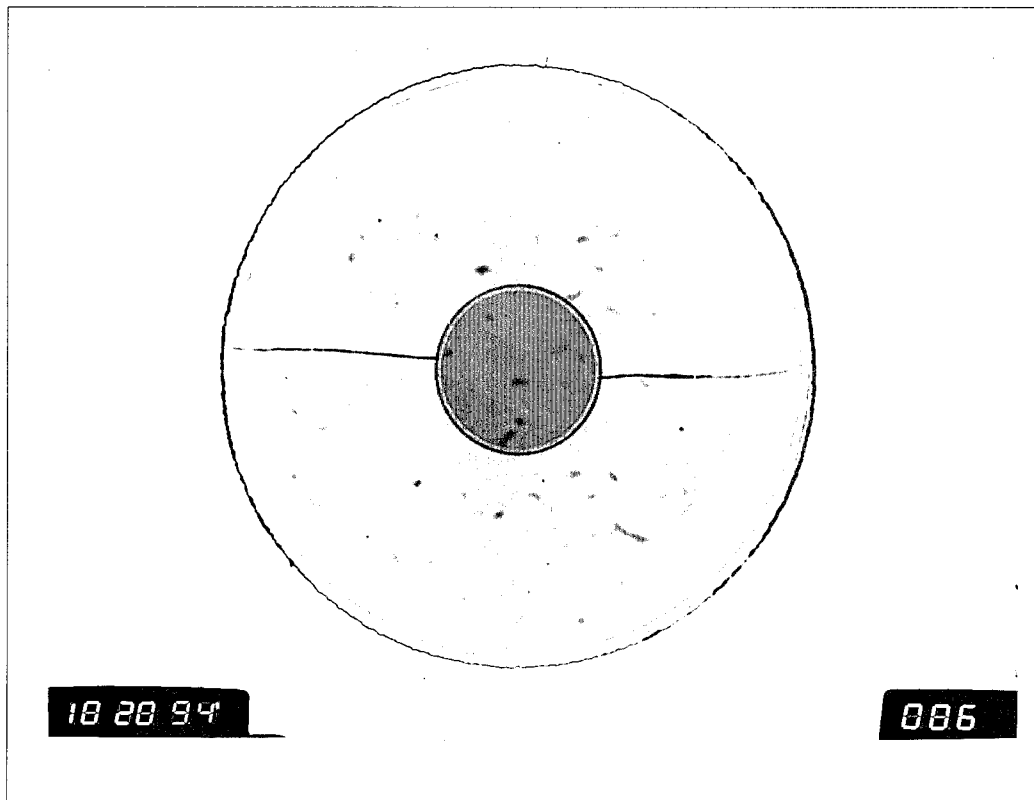


Figure 37. 90° Fiber Break (500x)

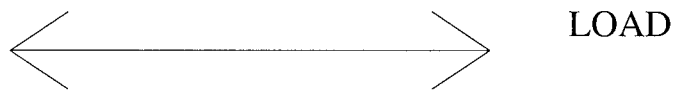
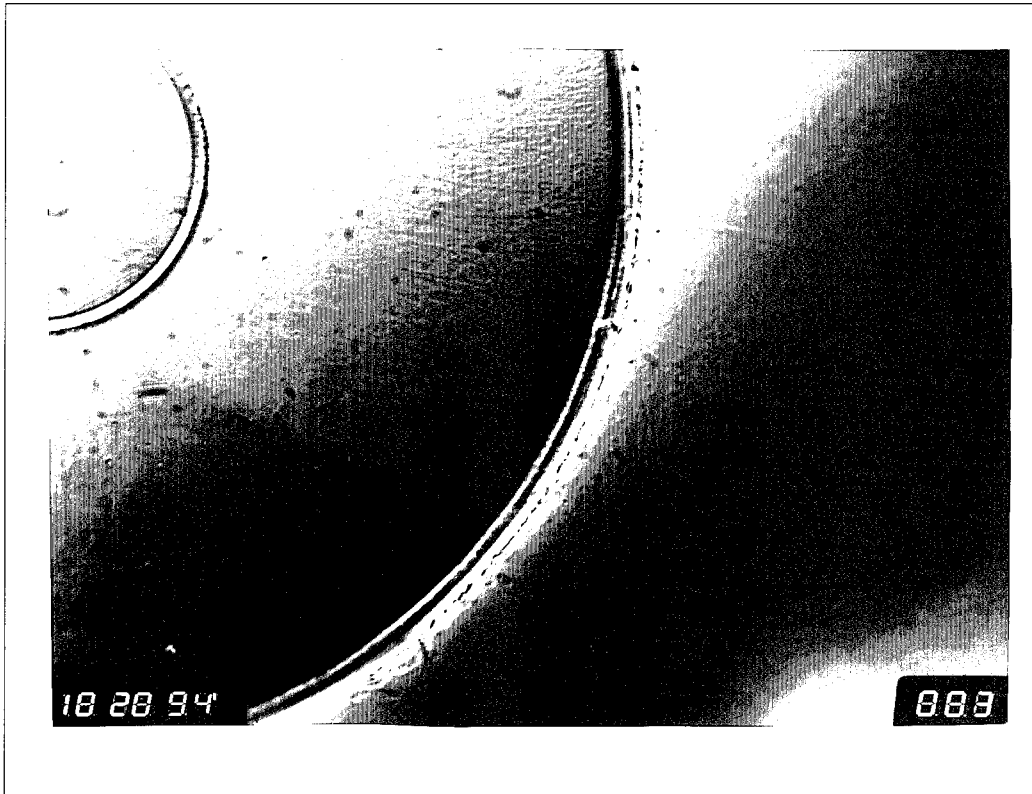


Figure 38. Reaction Zone Crack on 90° Fiber (560x)

tension and compression loading served to cause a great deal of reaction zone cracks among all the different stress level fatigue tests.

A fatigue test was run at a stress level of ± 270 MPa and stopped prior to failure. The purpose of this was to examine the specimen such that the hole and all accumulated damage, including the major and minor cracks, could be observed microscopically. The face of this specimen was polished down to the first set of fibers to reveal damage progression below the outer layer of matrix material.

Figure 39 shows the progression of a major crack from the edge of the hole. It is clear that the crack bridges the 0° fibers and proceeds entirely through the matrix. Fiber bridging is a condition in which fibers do not break at the fracture surface. The fibers span the crack and continue to carry load while the fatigue loading continues. The fiber bridging of the matrix cracks have a profound effect on the fatigue life of MMCs (see Figure 40). As the cracks open in the matrix under the tensile loading, the fibers in the region along the crack take on the load. These fibers attempt to resist this tensile load and exert a force opposite to the direction of loading. Eventually these fibers will be overloaded and begin to break behind the crack. With the combination of tensile and compressive loads during each cycle, the damage to the fiber/matrix interface of fibers both in front of and behind the crack tip is sufficiently high that crack propagation is never halted, as seen in Figure 25.

Figure 41 clearly shows that the effect of the fiber bridging on the 0° fibers. These fibers clearly debonded prior to the initiation of the fatigue crack. Once the fatigue

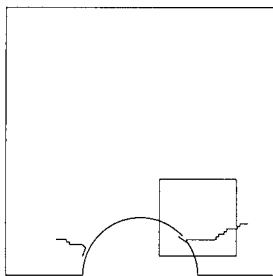
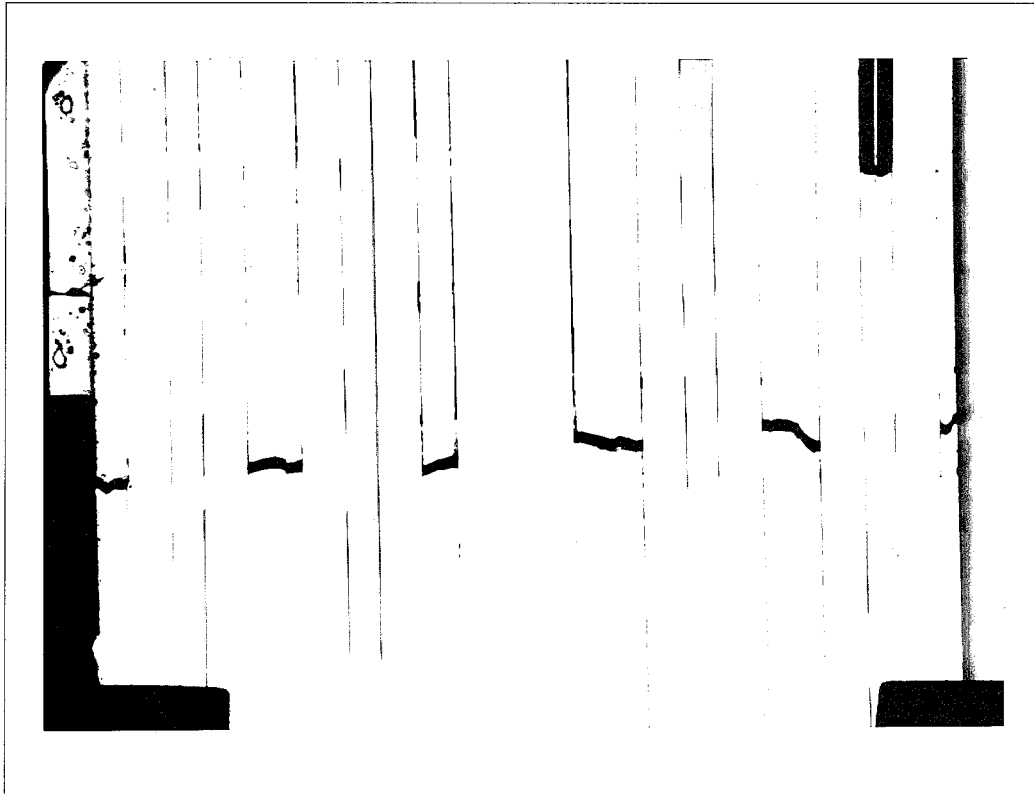
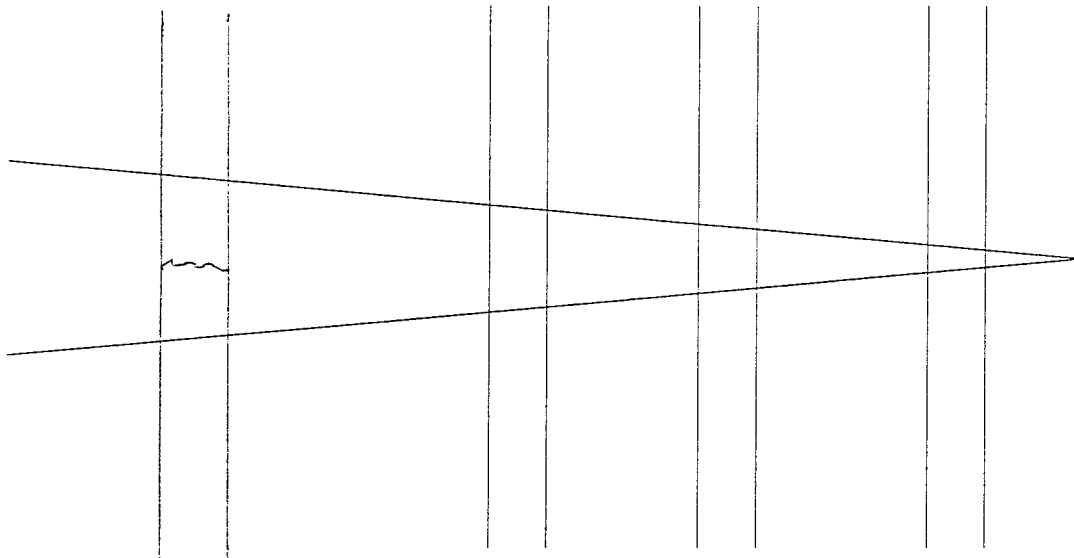


Figure 39. Fiber Bridging of Major Crack (120x)

BROKEN
FIBER

INTACT
FIBER

MATRIX
CRACK



TO HOLE

TO EDGE

Figure 40. Effect of Fiber Bridging

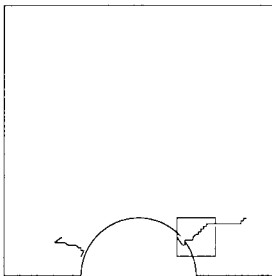
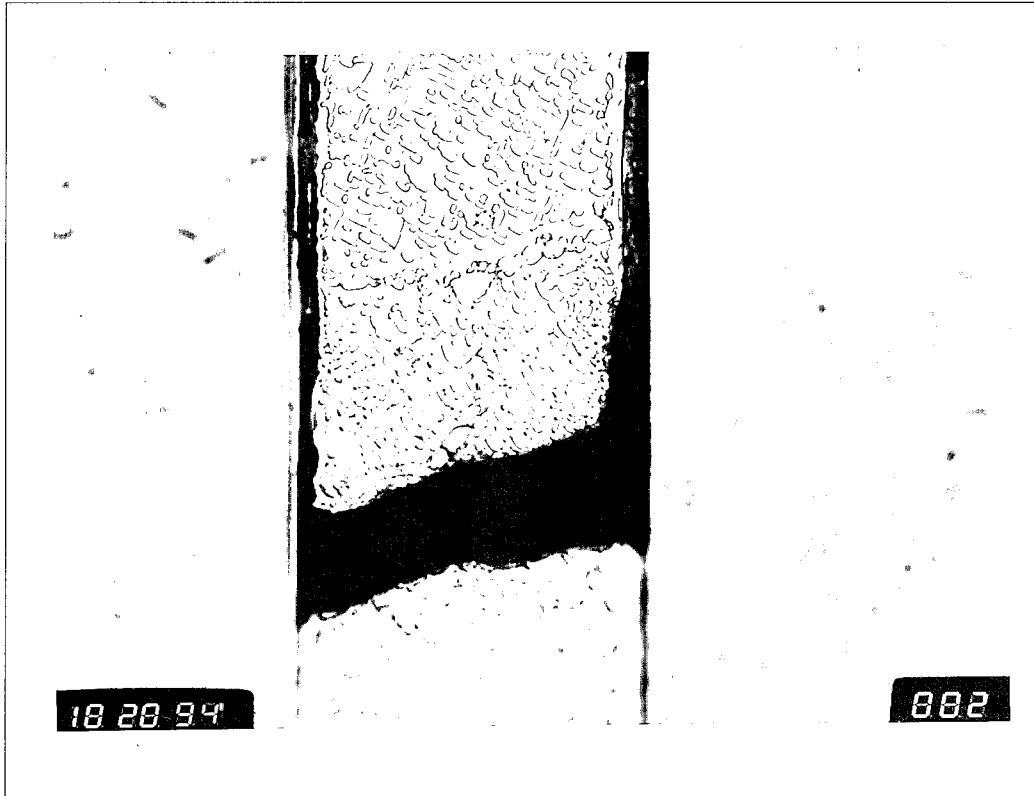


Figure 41. 0° Fiber Debond Causing Fiber Bridging of Major Crack (700x)

crack initiated, it progressed until it reached one of the debonded fibers, bridged the fiber, and continued on through the matrix.

To further determine how the cracks grew from the hole to the edge, the surface of the face-mounted specimen was etched to reveal slip bands. The presence of slip bands was not discovered, yet grain boundaries became quite clear. This revealed that the major cracks did not follow the grain boundaries, but exhibited transgranular behavior (see Figure 42).

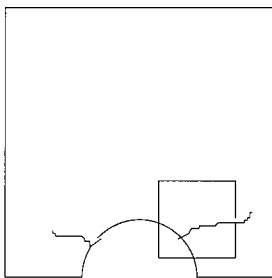
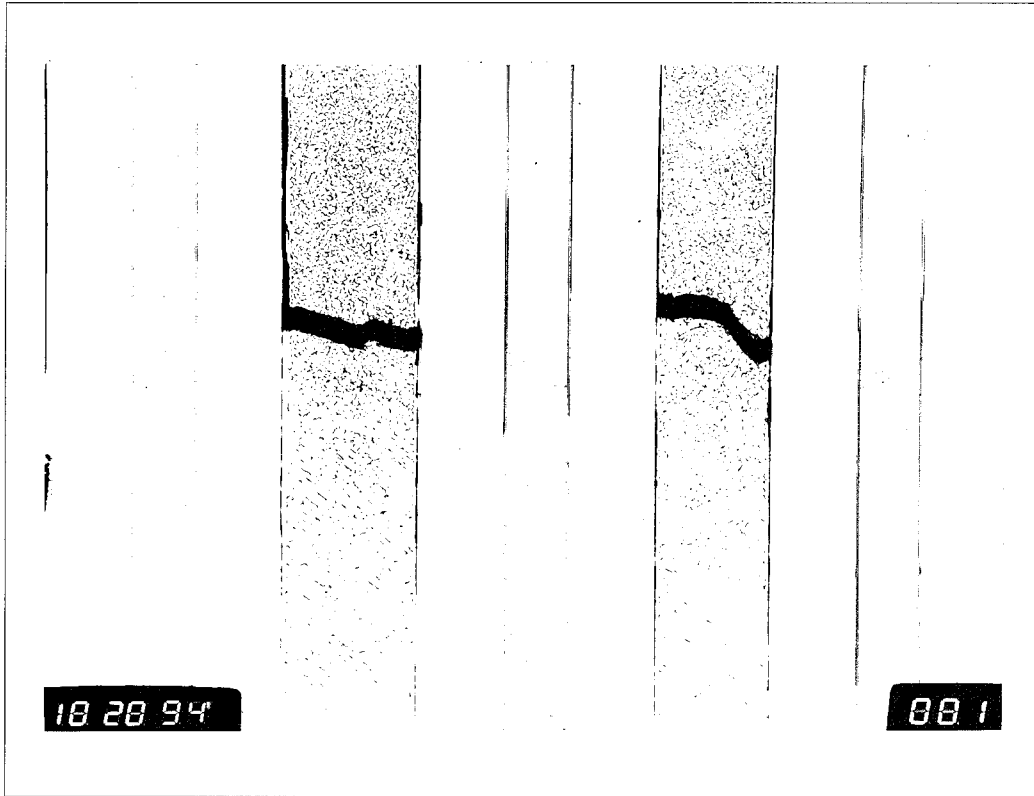


Figure 42. Transgranular Cleavage of Major Crack (220x)

V. Analysis and Discussion

Introduction

As mentioned previously, the aim of this study was to extend the existing experimental knowledge of fatigue damage mechanisms of an MMC by testing a tension-compression (TC) loaded, cross-ply lay-up with a notch (center hole) at the elevated temperature of 427 °C (800 °F). The previous chapter presented all the macromechanic and micromechanic results of this effort. This chapter will focus on a comparison with Baker's study (4), which incorporated the same set of conditions and material mentioned above but under tension-tension (TT) loading.

There has not been a clear cut manner in which to compare fatigue data collected under different R-ratios. However, Boyum's comparisons between tension-tension and tension-compression fatigue loading of an unnotched cross-ply laminate gave a useful insight about the type of criterion by which to compare tests with R-ratios of 0.1 and -1 (6:107-116). The most promising criterion was the *effective strain range* criterion, however the *maximum applied stress* criterion and *applied stress range* criterion were also employed and offered some insight.

This chapter will offer all three of the criteria for use in comparing this study's notched cross-ply TC tests with Baker's notched cross-ply TT tests. Also, a crack initiation and growth comparison will be made between the TC and TT notched specimens to determine if the different R-ratios and loading conditions have any effect on the initiation and progression of the cracks through the material.

Another comparison that will be made in this chapter is a fatigue life comparison on a stress range basis between this study, Baker's notched high temperature TT fatigue study (4), and Boyum's unnotched high temperature TT and TC fatigue results(6). It will be determined if the difference between fatigue lives for TT and TC of an unnotched specimen correspond to an equitable difference between fatigue lives for TT and TC of a notched specimen.

The attempt by researchers to determine mathematical models for fatigue crack growth has resulted in an analytical minefield. The main reason for this is that the assumption of similitude, that equal stress intensity will have equal consequences, breaks down when considering fatigue. Broek (5:266) states that "fatigue crack propagation is affected by an endless number of parameters, and the circumstances during the test will seldom be the same as in service." And *this* statement was made regarding the attempts to analytically characterize fatigue damage of monolithic materials, without even considering the added affects of transversely isotropic or orthotropic materials.

Despite this bleak outlook on the analytical realm of fatigue crack growth prediction in composites, there is a promising analytical tool that can determine microstresses within MMCs under thermomechanical and isothermal fatigue conditions. MMCs are multicomponent systems in which the dominant component, the fiber and matrix, changes with the loading condition, and also the elevated temperatures change the initial stress state of the components in the high temperature (HT) tests. This makes it useful to perform a *constituent stress* criterion which examines the microstresses in both the fiber and matrix. Since this data cannot be obtained experimentally, an analytical

technique is used. LISOL, the Laminate Inelastic Solver, which was developed by Robertson (18) at the Air Force Institute of Technology, is used to model the constituent microstresses in the TT and TC case for the notched cross-ply specimen.

Maximum Applied Stress Criterion

The maximum applied stress criterion typically works well for tension-tension data. However, it ignores the compression portion of the tension-compression fatigue cycle, and must be used with discretion.

Figure 43 shows the measured data from the TT and TC cases. It shows that on a maximum applied stress basis, the fatigue lives of the TT case were much longer than the TC case. It is apparent that despite the TT and TC specimens with equivalent maximum stresses experiencing the same tensile load, the compressive load of the TC specimens contributed to earlier failure.

This makes sense from a micromechanic standpoint when one considers the effect of compression on the notch. As the fatigue loading goes into the compression portion, the fibers around the hole will be compressed, further weakening their bonding with the matrix as well as aiding in the formation of the four fatigue cracks along the periphery of the hole.

Also, Boyum revealed that TC fatigue loading results in more damage to specimens than TT fatigue loading (6:109-111). The fiber/matrix debonding is more extensive in the TC case than in the TT case. In particular, there is higher degree of both 0° and 90° fibers debonding under TC loading than TT loading.

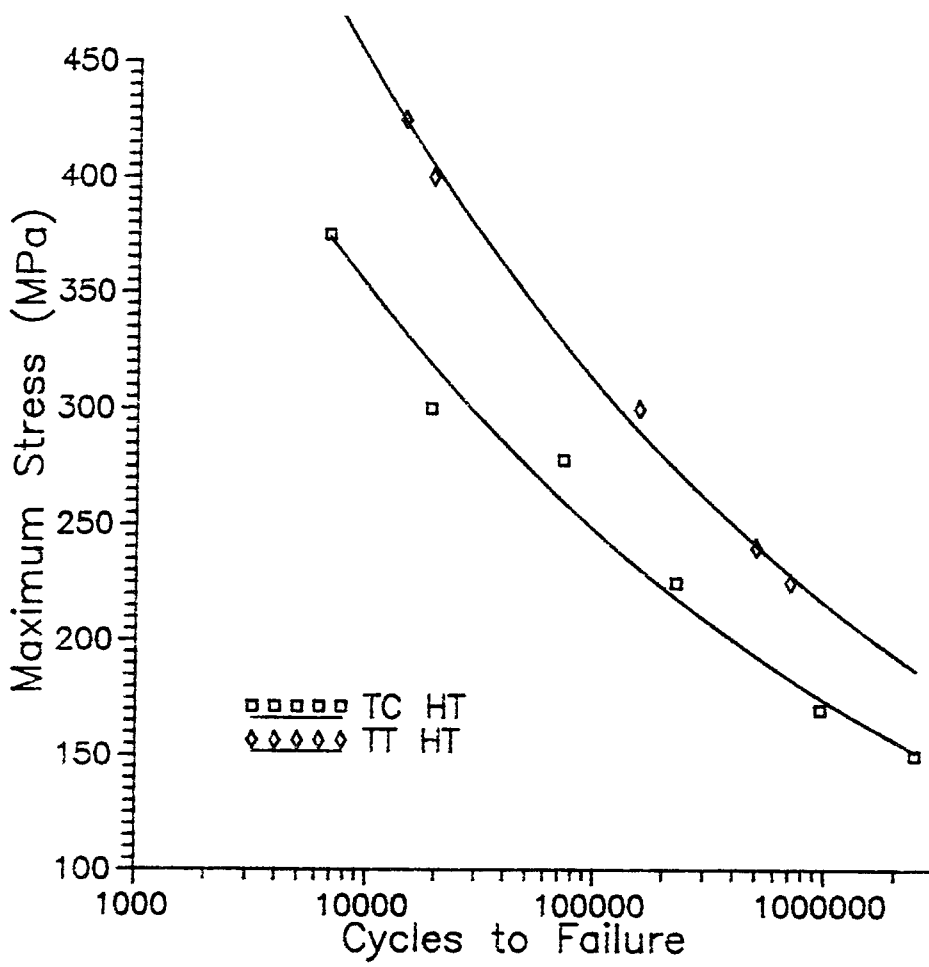


Figure 43. Maximum Stress S-N Curve: TC HT vs. TT HT

Stress Range Criterion

Figure 44 shows a distinct contrast with the results of the maximum applied stress criterion. This shows that on a stress range basis, the TT tests maintain longer fatigue lives than the TC tests. Therefore, despite the additional deformation mechanisms with the TC case, the compressive load comprising half of the load range in the TC case is not as detrimental as the load range comprised of tensile loads twice that value.

The tensile mean stress explains this difference. Mean stress is the average of the maximum and minimum stress:

$$\sigma_m = \frac{\sigma_{\max} + \sigma_{\min}}{2} \quad (2)$$

The TT specimens receive a positive, or tensile mean stress, while the TC specimens experience no mean stress. As discussed previously in Chapter 2, Verilli and Gabb (23) discovered that the mean stress has a substantial influence on the fatigue behavior, with tensile mean stresses being detrimental to fatigue life. Therefore, the tensile mean stress present in the TT tests have an adverse effect on the fatigue lives of the specimens when compared with the TC fatigue lives on the stress range basis.

The tensile mean stress for a notched specimen physically means that the four existing fatigue cracks in the TT specimen will remain open throughout the entire fatigue life. The TC specimens, having a tensile mean stress of zero, will be subjected to closure of the cracks for a significant portion of the fatigue lives.

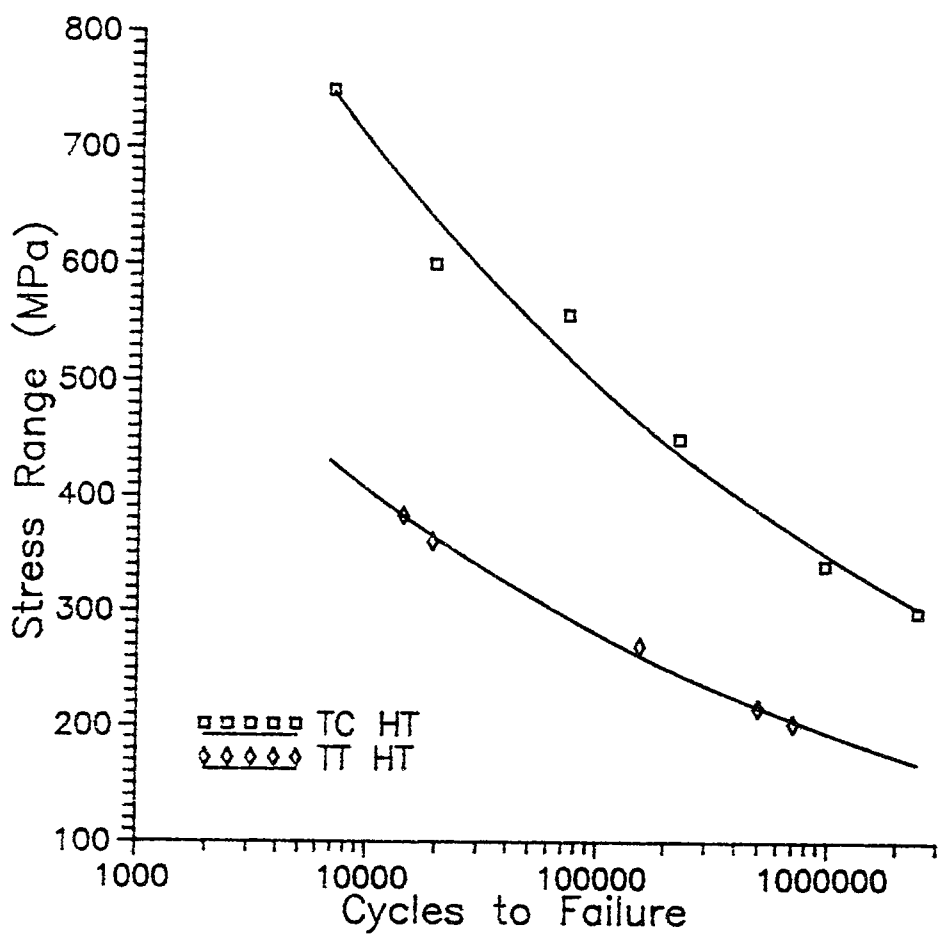


Figure 44. Stress Range S-N Curve: TC HT vs. TT HT

Effective Strain Range Criterion

Majumdar and Lerch (12) reported that the strain range criterion is a more fundamental parameter controlling the fatigue lives of MMCs. From their results they were able to conclude that the MMC fatigue life is strain range controlled, especially when considering the established fact that the fatigue life of metals is controlled by strain range.

Boyum (6:114-115) performed a full strain range criterion comparison between the unnotched cross-ply TT and TC fatigue conditions and found it to be an unsuitable measurement for comparison. That study found a better comparison could be made when one considered only the portion of the strain range which placed the matrix in tension. This was due to the fact that the cracks would only grow in the specimens under the tension portion of the fatigue loading, or approximately half the strain range of the TC tests.

Following the work of Elber (3) on determining an effective stress intensity factor, Boyum determined that the effective strain range, ϵ_{eff} , "can be estimated by dividing the strain range observed during the steady state strain portion of the fatigue life by a factor of two" (6:116). The effective strain range for the TC tests and the effective (which are also the full) strain range for the TT tests are plotted against the fatigue lives of each test in Figure 45. This clearly shows that the fatigue lives of the TC tests are shorter than the fatigue lives of the TT tests even when considering this effective strain range. This yields a better comparison at higher strain (i.e. stress) values than the stress range or maximum applied stress criteria, however it does not provide a good correlation between these

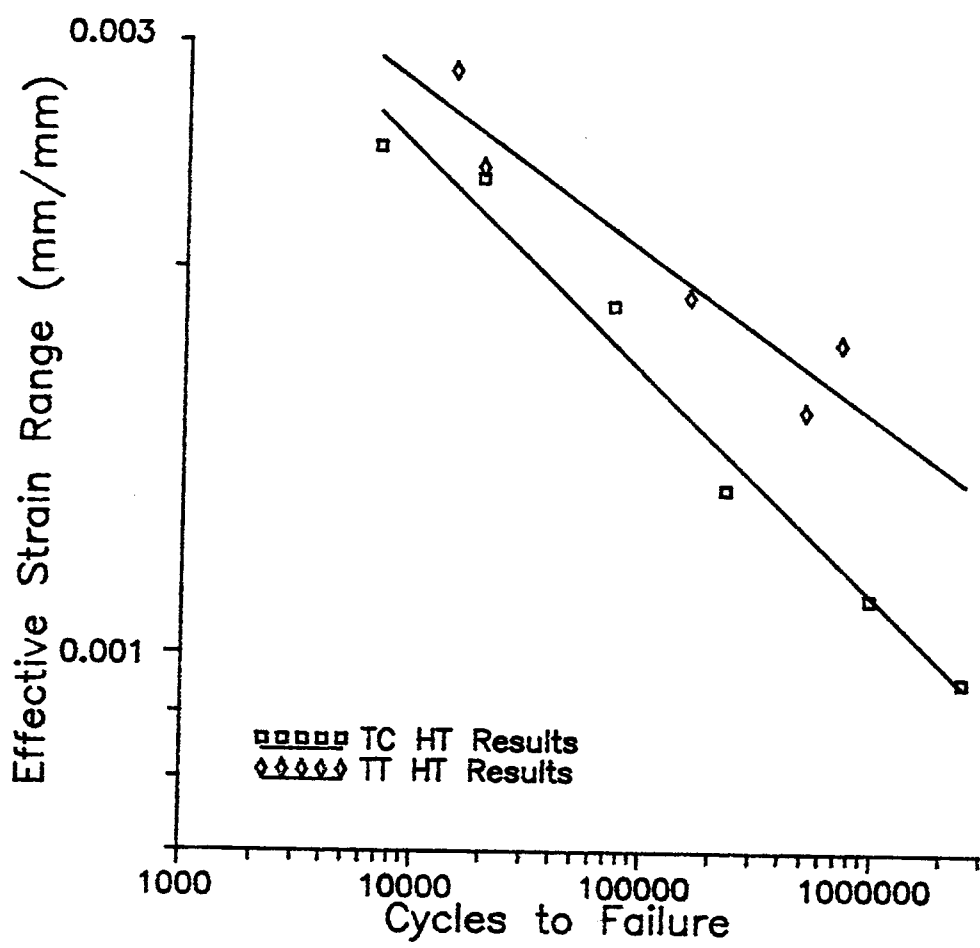


Figure 45. Effective Strain Range S-N Curve: TC HT vs. TT HT

cases (TT vs. TC) at lower strain (i.e. stress) values. This suggests that there is need for further study, such as the use of Goodman's diagram. This will require tests at different stress ratios involving different combinations of compression and tension loadings.

Crack Initiation and Growth Comparison

With crack propagation being the dominant damage mechanism during the fatigue loading, it is important to compare the experimental measurements of crack initiation and growth for the TT and TC notched tests. Crack initiation measurement is difficult by the fact that the exact cycle to initiation in both the TT and TC case is not known with absolute certainty. As mentioned previously in Chapter 4, face replicas were used to determine crack initiation by using the Scanning Electron Microscope (SEM), and there was often a long period of cycles when a replica was taken and no crack was observed, and the next replica when a crack was finally discovered. This study will present a method to determine whether the given value of the cycle to crack initiation is valid before making the crack initiation comparisons between the TC and TT cases.

The first step in this method is to take the number of the cycle at which crack initiation was observed and subtract the previous cycle at which an observation was made and no crack was found. This value, c_b , is the crack initiation bandwidth, and gives the number of cycles which were run on the specimen during which the crack actually initiated.

$$c_b = \text{observed cycles to init.} - \text{previous observed cycle} \quad (3)$$

Looking simply at this number is not necessarily a good parameter for determining the validity of the cycle to crack initiation value. For instance, if the crack initiation bandwidth is 10,000 cycles, which may seem like a long time in which a crack could have initiated, this may actually be a small amount of cycles between observations if that particular test had a fatigue life of 2 million cycles.

Therefore, it is necessary to normalize the crack initiation bandwidth with respect to the fatigue life of the test. This normalized crack initiation bandwidth, c_{nb} , is found by dividing the crack bandwidth for a particular test by that test's number of cycles to failure multiplied by 100%:

$$c_{nb} = (c_b / \text{cycles to failure}) \times 100\% \quad (4)$$

If the normalized crack initiation bandwidth was greater than 5% it was considered that there had been too long of an unobserved period of cycles in which the crack could have initiated, and that test was not considered to have an accurate measurement for the value of observed cycles to initiation. Table 3 shows a chart to assess whether the cycles to crack initiation value is acceptable for the TC case of this study, and Table 4 shows the same for Baker's TT study.

Table 3. TC HT: Crack Initiation Cycle Value Validity

Maximum Stress (MPa)	c_b	Cycles to Failure	c_{nb} (%)	Crack Initiation Value Valid (y/n)
150	90,000	2,451,504	3.67	yes
170	11,000	958,615	1.15	yes
278	1000	72,033	1.39	yes
375	1000	6716	14.89	no

Table 4. TT HT: Crack Initiation Cycle Value Validity

Maximum Stress (MPa)	c_b	Cycles to Failure	c_{nb} (%)	Crack Initiation Value Valid (y/n)
225	10,000	703,968	1.42	yes
240	5000	494,234	1.01	yes
300	2000	155,139	1.29	yes
400	2000	18,940	10.56	no
425	2000	14,202	14.08	no

Once the validity of each tests with reasonable crack initiation cycle values for both the TC and TT tests has been established, these values can be compared between the two cases. From this comparison, it will then be determined which case led to an earlier formation of cracks along the periphery of the hole. For the sake of comparison, the value of the cycle to crack initiation will be normalized with respect to fatigue life. This means the number of cycles to crack initiation will be divided by the number of cycles to failure for that test and will be multiplied by 100%.

Table 5 shows the following for the TC tests in which the measured cycle to initiation value was acceptable: the maximum stress, the observed cycle to initiation, the number of cycles to failure, and the percentage of the fatigue life until the crack initiated. An average value of the percentage of fatigue life until crack initiation is also given.

Table 6 shows the same for Baker's TT case.

Table 5. TC HT: Percentage of Life Until Crack Initiated

Stress Level (MPa)	Cycles to Initiation	Cycles to Failure	% of Life to Crack Initiation
150	100,000	2,451,504	4.08
170	11,000	958,615	1.15
278	1000	72,033	1.39
Avg.			2.21

Table 6. TT HT: Percentage of Life Until Crack Initiated

Stress Level (MPa)	Cycles to Initiation	Cycles to Failure	% of Life to Crack Initiation
225	50,000	703,968	7.10
240	25,000	494,234	5.06
300	12,500	155,139	8.06
Avg.			6.74

It can be seen through comparing Table 5 and Table 6 that the cracks initiate earlier in the fatigue life of the TC specimens than the TT specimens. This indicates that the compression portion of the loading of the TC case adds a higher degree of damage within the specimen to initiate cracks at an earlier stage than cracks from a specimen strictly under tension-tension fatigue loading.

It is also important to compare the progression of the cracks for the TT case and the TC case from the time of initiation until fracture of the specimen. Figure 46 shows a typical comparison for the TC test of ± 170 MPa (stress range of 340 MPa), and Baker's TT test (4:81) of maximum stress 300 MPa. It is clear that the major crack under TC progresses more quickly over the fatigue life of the specimen than the major crack under TT loading.

An important distinction can be made between the progression of the major crack for each case. The TC test shows a decline in the crack growth rate but no halting of the crack growth over the life of the specimen, while the TT test shows that the crack stopped growing for a portion of the fatigue life soon after initiation. It was explained earlier in Chapter 4 that the fiber bridging of the major cracks plays a role in this condition.

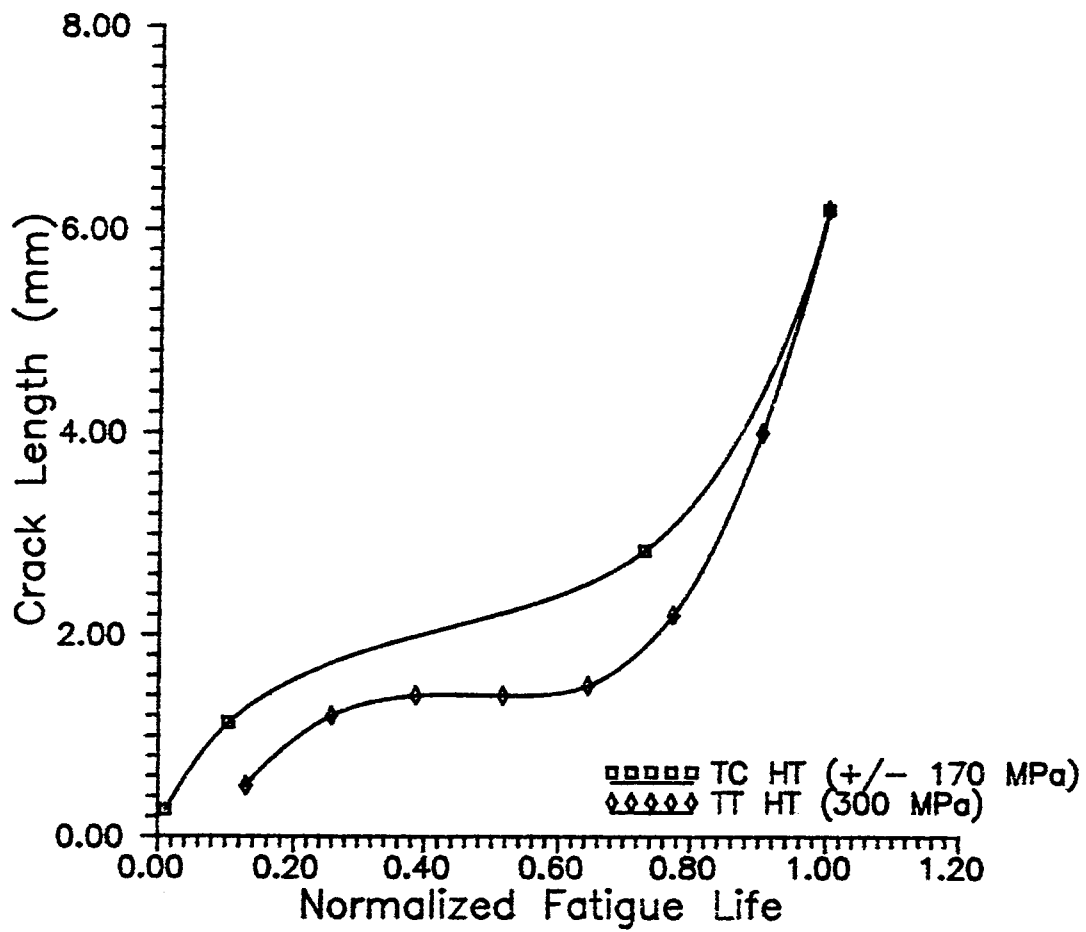


Figure 46. Crack Growth vs. Normalized Fatigue Life Comparison: TC HT vs. TT HT

For the TC fatigue loading condition, the fibers, as explained earlier in this chapter, experienced a greater degree of damage than the TT case, i.e. more debonding of all fibers at the fiber/matrix interface. As the crack opens under tension in the TC case, the fibers behind the crack tip have been bridged and take on the tensile load. Yet these fibers are more damaged than fibers in a TT specimen, due to their cycling under both tension and compression. The damaged fibers in the TC case exert a force to oppose the tensile load, and behind the crack tip these fibers begin to become overloaded and break (refer to Figure 40). As they break, the cracks continue to grow, placing more of the load on the damaged fibers, again causing more fibers to break. This accounts for the reason that the cracks continually grow in the TC fatigue loading case.

Figure 47 shows a comparison of the reduction of the normalized stiffness over the fatigue life of a notched TC HT test and a notched TT HT test with both having a similar stress range. The stiffness degradation gives a general indication of the amount of damage the composite is experiencing, i.e. a greater reduction in stiffness indicates more damage is accumulating within the material (refer to the macromechanic considerations section of chapter 4 for greater detail on this). It is seen in Figure 47 that the TC cycling has a higher amount of stiffness degradation, which indicates a greater amount of damage within the specimen. This aids in the explanation of the faster crack growth rate for the TC case over the TT case shown in Figure 46.

It would appear that the higher rate of crack initiation and growth, as well as the increased amount of damage, in the TC case is the dominant factor in their reduced fatigue lives as compared with the TT case. A greater amount of damage is evident in the

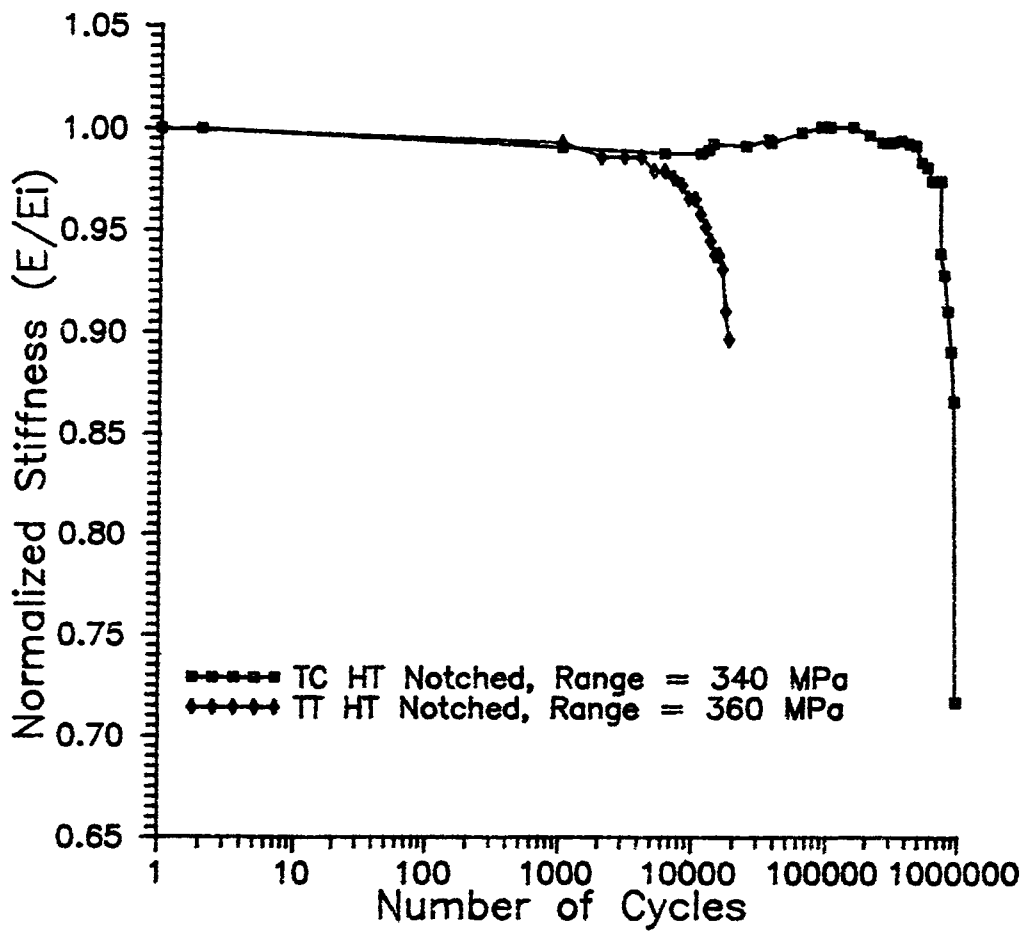


Figure 47. Stiffness Response Comparison: 170 TC HT vs. 400 TT HT

TC tests, such as the higher degree of fiber breaks found in TC specimens in regions away from the hole as compared with TT specimens. However, it is the growth of the major cracks that serves as the most important damage mechanism concerning the life of the specimen. As shown in this section, the TC tests initiated cracks earlier and progressed faster than the major cracks within the TT specimens. This corresponds with and corroborates the findings earlier in this chapter; for a given stress level, the fatigue lives of the TC notched cross-ply laminate will be shorter than the TT notched cross-ply.

Notched and Unnotched Specimen Fatigue Life Comparisons

In addition to comparisons between the tension-compression (TC) and tension-tension (TT) fatigue loading conditions of notched specimens, it is also important to make comparisons between the response of notched and unnotched specimens. These comparisons will be made in the form of a fatigue life using both the maximum applied stress value and the stress range basis.

Figures 48 and 49 show the fatigue lives of the high temperature (HT) TC notched specimens and Boyum's results for the high temperature TC unnotched specimens (6:93). It is clear that the notched specimens had shorter fatigue lives than the unnotched specimens when considering both maximum stress and the stress range. Thus, the addition of a center hole has a significant effect on the fatigue life of a cross-ply laminate lay-up MMC at high temperature.

Figure 50 shows a comparison of the fatigue lives of this study's TC HT notched specimens, Baker's TT HT notched specimens (4:38), and Boyum's TC and TT HT

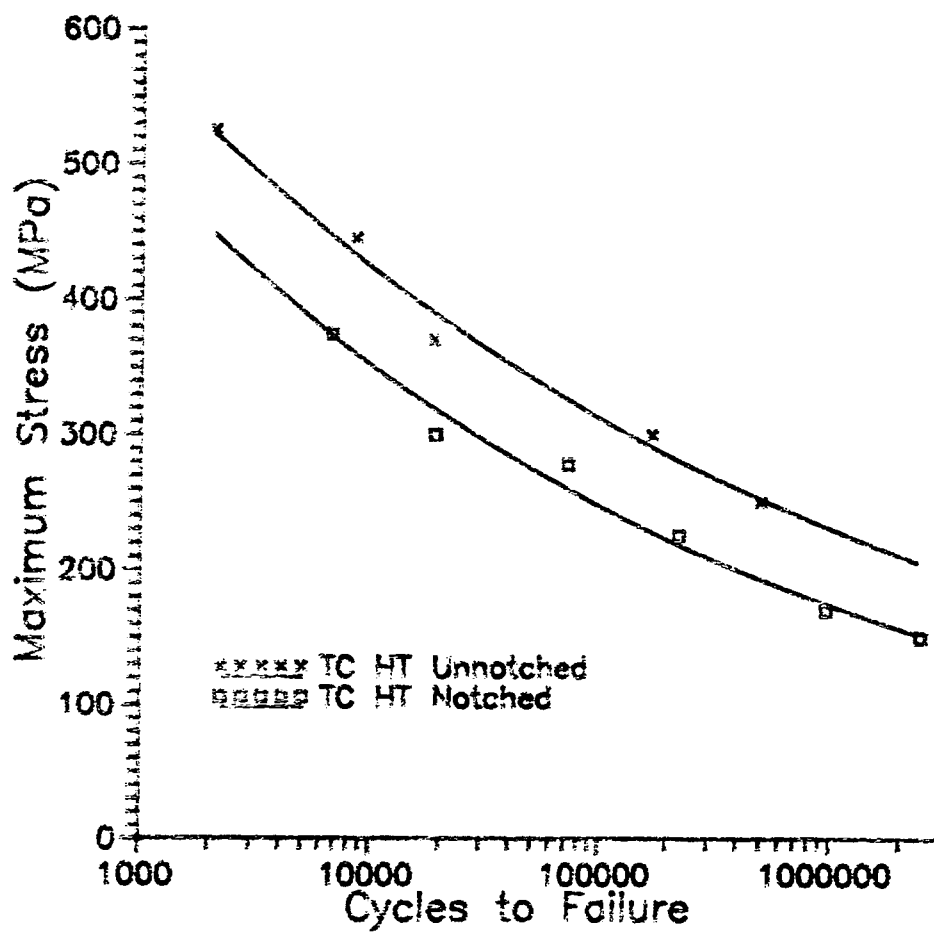


Figure 48. Maximum Stress S-N Curve: TC Notched vs. TC Unnotched

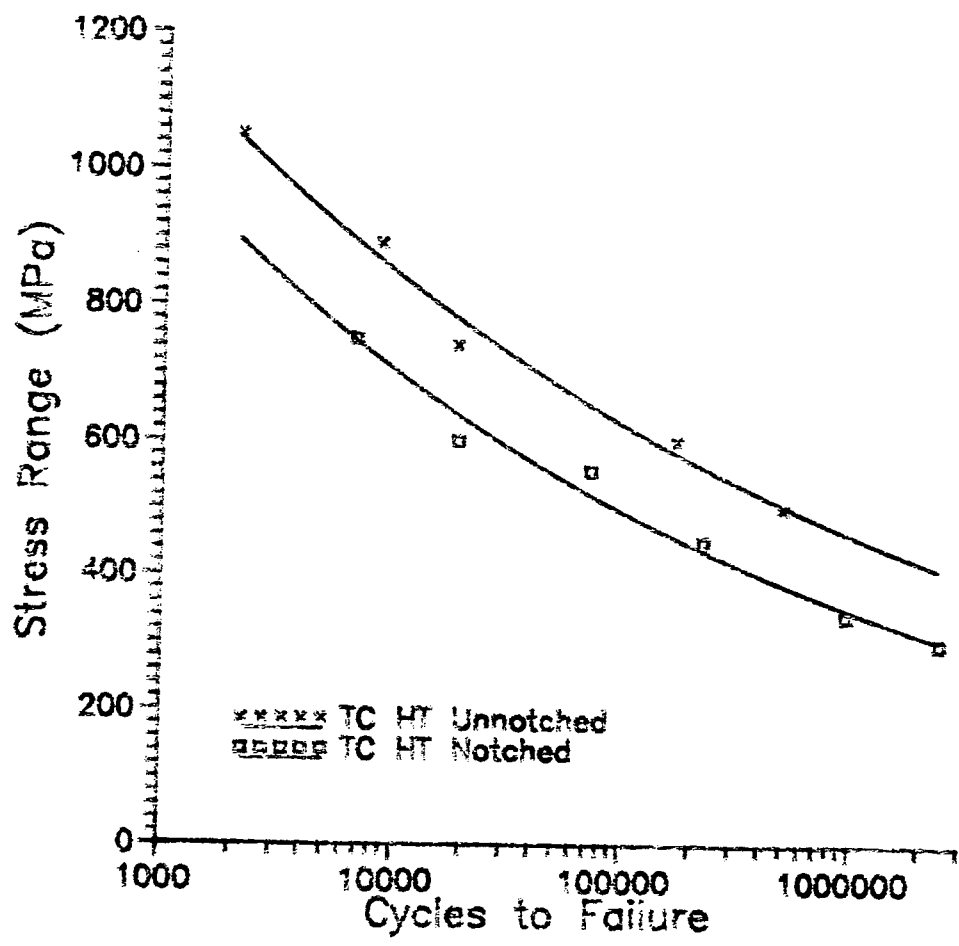


Figure 49. Stress Range S-N Curve: TC Notched vs. TC Unnotched

unnotched specimens (6:93). This shows that the fatigue condition with the shortest fatigue life at a particular stress level is the TC HT case which was investigated in this study. Therefore, on the maximum applied stress basis, the combination of tension and compression loading and the addition of a center hole plays a major role in the reduction of the fatigue life of this material.

Figure 51 presents a comparison of the fatigue lives of all four cases on a stress range basis. This graph gives a unique insight into the various conditions placed on this material. On the stress range basis, this figure shows that the addition of the notch has no effect on the fatigue life of the material if the cyclic loading condition at high temperature is tension-tension fatigue. However, the addition of the notch under fully reversed tension-compression at elevated temperature makes a clear difference in reducing the material's fatigue life.

As mentioned earlier in this chapter under the stress range criterion section, the mean stress has an important role in the fatigue life, with tensile mean stresses detrimental and compressive mean stresses beneficial to fatigue lives of specimens. Figure 51 shows on a stress range basis that the two TT cases (both notched and unnotched), which maintain positive or tensile mean stresses on the material, maintain the lowest fatigue lives at a given stress level. The two TC cases, which have zero mean stress, show that the effect of the notch makes a difference by reducing the fatigue life of the material as compared with unnotched material.

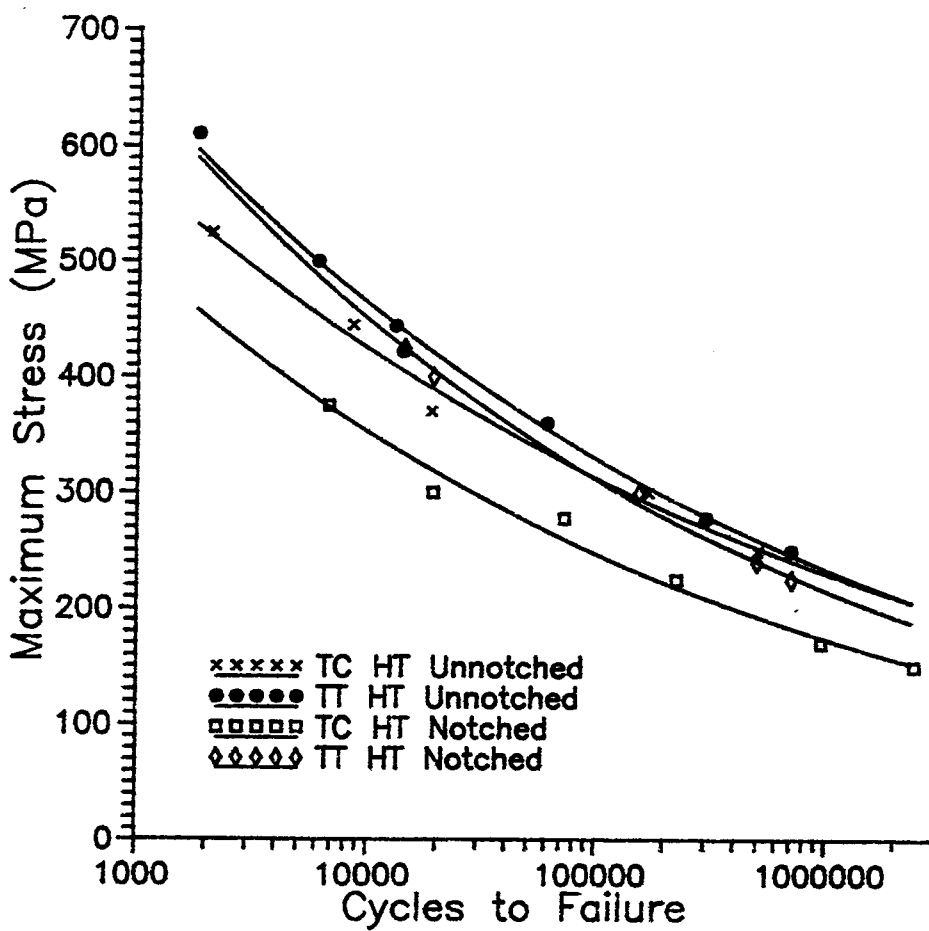


Figure 50. Maximum Stress Comparison of Fatigue Lives, Notched and Unnotched

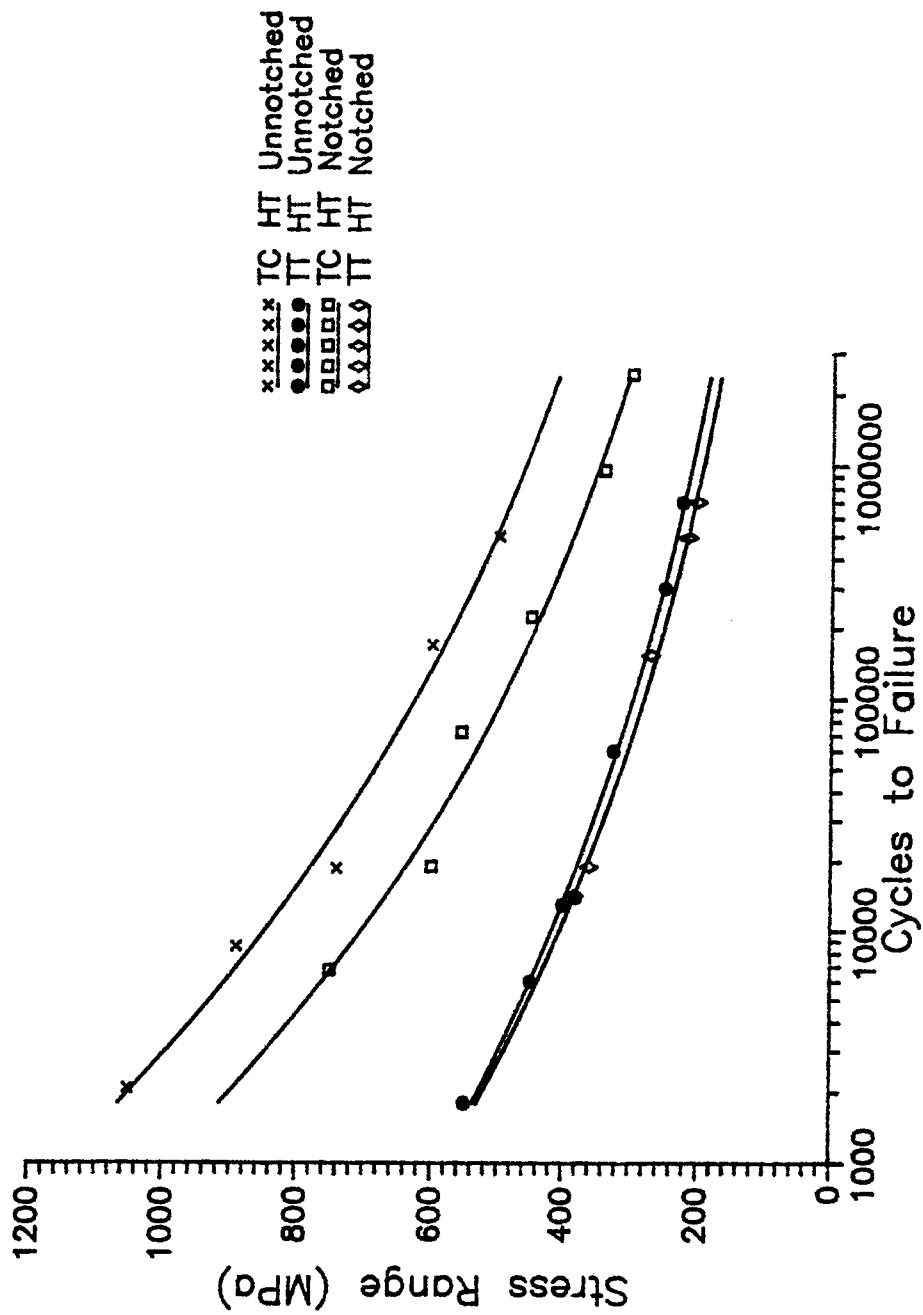


Figure 51. Stress Range Comparison of Fatigue Lives, Notched and Unnotched

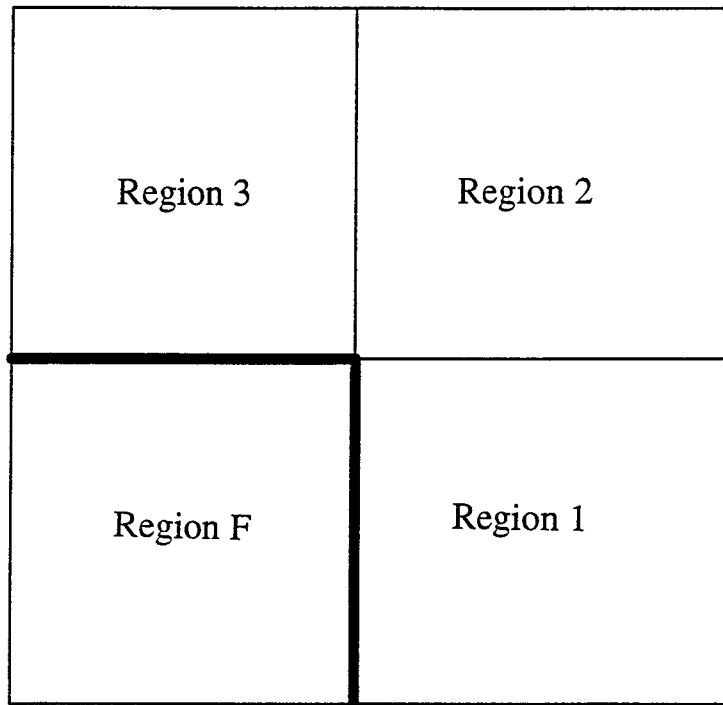
LISOL Analysis

LISOL is a FORTRAN computer code which was developed by Robertson (18) to perform a micromechanical analysis for thermoviscoplastic behavior of fiber-reinforced MMCs. The code uses a multi-cell model composed of a set of micromechanics equations that is based on the relaxation of the coupling effect between the normal and shear stresses for viscoplastic matrix materials.

Figure 52 shows the unit cell used in the LISOL program and its subsequent regions. Region 1, 2, and 3 are all matrix regions, and Region F is the fiber portion. Using the complete set of micromechanics equations found in (18), the program determines the microstresses for each of these regions for specified thermomechanical or isothermal fatigue conditions. The microstresses can also be obtained for each ply as well as the interface regions between the fiber and matrix.

The load history can be inputted by the user as a file or directly by typing in values for the length of time interval, temperature, loads in the global x, y, and z axes, and the increment between steps. For LISOL to give accurate microstress values, the beginning of the load history must account for the residual stresses due to the coefficient of thermal expansion mismatch between the matrix material and fiber that result from manufacturing of the material (see Appendix B for more details).

As seen in Chapter 4 under the stress-strain curves section, the TC case finds the tension and compression portions of the stress-strain curves to deviate as cracks are initiated and begin to progress through the specimen. However, Baker found that the TT case exhibited a linear response throughout the entire fatigue life of the tested specimens



————— = Fiber/Matrix Interface Regions

Region 1 = Matrix Region 1

Region 2 = Matrix Region 2

Region 3 = Matrix Region 3

Region F = Fiber Region

Figure 52. LISOL Unit Cell Model

(4:90). Therefore, it was decided that the LISOL program should be run for only 10 fatigue cycles (1 second at the frequency of 10 Hz), while the TC stress-strain curve can still be considered linear. To justify this linearity assumption over the entire stress-strain curve for the early cycles of the TC case, a linear regression was performed over the entire stress-strain curve of cycle 1 for the ± 225 MPa test. Stiffness values were 2.09% apart over the entire range of the curve, well within a range that validates the linearity assumption.

LISOL, as yet, does not have the capability of handling various geometries such as the effects of a center hole notch. Therefore, another assumption had to be made regarding the stress values for the fatigue tests. A simple fracture mechanics approach was used to handle this difficulty by multiplying stress values by a finite width stress concentration factor. Using the qualitative observation that crack growth progressed in a brittle cleavage region with little matrix plasticity (as revealed in the fractographic analysis section of Chapter 4) and the quantitative observation that no crack initiated within the first ten cycles of any test, the assumption is made that the finite width stress concentration factor initially developed by Lekhnitskii can be used to aid in the determination of stress levels, despite the fatigue loading of the tests.

To find this value, it is first necessary to determine the stress concentration factor for an infinite plate, K_t^∞ , as defined by:

$$K_t^\infty = 1 + \sqrt{\frac{E_L}{G_{LT}} - 2\nu_{LT} + 2\sqrt{\frac{E_L}{E_T}}} \quad (5)$$

where E_L is the longitudinal modulus, E_T is the transverse modulus, G_{LT} is the shear modulus, and ν_{LT} is the Poisson's ratio of the composite laminate. The next step is to determine the finite width correction factor through the equation:

$$\alpha = \frac{2 + (1 - \frac{d}{W})^3}{3(1 - \frac{d}{W})} \quad (6)$$

where d is the hole diameter and W is the width of the specimen. The finite width correction factor, α , is then multiplied by the stress concentration factor for an infinite plate, K_t^∞ , to obtain the finite width stress concentration factor, K_t . This is the value that is multiplied to the stress level of the fatigue test to determine the value that is inputted into LISOL to account for the effect of the center hole.

For the sake of comparison, the material properties chosen for this study were the same as those found by Baker in the TT study. These laminate properties were determined by Baker using the Metal Matrix Composite Analyzer, METCAN, developed by Hopkins and Murthy at NASA's Lewis Research Center (10). The values obtained were $E_L = 153.9$ GPa, $E_T = 153.9$ GPa, $\nu_{LT} = .2339$, $G_{LT} = 17.55$ GPa, and an ultimate strength of 704.0 MPa. Using these values as well as the dimensions given in Chapter 3 (hole diameter of 0.3175 cm and width of 1.905 cm), it was determined that the finite width stress concentration factor for the fatigue tests was $K_t = 3.31$.

Having determined all the necessary values, the cases of the notched cross-ply high temperature TT and TC fatigue were run on LISOL. Table 7 shows a comparison of the stress range felt by the matrix for each test of the TT and TC loading conditions. The

matrix microstress range was found 1 second into the fatigue cycle (or 10 cycles at a frequency of 10 Hz).

Table 7. Matrix Microstress Range Comparison: TC HT vs. TT HT

TC Max Applied Stress (MPa)	TC Matrix Stress Range (MPa)	TT Cycles to Failure	TT Max Applied Stress (MPa)	TT Matrix Stress Range (MPa)	TT Cycles to Failure
150	641.99	2,451,504	225	499.78	703,968
170	737.69	958,615	240	536.09	494,234
225	1006.32	225,785	300	681.21	155,139
278	1284.28	72,033	400	921.68	18,940
300	1362.30	18,925	425	981.84	14,202

As can be seen in Table 7, comparable maximum applied stress values give significantly different matrix stress ranges between TT and TC loading. For instance, the TC test with a maximum applied stress of 225 MPa showed a matrix stress range in the region around the hole of 1006.32 MPa, while the TT test with maximum applied stress of 225 MPa gave a matrix stress range of 499.78 MPa (approximately half the value of the TC case). This reinforces the experimental findings discussed earlier that the TC cases initiated cracks earlier than the TT cases. The compressive portion of the TC loading added more overall damage to the matrix in the region around the hole than TT loading, hence initiating cracks earlier and allowing the cracks to propagate faster.

Figures 53 and 54 show the comparisons of the maximum applied fiber and matrix microstresses for the TC HT and TT HT load cases. One must keep in mind that these figures show the maximum fiber and matrix stresses, that were determined from LISOL for a period of only *ten* cycles, and are being plotted against the *overall* fatigue lives (cycles to composite failure) for their respective tests. The comparisons in these

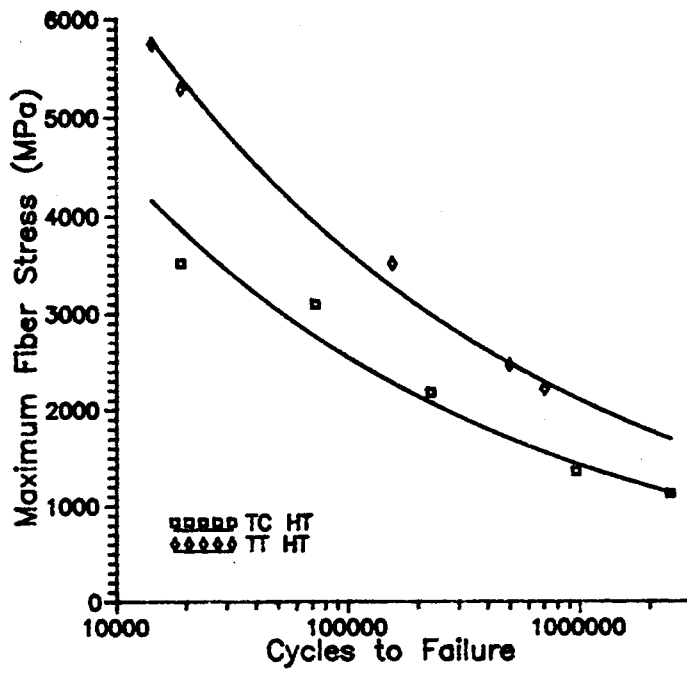


Figure 53. Maximum Fiber Stress vs. Fatigue Life: TC HT vs. TT HT

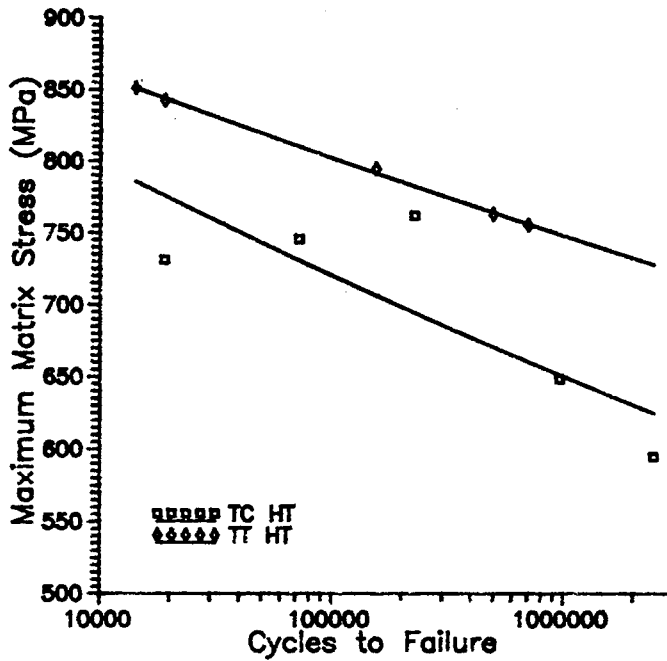


Figure 54. Maximum Matrix Stress vs. Fatigue Life: TC HT vs. TT HT

figures are made with the intent of determining whether the microstresses are a suitable parameter in determining the fatigue lives of an MMC under various loading conditions. Since the finite width stress concentration factor was used in LISOL to account for the center hole, the microstress values represent only stresses in the fiber and matrix in the immediate region around the hole. The two figures gave results in a similar manner as the comparisons of the actual experimental data. On the maximum fiber and matrix stress basis, the TT fatigue lives are longer than the TC lives.

A fiber and matrix stress range criterion also yields a similar comparison to the experimental results, shown in Figures 55 and 56. On a stress range basis, the TC specimens maintain longer lives than the TT specimens.

Boyum made the same comparisons of microstresses between TT RT and TC RT for an unnotched cross-ply using METCAN (6:129-131). The trends between the cases of unnotched TC and TT gave the same results as those shown in this study using LISOL. It is clear that LISOL is an effective tool when evaluating the microstresses of an MMC under isothermal fatigue conditions, however it does not appear to offer an accurate measure by which to compare data collected at R-ratios of 0.1 and -1.

A microstress comparison was also made in this study between Boyum's results for the unnotched TC HT fatigue tests (6:93) and this study's notched TC HT case using the fiber and matrix microstresses given by LISOL (see Figures 57 through 60). In this comparison, the notched TC condition microstresses were plotted against cycles to crack initiation. The reason for this was that the notched case used a stress concentration factor to account for the hole, and the resulting microstress values represented only the stresses

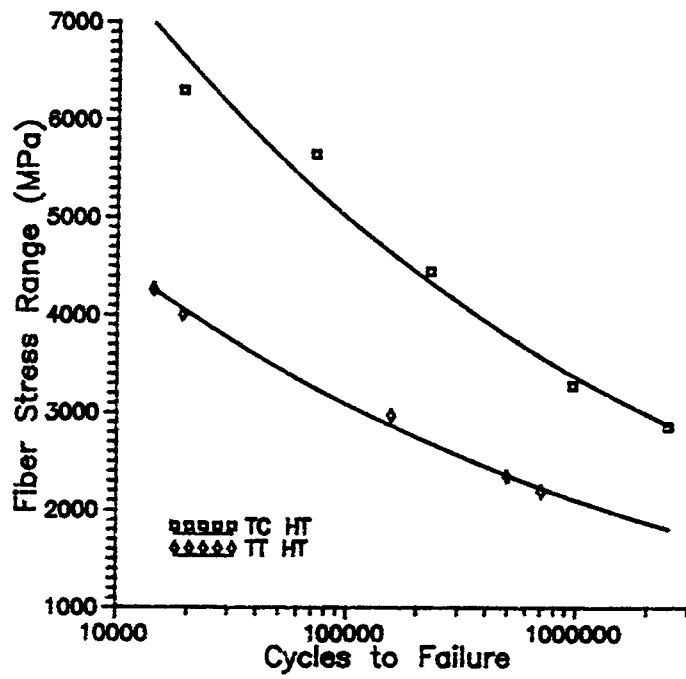


Figure 55. Fiber Stress Range vs. Fatigue Life: TC HT vs. TT HT

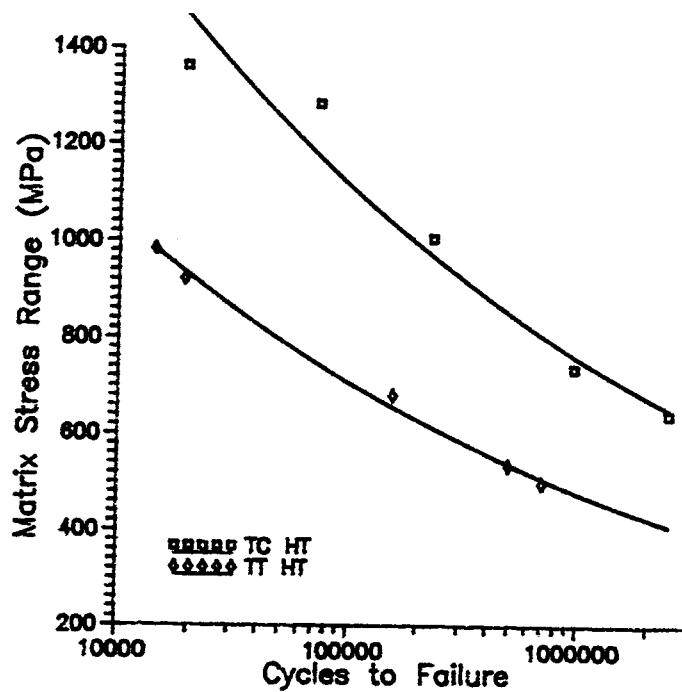


Figure 56. Matrix Stress Range vs. Fatigue Life: TC HT vs. TT HT

in the fiber and matrix in the region around the hole. Failure in the region directly around the hole occurred when a matrix crack initiated.

For the unnotched condition, the microstresses represent stress in the fiber and matrix throughout the entire specimen. Hence, failure of the specimen was when fracture of the specimen occurred. Therefore, the microstresses for the unnotched condition were plotted against the fatigue life of each test.

Figures 57 through 60 show that the microstresses for both the fiber and matrix were much higher for the notched condition than the unnotched condition when considering maximum stress values and stress ranges. This was expected due to the stress concentration effects of the center hole.

The microstress calculations made for the notched TC HT tests gave accurate indications as to the value of fiber and matrix stresses around the region of the hole early in the fatigue life of the material. However, none of the microstress comparisons appeared to offer a valid parameter in determining the fatigue life of tests under different R-ratios and notched/unnotched conditions. Further work needs to be done, such as use of Goodman's diagram as well as analytical studies to determine equations that account for the stresses exhibited by unbroken bridged fibers as they take on tensile and compressive loads.

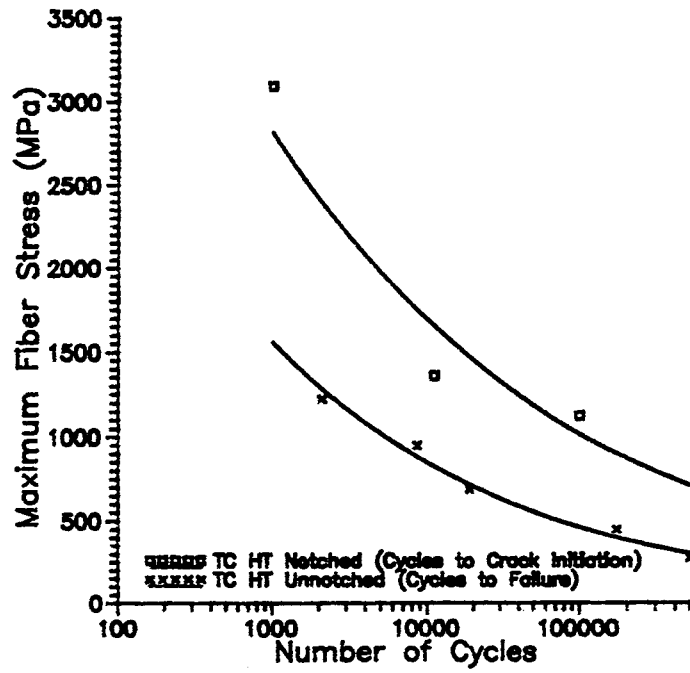


Figure 57. Maximum Fiber Stress vs. Cycles: Notched TC vs. Unnotched TC

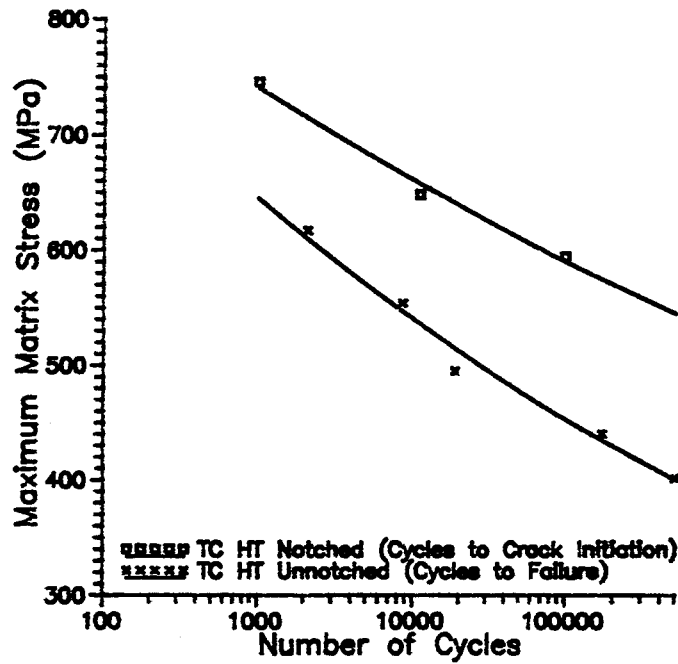


Figure 58. Maximum Matrix Stress vs. Cycles: Notched TC vs. Unnotched TC

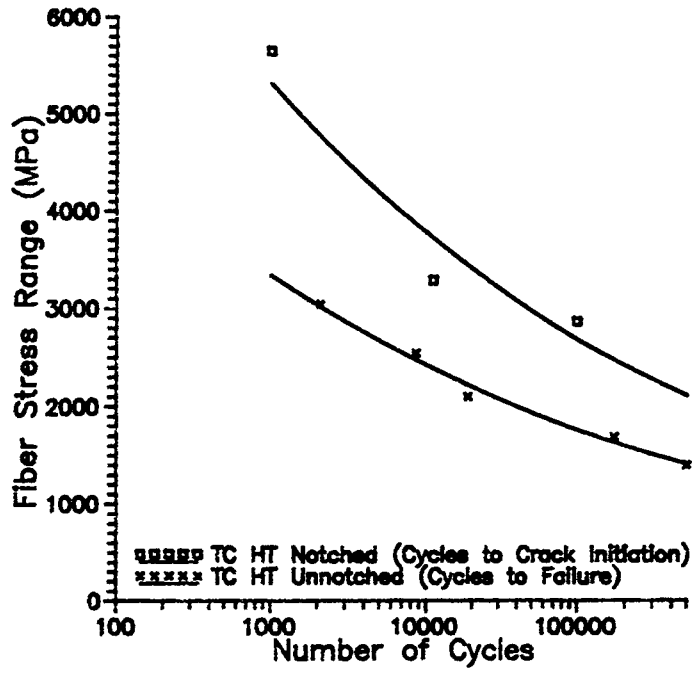


Figure 59. Fiber Stress Range vs. Cycles: Notched TC vs. Unnotched TC

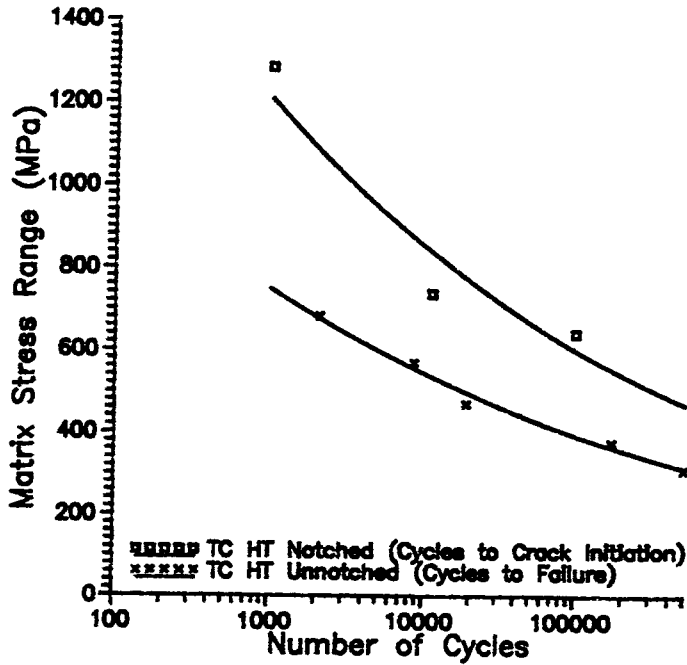


Figure 60. Matrix Stress Range vs. Cycles: Notched TC vs. Unnotched TC

VI. Conclusions and Recommendations

The purpose of this study was to further the existing knowledge of behavior and damage mechanisms for SCS-6/Ti-15-3 under fatigue loading conditions. In particular, this study focused on the tension-compression loading of a notched (center hole) MMC at an elevated temperature of 427 °C at a frequency of 10 Hz.

Replication in conjunction with fractographic and metallographic analysis of failed specimens showed a clear picture of the crack progression and the damage mechanisms. This study found that four cracks developed around the periphery of the hole. Two of these became dominant and proceeded through to the edge of the specimen, causing fracture. The crack proceeded through a brittle cleavage region in the matrix until a critical length was reached, at which time the crack grew catastrophically through the specimen causing a ductile region and matrix necking around the fibers.

The effect of the tension-compression fatigue condition on fatigue life was determined by making a comparison between fatigue lives from this study's tension-compression results and tension-tension fatigue data obtained by Baker (4:38). It was found that on the maximum applied stress basis, the fatigue lives of the tension-compression specimens were much shorter than the fatigue lives of the tension-tension specimens. This was due in some part to the additional damage from the compression portion of the loading that included increased fiber breaks and a higher degree of reaction zone cracks. Yet the most important factor in the lower fatigue lives of the tension-

compression case was the earlier initiation of the cracks along the periphery of the hole and the higher crack growth rate over the life of the specimen.

A comparison of fatigue lives was performed based on the effective strain range, which is one-half of the strain range for the tension-compression case and the full strain range of the tension-tension case. This effective strain range criterion showed that the fatigue lives of the tension-compression tests were shorter than the tension-tension tests.

A comparison was also made between the fatigue lives of the high temperature tension-compression notched specimens used in this study, high temperature tension-tension notched specimens from Baker's study (4:38), and the high temperature tension-compression and tension-tension unnotched specimens used in Boyum's study (6:93). On the maximum applied stress basis, it was found that this study's case of specimens experiencing tension-compression fatigue with the addition of the notch resulted in the lowest fatigue lives. This was a result of the stress concentration effect from the hole and the increased damage from the compressive portion of the loading. It was also found that on the stress range basis, the addition of the center hole made no difference in the fatigue life of the material if the loading condition was high temperature tension-tension fatigue only.

LISOL, the Laminate Inelastic Solver, was used to determine the microstresses in the fiber and matrix after one second into the fatigue life of the notched high temperature tension-compression and tension-tension cases. Fiber and matrix stresses for the two loading conditions, using both the maximum stress and stress range basis, were plotted against cycles to failure to determine if the microstresses would provide a parameter that

predicted the fatigue life for specimens experiencing different R-ratios. The microstresses did not prove to be a viable parameter for comparisons between the two loading conditions.

Microstresses for the fiber and matrix were also determined for the unnotched tension-compression fatigue loading case. A similar microstress comparison as between notched tension-compression (TC) and notched tension-tension (TT) was made, this time between notched tension-compression and unnotched tension-compression cases. However, in this comparison the notched TC condition microstresses were plotted against cycles to crack initiation. The reason for this was that the notched case used a stress concentration factor to account for the hole, and the resulting microstress values represented only the stresses in the fiber and matrix in the region around the hole. Failure in the region directly around the hole occurred when a matrix crack initiated.

For the unnotched condition, the microstresses represent stress in the fiber and matrix throughout the entire specimen. Hence, failure of the specimen was when fracture of the specimen occurred. Therefore, the microstresses for the unnotched condition were plotted against the fatigue life of each test.

This comparison showed that the microstresses for both the fiber and matrix were much higher for the notched condition than the unnotched condition when considering maximum stress values and stress ranges. This was expected due to the stress concentration effects of the center hole.

None of the microstress comparisons appeared to offer a valid parameter in determining the fatigue life of tests under different R-ratios and notched/unnotched

conditions. Further work needs to be done, such as use of Goodman's diagram as well as analytical studies to account for the stresses exhibited by unbroken bridged fibers as they take on tensile and compressive loads.

Characterization of a material's fatigue response is long and laborious. This study adds to the mosaic of knowledge concerning the fatigue response of MMCs. Yet there is more to be done to complete the picture. The tests in this study were isothermally controlled at a temperature of 427 °C and were sometimes run for a period of days. Testing will be required to determine the effects of creep that will begin take effect as long tests are run at high temperature. And there are still more conditions that must be studied under the tension-compression loading condition, including different lay-ups, temperatures, and possibly even tests that are not run at a constant amplitude. Among these conditions, one that will be important is the thermomechanical fatigue testing of notched cross-ply laminate MMCs under tension-compression loading. Considering the difficulties in analytically predicting the effects of fatigue cracking on MMCs, there are still many questions that must be answered through experimentation to ensure their full characterization and damage responses.

Appendix A: Stress-Strain Curves

The following figures show the stress-strain curves for each fatigue test in this study at four different cycles during their fatigue lives, starting from the initial cycle to the failure cycle. The curves are offset along the x-axis for the sake of clarity in comparing stress-strain results at various cycles in the fatigue life of each test. The sometimes rough and jagged data is a result of noise within the data acquisition equipment and slight extensometer slippage during fatigue cycling.

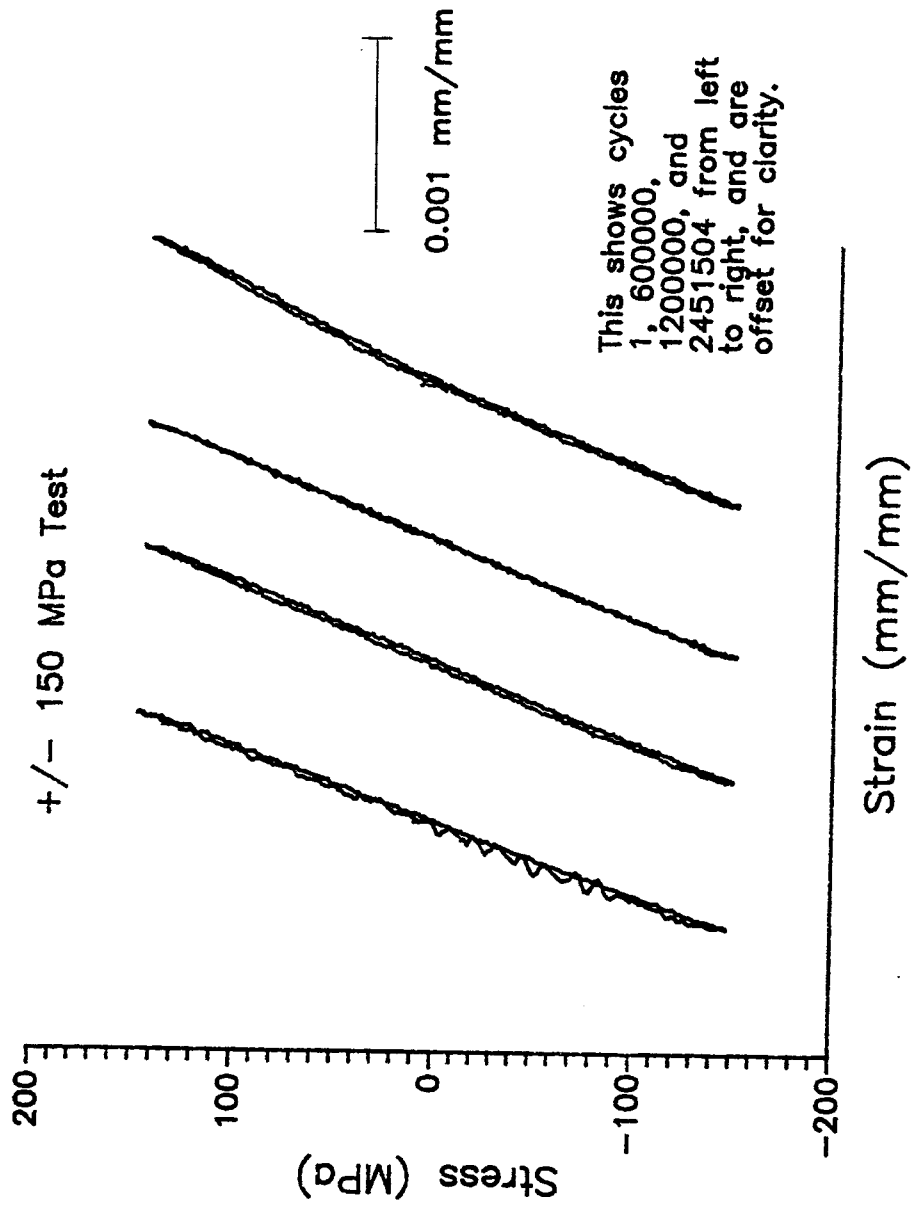


Figure 61. Stress-Strain Curves: ± 150 MPa Test

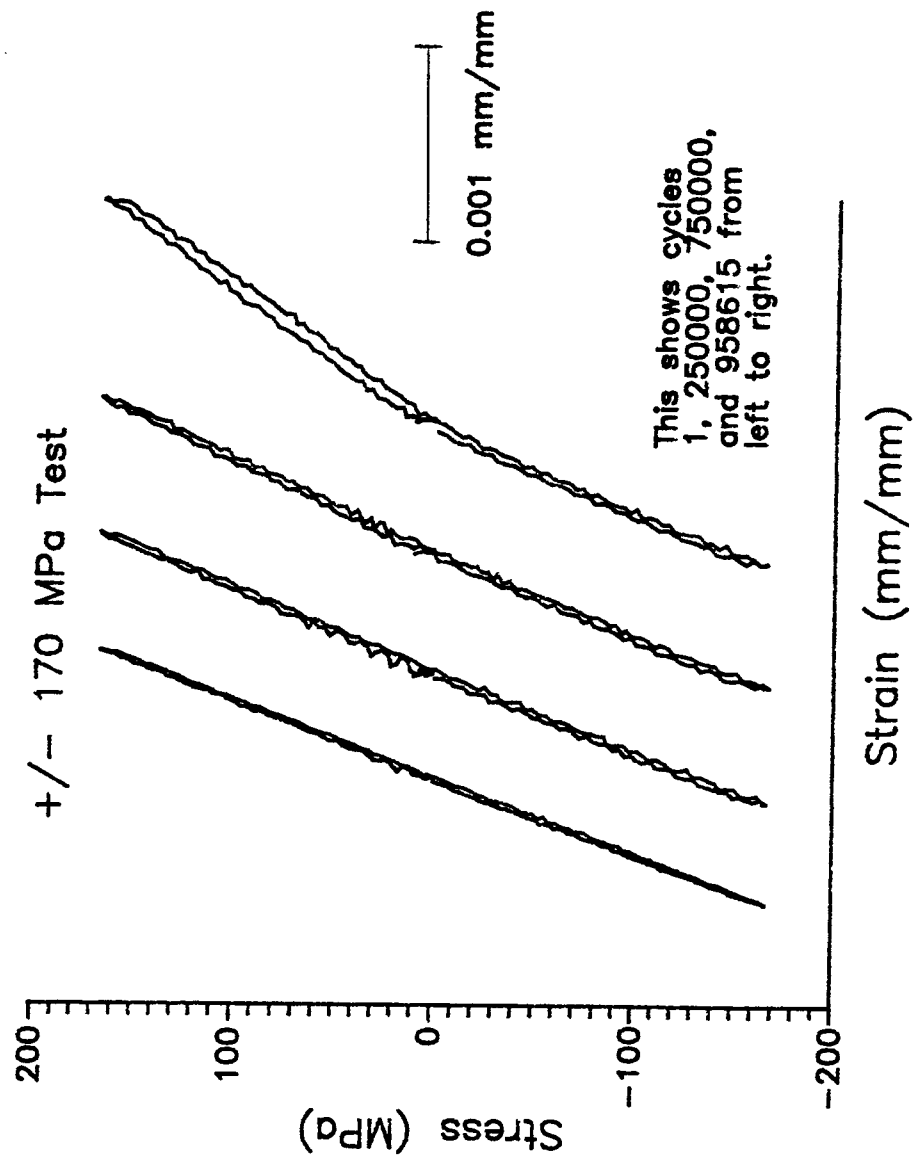


Figure 62. Stress-Strain Curves: ± 170 MPa Test

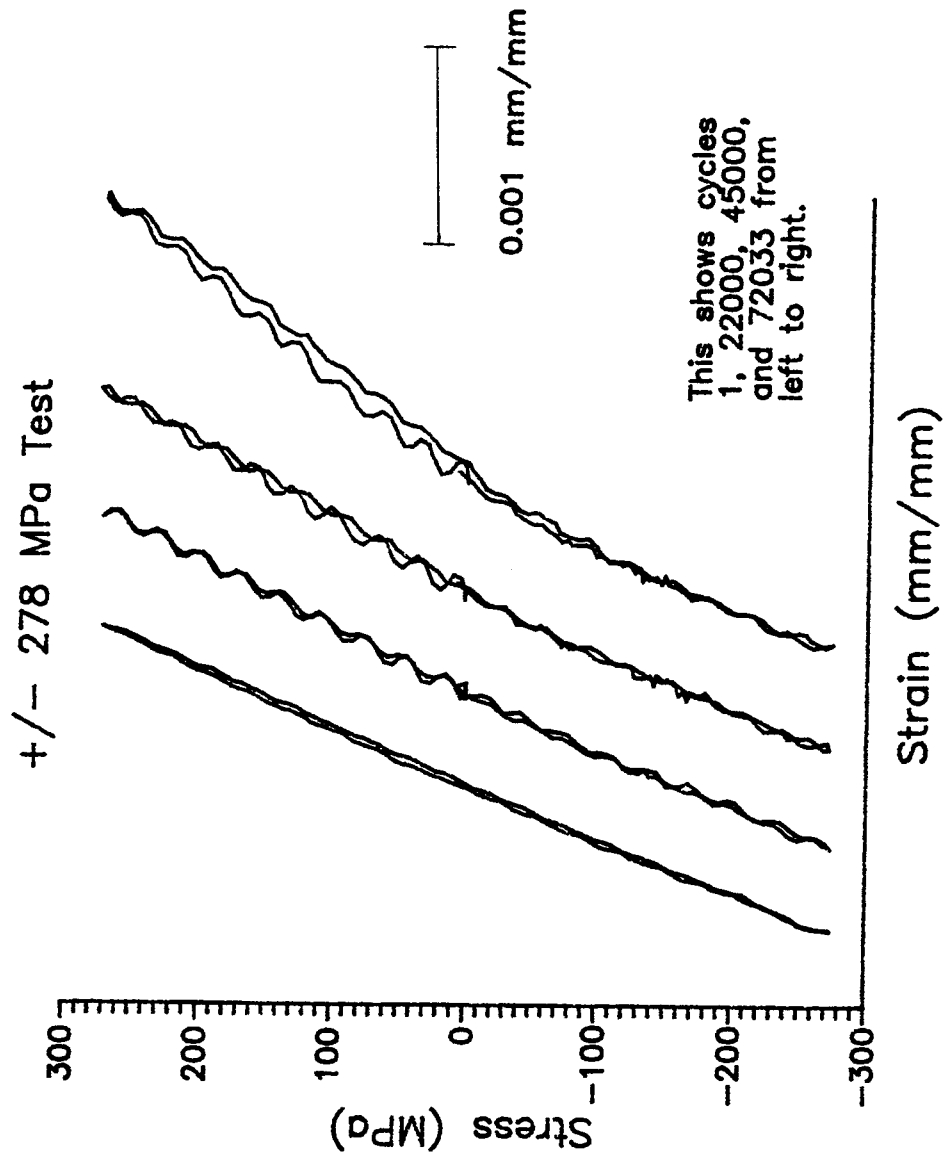


Figure 63. Stress-Strain Curves: ± 278 MPa Test

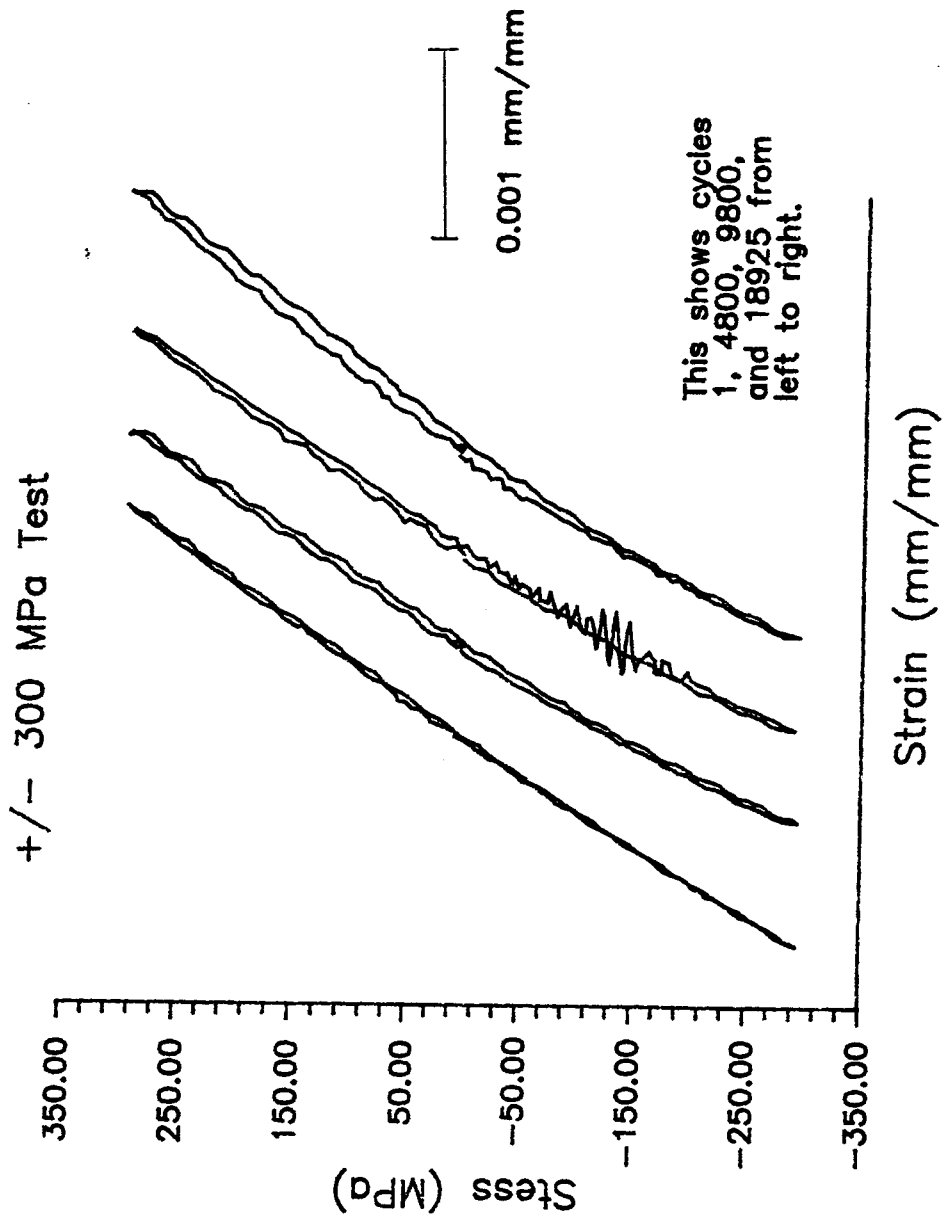


Figure 64. Stress-Strain Curves: ± 300 MPa Test

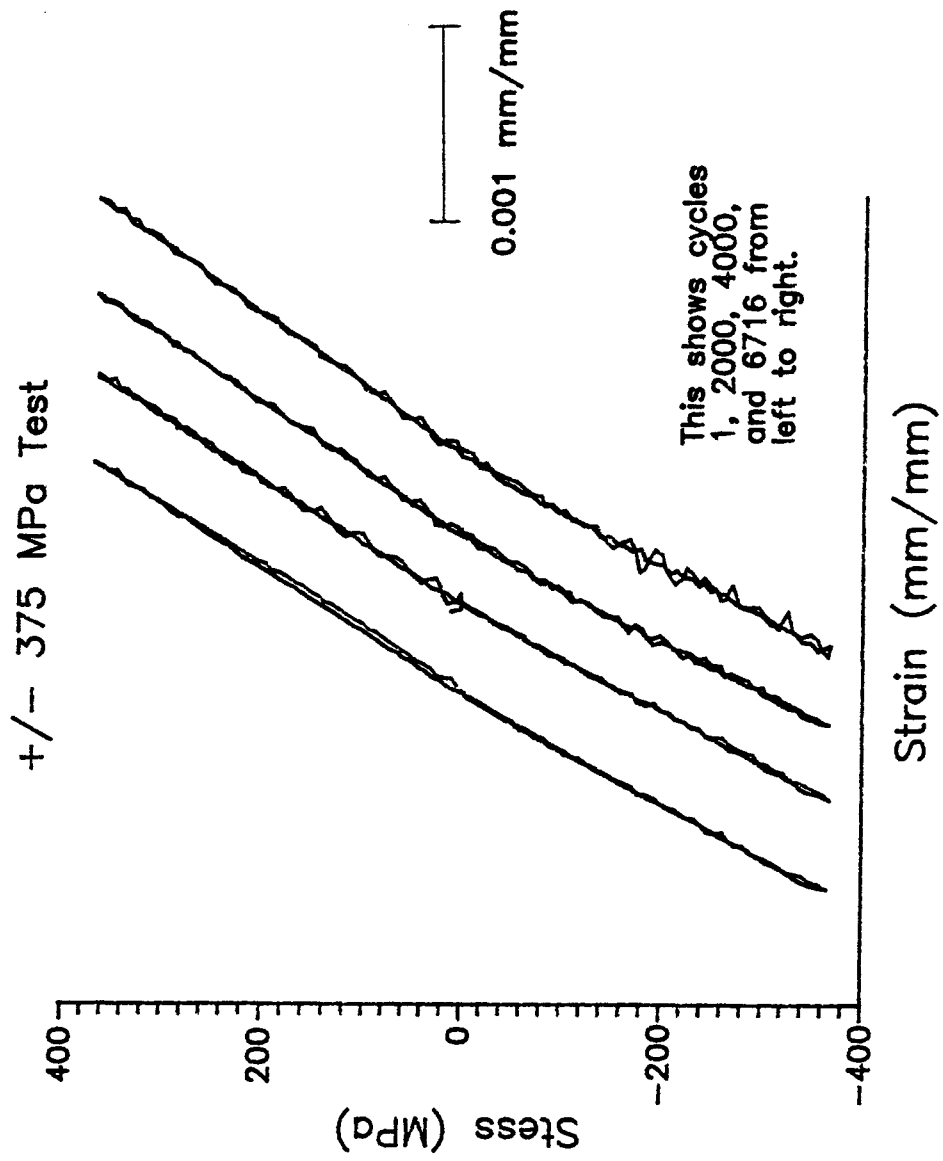


Figure 65. Stress-Strain Curves: ± 375 MPa Test

Appendix B: LISOL Files

The following is the input file for the material properties of SCS-6/Ti-15-3.

SCS6/Ti-15-3 Directional Hardening

Y Y N Y

```

10., 1.0, 0.350
21.11, 393., 0.2, 393., 0.2, 157.2
3.52911e-06, 3.52911e-06
93.33, 390., 0.2, 390., 0.2, 156.0
3.56562e-06, 3.56562e-06
204.44, 386., 0.2, 386., 0.2, 154.4
3.58091e-06, 3.58091e-06
315.56, 382., 0.2, 382., 0.2, 152.8
3.61545e-06, 3.61545e-06
426.67, 378., 0.2, 378., 0.2, 151.2
3.67056e-06, 3.67056e-06
537.78, 374., 0.2, 374., 0.2, 149.6
3.73890e-06, 3.73890e-06
648.89, 370., 0.2, 370., 0.2, 148.0
3.81488e-06, 3.81488e-06
760.00, 365., 0.2, 365., 0.2, 146.0
3.89375e-06, 3.89375e-06
871.11, 361., 0.2, 361., 0.2, 144.4
3.97195e-06, 3.97195e-06
1093.3, 354., 0.2, 354., 0.2, 141.6
4.09657e-06, 4.09657e-06

7, 0., 10000., 23.
25., 91.8, 0.36, 91.8, 0.36, 33.75
8.4800e-06, 8.4800e-06, 0., 0.
0., 0., 0., 0., 0.
1200., 4.5, 0., 1300., 3., 1.0e-08
.005, 1200., 3., 1.0e-08, 250.
315., 80.44, 0.36, 80.44, 0.36, 29.57
9.16e-06, 9.16e-06, 0., 0.
0., 0., 0., 0., 0.
1070., 2.9, 0., 1300., 3., 4.4e-06
.04, 1070., 3., 4.4e-06, 454.
427., 77.5, 0.36, 77.5, 0.36, 27.5
9.4e-06, 9.4e-06, 0., 0.
0., 0., 0., 0., 0.
1020., 2.7, 0., 1300., 3., 1.0e-05
.05, 1020., 3., 1.0e-05, 550.
482., 72.24, 0.36, 72.24, 0.36, 26.56
9.71e-06, 9.71e-06, 0., 0.
0., 0., 0., 0., 0.
850., 1.6, 0., 1300., 3., 1.
5, 850., 3., 1.0, 1100.
566., 64.4, 0.36, 64.4, 0.36, 23.68
9.98e-06, 9.98e-06, 0., 0.

```

0., 0., 0., 0., 0.
700., 1.05, 0., 1300., 3., 0.79
8., 700., 3., 0.79, 2400.
649., 53.00, 0.36, 53.00, 0.36, 19.49
10.260e-06, 10.260e-06, 0., 0.
0., 0., 0., 0., 0.
600.0, 0.7, 0., 1300., 3., 0.2
10.00, 600.0, 3., 0.2, 3800.
900., 25.00, 0.36, 25.00, 0.36, 9.19
10.5e-06, 10.5e-06, 0., 0.
0., 0., 0., 0., 0.
150., 0.5, 0., 1300., 3., 0.2
20., 150., 3., 0.2, 5000.

3, -75.

25., 95., .04
130., .20

538., 75., .04
60., .05

650., 75., .04
60., .05

0.0

The load history can be inputted by the user as a file or directly by typing in values for the length of time interval, temperature, loads in the global x, y, and z axes, and the increment between steps. For LISOL to give accurate microstress values, the beginning of the load history must account for the residual stresses due to the coefficient of thermal expansion mismatch between the matrix metal and fiber. The user can account for these residual stresses by inputting the first line of the load history as a time increment of 0.01 seconds, temperature of 815 °C, no load in any axes, and an increment between steps of 1. This is typed in as :

0.01 815 0 0 0 1

The following line must account for a cool down to room temperature and will determine the residual stresses. Suitable values for this line of input are 2000 seconds, 25 °C, 0 loads in all directions, and an increment of 25. The user may then enter the thermomechanical or isothermal fatigue conditions and specify the number of cycles to be calculated. The following is an example load history input file for the notched tension-compression high temperature case of ± 300 MPa (multiplied by a finite width stress concentration factor of 3.31).

N Y	7	4	7	10	
0.01	815	0	0	0	1
2000	25	0	0	0	20
2500	427	0	0	0	25
0.025	427	496.5	0	0	3
0.025	427	0	0	0	3
0.025	427	-496.5	0	0	3
0.025	427	0	0	0	3

The associated output file for the microstresses is:

Composite Stress Component 1-1/XX	Fib Reg Stress Component 1-1/XX	Mat Reg 2 Stress Component 1-1/XX
0.000000000	0.001998054	0.000540634
0.000000000	-1021.711791992	472.534729004
0.000000000	-508.339447021	224.549133301
496.500000000	1124.936767578	594.489196777
0.000000000	-452.241912842	238.096450806
-496.500000000	-1726.237182617	-44.972671509
0.000000000	-454.044067383	237.793731689
496.500000000	1124.856933594	594.611572266
0.000000000	-453.800598145	237.857192993
-496.500000000	-1729.297851562	-45.645374298
0.000000000	-454.642486572	237.716979980
496.500000000	1124.836181641	594.678771973
0.000000000	-454.523895264	237.749954224
-496.500000000	-1731.174926758	-46.057273865
0.000000000	-455.036590576	237.664093018
496.500000000	1124.796386719	594.707031250
0.000000000	-454.966186523	237.681076050
-496.500000000	-1732.486938477	-46.347518921
0.000000000	-455.324066162	237.621185303
496.500000000	1124.791015625	594.732116699
0.000000000	-455.271240234	237.633911133
-496.500000000	-1733.478881836	-46.567008972
0.000000000	-455.541046143	237.588821411
496.500000000	1124.786254883	594.750976562
0.000000000	-455.500946045	237.598464966
-496.500000000	-1734.265014648	-46.740943909
0.000000000	-455.714263916	237.562866211
496.500000000	1124.781738281	594.765747070
0.000000000	-455.682617188	237.570495605
-496.500000000	-1734.914062500	-46.884422302
0.000000000	-455.858306885	237.541183472
496.500000000	1124.747070312	594.770507812
0.000000000	-455.837066650	237.546295166
-496.500000000	-1735.459594727	-47.005119324
0.000000000	-455.984497070	237.521728516
496.500000000	1124.740844727	594.780029297
0.000000000	-455.963195801	237.526901245
-496.500000000	-1735.930541992	-47.109405518
0.000000000	-456.090240479	237.505706787
496.500000000	1124.740600586	594.789428711
0.000000000	-456.071014404	237.510345459
-496.500000000	-1736.343994141	-47.200855255
0.000000000	-456.182250977	237.491790771

The load history input file for the high temperature tension-tension case of 240

MPa (multiplied by a stress concentration factor of 3.31) is:

NY	5	4	5	0	
0.01	815	0	0	0	1
2000	25	0	0	0	20
2500	427	0	0	0	25
0.05	427	794.4	0	0	3
0.05	427	79.44	0	0	3

The associated output file for the microstresses of this case is:

Composite Stress Component 1-1/XX	Fib Reg Stress Component 1-1/XX	Mat Reg 2 Stress Component 1-1/XX
0.000000000	0.001998054	0.000540634
0.000000000	-1021.711791992	472.534729004
0.000000000	-508.339447021	224.549133301
794.400024414	2392.589355469	788.805603027
79.440002441	46.391162872	253.620773315
794.400024414	2415.729003906	779.527221680
79.440002441	68.745635986	244.016265869
794.400024414	2427.604003906	774.762573242
79.440002441	80.221244812	239.086883545
794.400024414	2435.410156250	771.633605957
79.440002441	87.765762329	235.850738525
794.400024414	2441.153564453	769.335327148
79.440002441	93.317687988	233.473999023
794.400024414	2445.663574219	767.534118652
79.440002441	97.677558899	231.611373901
794.400024414	2449.358398438	766.061340332
79.440002441	101.249382019	230.088806152
794.400024414	2452.478271484	764.820495605
79.440002441	104.265563965	228.805694580
794.400024414	2455.170654297	763.752075195
79.440002441	106.868843079	227.700622559
794.400024414	2457.535644531	762.815246582
79.440002441	109.154960632	226.732086182

Bibliography

1. Adams, Donald F. "Test Methods for Composite Materials," Seminar Notes, Composite Materials Research Group, University of Wyoming. Lancaster: Technomic Publishing Company, March 1991.
2. Agarwal, B.D. and Brautman, L.J. *Analysis and Performance of Fiber Composites*. New York: John Wiley & Sons, Inc., 1990.
3. Bannantine, Julie A. and others. *Fundamentals of Metal Fatigue Analysis*. New Jersey: Prentice Hall, 1990.
4. Baker, Capt. Robert P. *Investigation of Fatigue Behavior in Notched Cross-Ply Titanium Metal Matrix Composite at Elevated Temperature*. MS Thesis, AFIT/GAE/ENY/92D-03. School of Engineering, Air Force Institute of Technology (AU), Wright-Patterson AFB, OH, December 1992.
5. Broek, David. *Elementary Engineering Fracture Mechanics, Fourth Revised Edition*. Dordrecht: Kluwer Academic Press, 1991.
6. Boyum, Capt. Elizabeth A. *Investigation of Tension-Compression Fatigue Behavior of a Cross-Ply Metal Matrix Composite at Room and Elevated Temperatures*. MS Thesis, AFIT/GAE/ENY/93-D-6. School of Engineering, Air Force Institute of Technology (AU), Wright-Patterson AFB, OH, December 1993.
7. Gabb, T.P., Gayda, J. and MacKay, R.A., "Isothermal and Nonisothermal Fatigue Behavior of a Metal Matrix Composite," *Journal of Composite Materials*, Vol. 24, June 1990, pp. 667-686.
8. Greszczuk, L.B., "Stress Concentrations and Fatigue Criteria for Orthotropic and Anisotropic Plates with Circular Openings," *Composite Materials: Testing and Design (Second Conference)*, ASTM STP 497, American Society for Testing and Materials, 1972, pp. 363-381.
9. Hillberry, B.M., and Johnson, W.S., *Prediction of Matrix Fatigue Crack Initiation in Notched SCS-6/Ti-15-3 Metal Matrix Composites*. NASA TM 104141. NASA Langley Research Center, 1991.
10. Hopkins, D.A. and Chamis, C.C., *A Unique Set of Micromechanics Equations for High Temperature Metal Matrix Composites*, NASA TM 87154. NASA Lewis Research Center, 1985.

11. Johnson, W.S., "Fatigue Testing and Damage Development in Continuous Fiber Reinforced Metal Matrix Composites," *Metal Matrix Composites: Testing, Analysis, and Failure Modes*, ASTM STP 1032, W. S. Johnson, Ed., American Society for Testing and Materials, Philadelphia, 1989, pp. 194-221.
12. Majumdar, B.S. and Lerch, B.A. "Fatigue Mechanisms in a Ti-Based Fiber-Reinforced MMC and Approaches to Life Prediction." Submitted to Titanium Matrix Composites Workshop, La Jolla, California, June 1993.
13. Majumdar, B.S. and Newaz, G.M. "Inelastic Deformation of Metal Matrix Composites: Compression and Fatigue," Submitted for publication. Battelle Memorial Institute, Columbus, OH 43201.
14. Mall, S. and Portner, B., "Characterization of Fatigue Behavior in Cross-Ply Laminate of SCS-6/Ti-15-3 Metal Matrix Composite at Elevated Temperature," ASME Journal of Engineering Materials and Technology, Vol. 114, No. 4, October 1992, pp. 409-415.
15. Naik, R.A. and Johnson, W.S., "Observations of Fatigue Crack Initiation and Damage Growth in Notched Titanium Matrix Composites." Paper presented at the ASTM Third Symposium on Composite Materials: Fatigue and Fracture. Orlando, FL, November 6-9, 1989.
16. Newaz, G.M. and Majumdar, B.S., "Crack Initiation Around Holes in a Unidirectional MMC under Fatigue Loading," Accepted for publication in Engineering Fracture Mechanics. Battelle Memorial Institute, Columbus, OH 43201.
17. Portner, Barry D. *Investigation of Fatigue Damage in Metal Matrix Composite Under Elevated Temperature*. MS Thesis, AFIT/GAE/ENY/90D-20. School of Engineering, Air Force Institute of Technology (AU), Wright-Patterson AFB, OH, December 1990.
18. Robertson, D.D. and Mall, S. "Micromechanical Analysis for Thermoviscoplastic Behavior of Unidirectional Fibrous Composites," *Composites Science and Technology*, 50, July 1993, pp. 483-496.
19. Sanders, Brian. *Characterization of Fatigue Behavior in a Metal Matrix Composite (SCS-6/Ti-15-3) at Elevated Temperature*. Doctoral Dissertation, AFIT/DS/ENY/92J. School of Engineering, Air Force Institute of Technology (AU), Wright-Patterson AFB, OH, January 1992.
20. Smith, K.N., Watson, P., and Topper, T.H., "A Stress-Strain Function for the Fatigue of Metals," *Journal of Materials*, JMLSA, 5, December 1970, pp. 767-778.

21. Talreja, Ramesh. *Fatigue of Composite Materials*. Lancaster: Technomic Publishing Company, 1987.
22. Tsai, Stephen W. *Composites Design*. Dayton: Think Composites, 1987.
23. Verilli, M.J. and Gabb, T.P. "High Temperature TC Fatigue Behavior of a Tungsten Copper Composite," Fourth Symposium on Composite Materials: Fatigue and Fracture, ASTM Conference Proceedings, March 1991.

Vita

Second Lieutenant Matthew W. Yocum was born 18 November 1971 in Covington, Kentucky. He graduated from Boone County High School, in Florence, Kentucky, in 1989. That summer he entered the United States Air Force Academy where he majored in Engineering Science. Upon his graduation from USAFA in 1993, his first assignment was to enter the Air Force Institute of Technology in July 1993, during which he published his first work, a poem in an anthology by the National Library of Poetry.

Permanent Address: 103 N. Watchtower Dr.
Wilder, KY 41076

REPORT DOCUMENTATION PAGE

Form Approved
OMB No. 0704-0188

Public reporting burden for this collection of information is estimated to average 1 hour per response, including the time for reviewing instructions, searching existing data sources, gathering and maintaining the data needed, and completing and reviewing the collection of information. Send comments regarding this burden estimate or any other aspect of this collection of information, including suggestions for reducing this burden, to Washington Headquarters Services, Directorate for Information Operations and Reports, 1215 Jefferson Davis Highway, Suite 1204, Arlington, VA 22202-4302, and to the Office of Management and Budget, Paperwork Reduction Project (0704-0188), Washington, DC 20503.

1. AGENCY USE ONLY (Leave blank)		2. REPORT DATE December 1994	3. REPORT TYPE AND DATES COVERED Master's Thesis	
4. TITLE AND SUBTITLE INVESTIGATION OF TENSION-COMPRESSION FATIGUE BEHAVIOR OF A NOTCHED CROSS-PLY METAL MATRIX COMPOSITE AT ELEVATED TEMPERATURE			5. FUNDING NUMBERS	
6. AUTHOR(S) Matthew W. Yocum, Second Lieutenant, USAF				
7. PERFORMING ORGANIZATION NAME(S) AND ADDRESS(ES) Air Force Institute of Technology, WFAFB, OH 45433			8. PERFORMING ORGANIZATION REPORT NUMBER AFIT/GAE/ENY/94D-8	
9. SPONSORING / MONITORING AGENCY NAME(S) AND ADDRESS(ES) Dr. Walter Jones AFOSR/NA Wright-Patterson AFB, OH 45433			10. SPONSORING / MONITORING AGENCY REPORT NUMBER	
11. SUPPLEMENTARY NOTES				
12a. DISTRIBUTION / AVAILABILITY STATEMENT Approved for public release; distribution unlimited			12b. DISTRIBUTION CODE	
13. ABSTRACT (Maximum 200 words) This research extends the existing knowledge of MMC fatigue damage mechanisms by studying the tension-compression fatigue behavior of a notched cross-ply laminate MMC at elevated temperature. A [0/90] _{2S} SCS-6/Ti-15-3 laminate with a center hole was subjected to tension-compression fatigue at 427 °C (800 °F). Stress and strain data was taken to evaluate macro-mechanic behavior of the material. Microscopy and fractography were performed to characterize the damage on a micro-mechanical level. Crack initiation and progression was monitored using acetate face replicas. Four cracks were found to develop around the periphery of the hole, two of which became dominant and proceeded through to the end of the specimen. On a maximum applied stress basis, tension-compression notched specimens had shorter fatigue lives than tension-tension notched specimens. Also, tension-compression adds more damage due to the compressive portion of the loading, and tension-compression loading increased the time to crack initiation for a given maximum stress and increased the rate of crack propagation over tension-tension cases.				
14. SUBJECT TERMS Metal Matrix Composite, Elevated Temperature, Fatigue Testing, Tension-Compression Fully-reversed, Titanium, Silicon Carbide			15. NUMBER OF PAGES 145	
			16. PRICE CODE	
17. SECURITY CLASSIFICATION OF REPORT Unclassified	18. SECURITY CLASSIFICATION OF THIS PAGE Unclassified	19. SECURITY CLASSIFICATION OF ABSTRACT Unclassified	20. LIMITATION OF ABSTRACT UL	